Parameterisation of Tyres with Large Lugs

by

Carl Martin Becker

A dissertation submitted in partial fulfilment

of the requirements for the degree of

Doctor of Philosophy (Mechanical Engineering)

in the

Faculty of Engineering, Built Environment and Information Technology (EBIT)

University of Pretoria

November 2021

Abstract

Title: Parameterisation of Tyres with Large Lugs

Author: Carl Martin Becker

Study Leader: Prof P.S. Els

Department: Department of Mechanical and Aeronautical Engineering

Degree: Philosophiae doctor (Mechanical Engineering)

Vehicle development relies heavily on simulation results throughout the vehicle industry; however, simulation results are only as reliable as the input data used to parameterise the models. In vehicle dynamics simulations the terrain and tyres are two very important aspects that are often disregarded or the models over simplified.

Profiling terrain and testing tyres are not trivial or inexpensive exercises, thus it is extremely important to obtain representative measurements. Tyre characteristics are dependent on the terrain characteristics, so it is vital to use representative artificial terrains in laboratory tyre characterisation tests. In this study the artificial and field terrains are measured, characterised together with tyre tests on these terrains. Measuring equipment and tyre test rigs, in the form of terrain profilometers, wheel force transducers, static/non-rolling, dynamic/rolling and damping tyre test rigs are also conceptualised, designed, manufactured, commissioned and used to characterise an agricultural tyre with large lugs.

This study compares friction coefficient measurements on dry non-deformable on-road surfaces in a laboratory and field test tracks on the same agricultural tyre with large lugs.

It is found that the microtexture of the different surfaces needs to correlate in order to have comparable laboratory and field tests results. For the concrete field test surfaces in question, the recommended laboratory test surface needs to have a surface roughness value of $10 < R_a < 15 \mu m$. This roughness is equivalent to a P180 grit to P220 grit sandpaper, however, using only the sandpaper grade is not a good measure to use. A more accurate method is to compare the Displacement Spectral Densities of the field test surface with that of the sandpaper intended to be used in the laboratory. The spatial frequency of interest that needs to be compared is between 10^4 and 10^6 cycles/m, which corresponds to the surface roughness value.

During the operational life of a tyre the longitudinal, lateral, vertical and damping characteristics change as the tyre wears down. This study investigates the change in tyre characteristics with tyre wear at a single load condition, two inflation pressures and three tread wear conditions on a flat surface and over a cleat. Increasing trends are noted with change in traction and tyre stiffnesses as the tyre wear changes.

Motion resistance of tyres directly contribute to the operational costs of all vehicles. Different methods used to measure the motion resistance of a tyre with large lugs are compared on non-deformable terrain. Some basic considerations that need to be considered during motion resistance measurements are the very low longitudinal forces that need to be measured compared to the large vertical load carried by the tyre and tyre operating conditions.

These findings and development of measuring equipment and tyre test rigs will assist researchers and industry to improve handling, ride comfort and energy efficiency of, amongst other, agricultural and construction vehicles.

Acknowledgements

I would like to extend my gratitude to the following people, but not limited to, who assisted me in completing this thesis:

Table of Contents

List of figures

List of Tables

List of Symbols

Symbol	Description	Unit
A	Vehicle Frontal Area	m^2
A_r	Roughness Coefficient	
A_{year}	Tyre age	years
a	Acceleration	m/s^2
C	Damping Coefficient	Ns/m
C_d	Drag Coefficient	
C_r	Motion Resistance Coefficient	
C_{rDB}	Motion Resistance Coefficient Towed vehicle	
C_{vr}	Vehicle Motion Resistance Coefficient	
$d_{\perp OG}$	Distance from the Center of Mass to Hitch Point	m
$D_{longStatic}$	Longitudinal Displacement of Contact Patch	m
D_{rim}	Rim Diameter	inch
$D_{vehicle}$	Longitudinal Displacement of Vehicle	m
D_{wheel}	Longitudinal Displacement of Wheel	m
E	Young's Modulus	GPa
F	Frequency	Hz
$F_{adhesion}$	Adhesion Component in Friction Force	N
F_{Fric}	Friction Force	N

$F_{hysteresis}$	Hysteresis Component in Friction Force	N
F_{pl}	Parasitic Losses	N
F_r	Motion Resistance Force	N
F_{r01}	Motion Resistance Force Measurement on Drum One	N
F_{r02}	Motion Resistance Force Measurement on Drum Two	N
F_{r25}	Motion Resistance Force at 25 degrees Celsius	N
F_{static}	Static Vertical Wheel Load	N
F_x	Longitudinal Force	N
F_{xDB}	Longitudinal Force Measured During Towed Vehicle	N
F_z	Vertical Load	N
g	Gravitational Acceleration	m/s^2
$H1$	Road Index	
$H2$	Surface Index	
$H2_{field}$	Surface Index of Field/ Outdoor Test Surface	
$H2_{lab}$	Surface Index of Laboratory Test Surface	
I_{fw}	Moment of Inertia of Front Wheel	kgm^2
I_G	Moment of Inertial About the Center of Gravity	kgm^2
I_{lug}	Moment of Inertia of Lug for Longitudinal Deformation	kgm^2
I_o	Moment of Inertial About the Tow Hitch	kgm^2
I_{rw}	Moment of Inertia of Rear Wheel	kgm^2
I_{tread}	Moment of Inertia of Lug for Vertical Deformation	kgm^2
k	Spring Stiffness	N/m
K_{Fz}	Vertical Stiffness	kN/m

K_r	Drum Diameter Correction Factor	
K_t	Temperature Constant	
l	Sample length of profile	mm
l_{lug}	Tread Length	mm
l_{tread}	Tread Depth	mm
L	Contact Patch Length	mm
L_h	Distance from the Tow Hitch to the Center of Tyres	m
L_m	Load on Tyre Normal to Drum	N
m	Mass of the DTT During Damping Measurements	kg
M	Vehicle Mass	kg
M_r	Reactive Bending Moment	N/m
n	Number of Cycles	
n_{RI}	Road Index	
N_{rotate}	Wheel Rotations During Brake Application	
P_{bar}	Tyre Inflation Pressure	bar
r	Test Drum Radius	m
r_{rr}	Tyre Rolling Radius	m
r_1	Radius Drum 1	m
r_2	Radius Drum 2	m
r_T	One Half of the Nominal Tyre Diameter	m
R_a	Average Surface Roughness	μm
R_{drum}	Drum Radius	m
R_p	Maximum Peak Height	μm

R_{RL}	Road Load	N
R_{RL_cd}	Road Load from Coast Down	N
$R_{RL-comp}$	Road Load with Inertial Compensation	N
R_q	Mean Square Value of the Surface Roughness	μm
R_y	Maximum Profile Valley Depth	μm
R_z	Maximum Height of Surface Roughness	μm
s	Shore A Hardness	
$Slip_{Lat\_mm}$	Lateral Displacement Component	mm
S_{xx}	Vertical DSD of road profile	
S_z	Vertical DSD	
t_{amb}	Temperature Ambient	°C
t_i	Time Instance	sec
T_{no_load}	Drum Torque Required with No Load Applied	Nm
T_{pl}	Torque on Drum from Parasitic Losses	Nm
T_t	Torque on Drum	Nm
V	Vehicle Speed	km/h
W	Contact Patch Width	mm
W_N	Vehicle Weight	N
W_{rim}	Rim Width	inch
W_W	Vehicle Wheel Load	N
x_0	Amplitude of Initial Peak	mm
$x(d)$	Road Profile	mm

x_n Amplitude of nth Peak   mm

$x(t_i)$ Amplitude of Underdamped Free Vibration Response   mm

X_δ FFT of Road Profile

X_δ^* Complex Conjugate of X_δ

Greek letters

α	Angular Acceleration	rad/s
β	Lateral Slip Angle	°
δ	Logarithmic Decrement	
δ_{lug}	Longitudinal Lug Deformation	mm
δ_{lugFz}	Vertical Lug Deformation	mm
θ	Track Gradient	°
ρ	Air Density	kg/m^3
τ	Undamped Period	sec
τ_d	Mean Damped Period	sec
φ	Spatial Frequency	cycles/m
ζ	Damping Ratio	
μ	Friction Coefficient	
ω_n	Natural Frequency	Hz

Abbreviations and acronyms

DIC	Digital Image Correlation
DSD	Displacement Spectral Density
DT	Drivetrain
DTT	Damping Test Trailer

DTTT   Dynamic Tyre Test Trailer

FFT   Fast Fourier Transform

GPS   Global Positioning System

HSSTM   Hybrid Soft Soil Tire Model

MF   Magic Formula

OEM   Original Equipment Manufacturer

PIARC   Permanent International Association of Road Congresses

PSD   Power Spectral Density

RMS   Root Mean Square

STTR   Static Tyre Test Rig

T2CAM   Tyre-Terrain Camera System

VDG   Vehicle Dynamics Group

WFT   Wheel Force Transducer

1. Introduction

Tyres are the only components in the wheeled-vehicle system that connects the vehicle with the terrain over which the vehicle travels. This is the case for vehicles traveling on non-deformable and deformable terrain. Agricultural equipment can tow implements for example a plough which is used to turn and break up soil. This adds a completely different dynamic to the vehicle system and will not be considered in the current study. Agricultural equipment also travels between fields on public roads at higher operating speeds. This study will focus on agricultural vehicles traveling on non-deformable on-road terrain.

On large off-road vehicles, as with passenger cars, the tyres play a very important role in the dynamic behaviour of the vehicle as all of the tractive forces (lateral and longitudinal directions) acting on the vehicle goes through the tyre to the terrain. Tyres are manufactured from several materials ranging from metals to rubber.

In the 1800s tyres were bands made from leather followed by steel as used on wooden wagon wheels. The first patented pneumatic tyre appeared in 1847, which was invented by Robert William Thomson, (Du Cross, 1938). The first practical pneumatic tyre was made in Belfast by John Boyd Dunlop in 1888. The discovery of vulcanization of natural rubber using sulphur accelerated the development of tyres followed by invention of synthetic rubber in the 1920s. The first tractors using rubber tyres were designed in the 1930's. Prior to this development, tractors used steel rims with steel lugs (Rukes, 2002). Michelin developed and patented the first radial tyre construction method in 1946. The majority of tyre research and development was done on passenger cars.

Off-road tyres are produced in a large array of sizes and load ratings with much less standardisation compared to passenger car tyres. Production volumes can range from a handful to millions of tyres. A multitude of parameters need to be taken into consideration when selecting a tyre to be used on a vehicle. All of these parameters contribute to tyre characteristics and vary as they are all interconnected and have a direct or indirect effect on each other as well as the response of the tyre and as a result the response of the vehicle. These parameters can be listed as the following and are not limited to: solid rubber tyre or pneumatic tyre, static vertical load (laden and unladen), expected dynamic vertical load, carcass construction (influenced by tyre size, width, profile height, speed rating, load rating, inflation pressure, etc.), rubber compound, tread pattern, wear condition, tyre age, ambient temperature (e.g. artic use, desert use or daily fluctuation in temperature), operating speed, efficiency, type of terrain (deformable vs. non-deformable terrain), surface roughness, friction condition (dry, wet or ice), daily operating use (racing, commuting, commercial, construction, agricultural or even aviation) all of which directly relates to vehicle handling or passenger/cargo ride comfort. These parameters can also be divided into many more sub divisions that can go down to molecular level.

Agricultural vehicles are being used more on asphalt/non-deformable terrain as commercial farms are ever increasing in size. As a result, modern farmers need to travel with agricultural vehicles over long distances on public roads from one field to the next. This drives the operating conditions of these vehicles to the limit as it is required that these vehicles travel at the maximum possible speed. As operational costs are always forced to a minimum, agricultural vehicles may operate with tyres ranging from new to fully used condition with 100% down to almost 0% tread on them.

During the operational life of a tyre, the tyre characteristics change as the tyre wears down to the limit. This is not always taken into consideration by the Original Equipment Manufacturer (OEMs). It is expected from the end user to conduct the required maintenance on the vehicle. The change in tyre characteristics on agricultural tyres are significant due to the size of the tread blocks on these tyres. New tread designs on agricultural tyres are also increasing the forces on the drivetrain as the tyres are designed for on-road use with even more rubber in contact with the road. Wright et al., (2019) indicated that tyre wear and aging does not have a significant change in Sports Utility Vehicle's (SUV) tyre characteristics, however the tread depth on SUV tyres are in order of the carcass thickness compared to agricultural and construction tyres where the tread thickness is up to 10 times the carcass thickness. The thick tread blocks on these agricultural tyres contribute significantly to the stiffness and mass of the tyre, thus as the tread wears down, the tyre characteristics change. Aging of tyre was a problem in the past, however, modern tyres are manufactured with additives to improve ozone resistance and ensure consistent properties over long periods (Witzel, 2018).

Over the last two decades considerable advances have been made in the levels of detail design and simulation of large off-road vehicles. This includes the construction, mining and agricultural industries amongst others. The advances in simulation have been driven as many of these large vehicles, which still fits within the legal road limits, are being used on public roads thus they need to comply with more strict national road traffic regulations all over the world. Even with the larger vehicles the OEM has to compete with increased production requirements, which requires higher vehicle operating speeds and better efficiency thus the motion resistance of agricultural tyres is now of more interest. This has

forced OEMs to invest in more detailed simulation orientated design processes to increase safety and efficiency of the vehicles. The increase in production operating conditions typically drives improved handling and ride comfort characteristics and lower operating costs as the vehicles need to travel safely at higher speeds over longer distances. The tyres play a very important role in all of these considerations, thus improved tyre models of agricultural tyres are required in order to obtain accurate simulation results.

Obtaining tyre data is not a trivial or inexpensive exercise, as a result tyre manufactures are reluctant to freely supply tyre data. Tyre manufactures only supply high-end clients with limited tyre data or they simply do not have the required data. Test equipment suitable for large agricultural and off-road vehicles are very limited due to the size of the tyres, the required operating load and logistics around testing these large tyres at the designed operating conditions.

Every tyre model used in simulations requires different sets of parameterisation data. Different tyre parameterisation test methods exist and vary from laboratory tests to field tests on different surfaces. Tyre parameters include longitudinal, lateral and vertical stiffness and is in some cases proportional to the inflation pressure or may be dependent on the carcass construction. The tyre-terrain interaction parameters are dependent on the friction coefficient between the tyre and terrain, which is dependent on the contact area which directly effects the motion resistance and maximum traction available. Each test surface has different surface roughness and will result in different measured tyre characteristics.

During this study and over the last decade the author was an integral part of the conceptualisation, design, development, manufacturing, commissioning and testing of multiple instruments and test rigs that range from terrain profilers, wheel force transducers, static/non-rolling, dynamic/rolling and damping tyre test rigs that form part of the unique range of research equipment used by the Vehicle Dynamics Group at the University of Pretoria.

Multiple journal and conference papers have been published that are relevant to the current study and contributed to the test methods and final results:

1. Becker, C.M. and Els, P.S., 2020, Motion Resistance Measurements on Large Lug Tyres, Journal of Terramechanics, Vol. 88, pp.17–27.

2. Becker, C.M. and Els, P.S., 2021, Laboratory tyre testing vs. Field Test Friction Results, submitted for publication in peer-reviewed journal.

3. Becker, C.M. and Els, P.S., 2021, Agricultural Tyre Stiffness Change as a Function of Tyre Wear, submitted for publication in peer-reviewed journal.

4. Becker, C.M. and Els, P.S., 2018, Static and dynamic parameterization test rigs for large tyres, Proceedings of the joint 10th Asia-Pacific Conference of ISTVS and 39th Annual Meeting of Japanese Society for Terramechanics, Kyoto, Japan.

5. Becker, C.M. and Els, P.S., 2015, The applicability of the friction circle concept to off-road tyres, Proceedings of the 13th European Conference of the ISTVS, Rome, Italy.

6. Becker, C.M. and Els, P.S., 2014, Profiling of rough terrain, International Journal of Vehicle Design, Vol. 64, Nos. 2/3/4, pp. 240-261.

7. Becker, C.M. and Els, P.S., 2012, Wheel Force Transducer Measurements on a Vehicle in Transit, Proceedings of the 12th European Regional Conference of the ISTVS, Pretoria, South Africa.

8. Els, P.S. and Becker, C.M., 2011, Characterisation of off-road tyres, Proceedings of the 17th International Conference of the ISTVS, Blacksburg, USA.

9. Els, P.S. and Becker, C.M., 2010, Characterisation and Modelling of Off-road Tyres, Proceedings of the Joint 9th Asia-Pacific ISTVS Conference and Annual Meeting of the Japanese Society for Terramechanics, Sapporo, Japan.

This study compares friction coefficient measurements on dry non-deformable surfaces in a laboratory and field test tracks on the same agricultural tyre. The macrotexture and microtexture of multiple surfaces are measured and compared. The change in tyre characteristics with tyre wear at a single load condition, two different inflation pressures and three tread wear conditions are investigated. Different methods used to measure the motion resistance of the agricultural tyre with large lugs and large gaps between the lugs are compared on non-deformable terrain and measured during multiple tyre wear stages.

2. Literature Review

A number of studies were conducted in the 1970s to the 1990s to obtain tyre data. Crolla and Maclaurin (1985) already described the importance and contribution that simulation makes in the design stage. Many studies have been conducted with regard to on-road vehicle tyres, on-road vehicle dynamics, etc. Simulation for on-road vehicles are very well established up to the point where homologation of new vehicles is possible based on simulation results, instead of real-world testing (TüV SüD, 2021). Limited information regarding the suspension characteristics of agricultural tyres is available as described by Stayner et al., (1984). Lines (1991) indicated that poor information about the agricultural tyre's behaviour over any terrain has a very large effect on the simulation errors. Simulation results are only as reliable as the input data and in vehicle ride or handling simulations, the primary excitation into the system is via the tyres, thus the importance of having reliable tyre data for accurate tyre modelling and vehicle simulation. With the tyres being the only suspension on many agricultural and construction vehicles, the importance of accurate tyre models is even more critical. The advances made in tyre technology and construction to date has placed a large question mark on the reliability on the limited historical collection of tyre data available especially in the agricultural and construction industry. Other vehicle performance factors taken into consideration of which tyres contribute to, range from off-road traction and soil compaction to on-road handling, ride comfort, braking and motion resistance.

2.1. Tyre Models

In the simulation environment multiple models are used to simulate a vehicle driving over a terrain. A high-level representation of the models within a simulation vehicle model is shown in Figure 1.
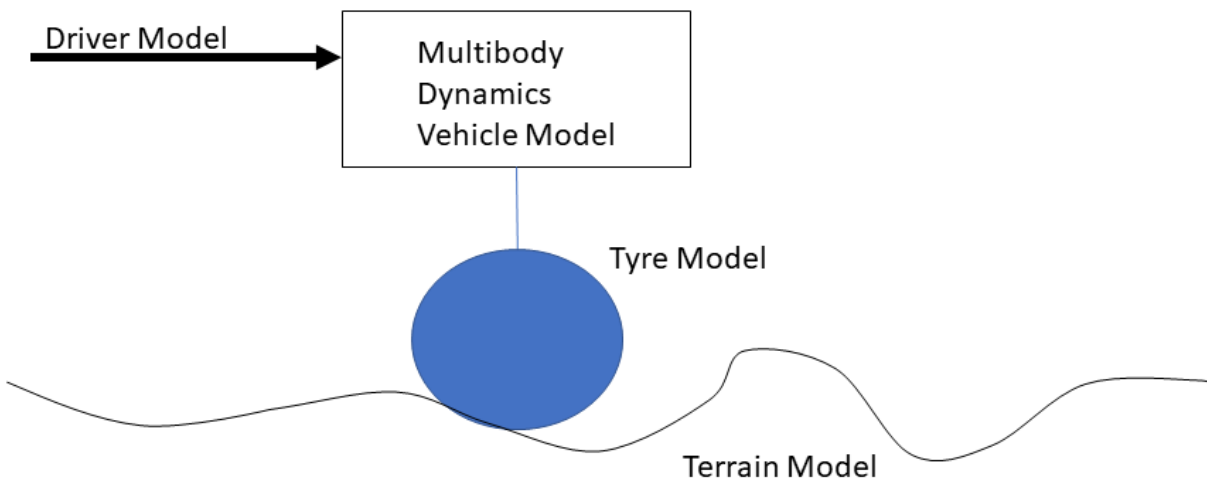
Figure 1: High level representation of the models in a vehicle simulation model.

These models include, but are not limited to, a driver model, multibody dynamics vehicle model, tyre model and terrain model. The multibody dynamics vehicle model may include vehicle suspension, vehicle body inertia, mass properties, torsional stiffness, etc. The multibody dynamics vehicle model may be very simplistic or very detailed and complicated, it all depends on the intent of the simulation model. A driver model is used to move the multibody dynamics vehicle model in the simulation environment. A tyre model is used to simulate the interaction between the vehicle and the terrain. The tyre model can vary form a very simplistic point follower to a very detailed finite element model

of the tyre. The same is true for terrain models. Depending on the intent of the simulation model, the terrain model can vary from a 2-dimensional line representing a profile of the terrain, a 3-dimensional profile of un-deformable terrain, up to a Discrete Element Model, with sand granules or deformable terrain.

When we only look at the tyre models one will find that different tyre models exist and each tyre model has different advantages. Tyre models fall broadly into two types of models namely:

    i.   Empirical or semi-empirical models, for example a Pacejka/ Magic Formula model, Hybrid Soft Soil Tire Model, etc.

    ii.   Physics based models, for example FTire, RMOD-K, Hohenheim, etc.

These models need to simulate the tyre's response to an input from the terrain. As the tyres are the primary input to the vehicle dynamics model it is very important to have a representative tyre model for the analysis intended with the simulation. This means the user needs to know what parameter will be examined in the simulation model before a tyre model can be selected. Only a few tyre models will be referred to in this section in an attempt to explain the different levels of complexity and parameter requirements for different tyre models.

ADAMS is a multibody dynamics and motion analysis software supplied by MSC Software Corporation (MSC Software, 2014). It is one of many software packages available on the market used for multibody dynamics analysis. ADAMS supplies the user with a very informative tyre model selection chart, shown in Figure 2, that can assist the user in selecting the most appropriate tyre model available in ADAMS for the simulation at hand.

When the user knows which tyre model needs to be used, parameterisation data can be

acquired and a model developed.

MD Adams	Event / Maneuver	ADAMS/ Handling Tire							Specific Models	
		PAC2002[1]	PAC-TIME[1]	PAC89[1]	PAC94[1]	FIALA[1]	5.2.1.[1]	UA Tire[1]	PAC-MC[1]	FTire
Handling	Stand still and start	+	o/+	o/+	o/+	o/+	o/+	o/+	o/+	+
	Parking (standing steering effort)	+	-	-	-	-	-	-	-	+
	Standing on tilt table	+	+	+	+	+	+	+	+	+
	Steady state cornering	+	+	o/+	+	o	o	o/+	+	o/+
	Lane change	+	+	o/+	+	o	o	o/+	+	o/+
	ABS braking distance	+	o/+	o/+	o/+	o	o	o/+	o/+	+
	Braking/power-off in a turn	+	+	o	o	o	o	o	+	o/+
	Vehicle Roll-over	+	o	o	o	o	o	o	o	+
	On-line scaling tire properties	+	-	-	-	-	-	-	-	o
Ride	Cornering over uneven roads *	o/+	o	o	o	o	o	o	o	o/+
	Braking on uneven road *	o/+	o	o	o	o	o	o	o	+
	Crossing cleats / obstacles	-	-	-	-	-	-	-	-	+
	Driving over uneven road	-	-	-	-	-	-	-	-	+
	4 post rig (A/Ride)	+	o/+	o/+	o/+	o/+	o/+	o/+	o/+	o/+
Chassis Control	ABS braking control	o/+	o	o	o	o	o	o	o	+
	Shimmy[2]	o/+	o	o	o	o	o	o	o	+
	Steering system vibrations	o/+	o	o	o	o	o	o	o	+
	Real-time	+	-	-	-	-	-	-	-	-
	Chassis control systems > 8 Hz	o/+	-	-	-	-	-	-	-	+
	Chassis control with ride	-	-	-	-	-	-	-	-	+
Dura- bility	Driving over curb	-	-	-	-	-	o	o	-	o/+
	Driving over curb with rim impact	o	-	-	-	-	o	o	-	o/+
	Passing pothole	-	-	-	-	-	o	o	-	o/+
	Load cases	-	-	-	-	-	o	o	-	o/+

-	Not possible/Not realistic	* wavelength road obstacles > tire diameter
o	Possible	[1] use_mode on transient and combined slip
o/+	Better	[2] wheel yawing vibration due to
+	Best to use	supension flexibility and tire dynamic response

Figure 2: ADAMS tyre model selection chart, (MSC Software,2014), with important sections circled for off-road simulations.

From Figure 2 it can be seen that:

i.   A wide variety of tyre models can be used for stationary tests on a tilt table

ii.   Several models can be used to simulate handling and braking on smooth terrain

iii. Only FTire is suitable for simulating a vehicle driving over rough terrain or simulating a chassis control system

iv.   No good solution available for durability analysis

v.   The circled sections are especially important for off-road simulations.

The Pacejka tyre model, also known as the Magic Formula, MF, was formulated by Dr. H.B Pacejka in the 1980s (Bakker, et al., 1987). The model is widely known and used for handling simulations on smooth terrains, but has limitations when it comes to ride comfort simulations (Becker, 2009). The model is semi-empirical and completely dependent on the experimental data for friction. The following data sets are required to parameterise a Pacejka model:

- Longitudinal force vs. % longitudinal slip at three vertical loads

- Lateral force vs. slip angle at three vertical loads

- Vertical stiffness and damping at three vertical loads

Curve fits are made to the test data which is stored in lookup tables in the simulation model. Changes in tyre operating conditions, for example a different inflation pressure, requires that a new MF model needs to be parameterized.

The original Pacejka tyre model, known as PAC89, as implemented by ADAMS, has evolved over the years with updates and has become known as PAC94, PAC2002 and PAC-MC, with PAC-MC being a motorcycle tyre model. With the basic MF model primarily focused on handling simulations, several additions have been made over the years to improve the performance of the models over uneven and rough terrain. ADAMS/Tire implements four contact models that can be selected, for use with the Pacejka tyre models.

These four contact models are:

- Single Point Contact

- 3D Equivalent Volume Contact

- 3D Enveloping Contact

- Tyre cross-section profiles contact method.

Stallmann (2013), conducted a very informative study where the accuracy of the PAC89 models with different contact models were compared to the physics-based FTire model. It was found that by adding the 3D Equivalent Volume Contact model to the PAC89 tyre model, acceptable results could be obtained over rough terrain.

The following tyre models are stand-alone models that are run via co-simulations.

Sandu et al, (2020), developed the Hybrid Soft Soil Tire Model (HSSTM) which is a semi-empirical tyre model that can efficiently estimate tyre forces and moments on non-deformable or deformable terrain. The parameters required to generate a model range from tyre geometry, footprints, loading radius, modal analysis, finite element model results to static longitudinal stiffness, radial stiffness and lateral stiffness at multiple camber angles. More detailed tyre parameters in the form of belt and sidewall stiffness' are also evaluated in the HSSTM. Dynamic tests in the form of lateral force vs. slip angle and longitudinal force vs. % longitudinal slip tests are again used to validate the tyre model, as shown by the flow diagram in Figure 3.
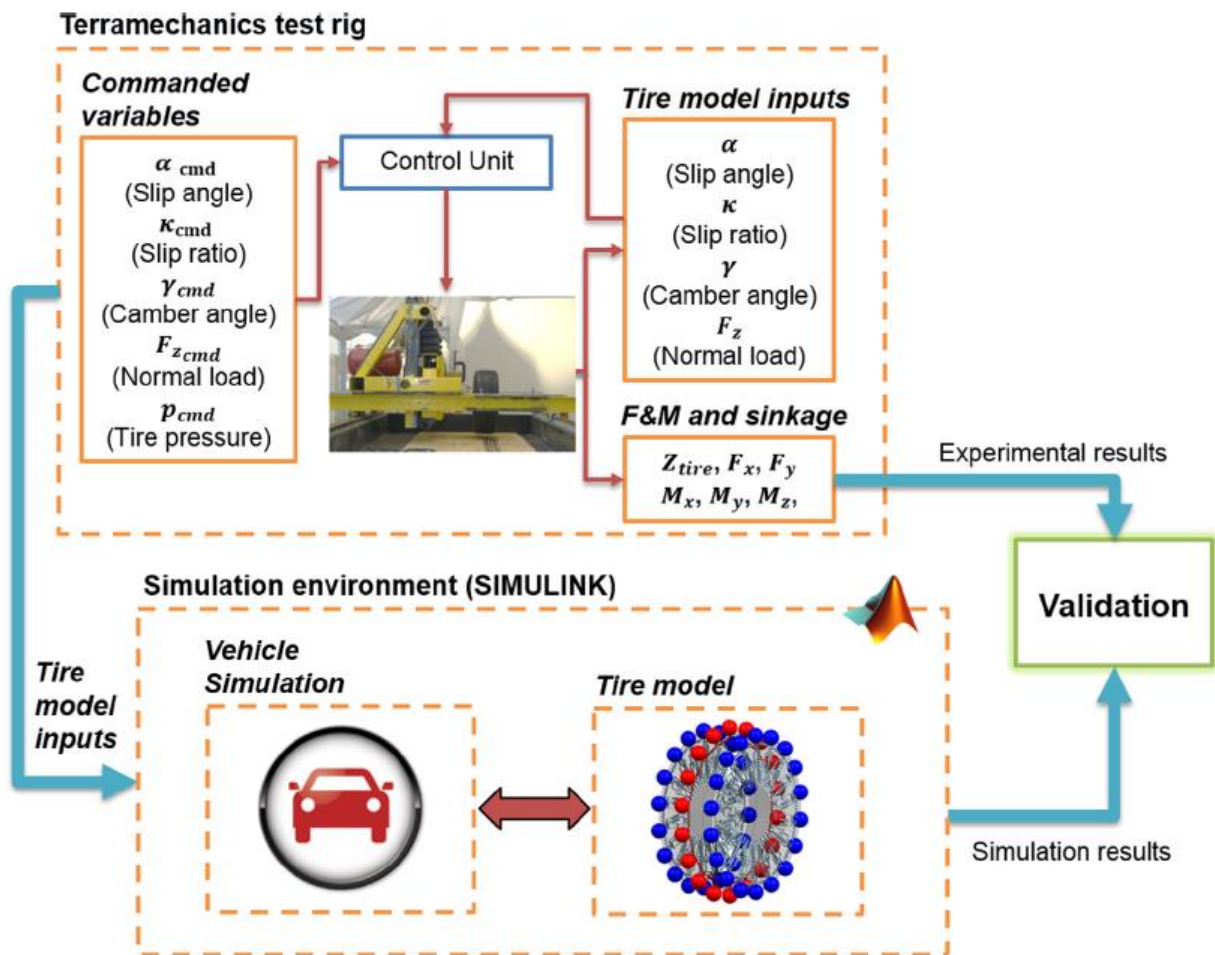
Figure 3: Validation routine of the HSSTM, Sandu, et al, (2020)

The Hohenheim tyre model is a physics-based tyre model specifically developed for agricultural tyres as described by Witzel (2018). The original models used a single point contact, however the updated version use a multi spoke contact approach, where the spoke lengths are adjusted to incorporate the radial runout which is often present on agricultural tyres. The Hohenheim tyre model consists of a selection of Voigt-Kelvin elements and does not use slip as an input. These elements/spokes are orientated radially, tangentially and axially to the wheel hub as shown in Figure 4. The spokes are

only solved for the bottom section of the tyre in order to decrease simulation time. A Real-time solving factor of 0.6 is achieved with this model.
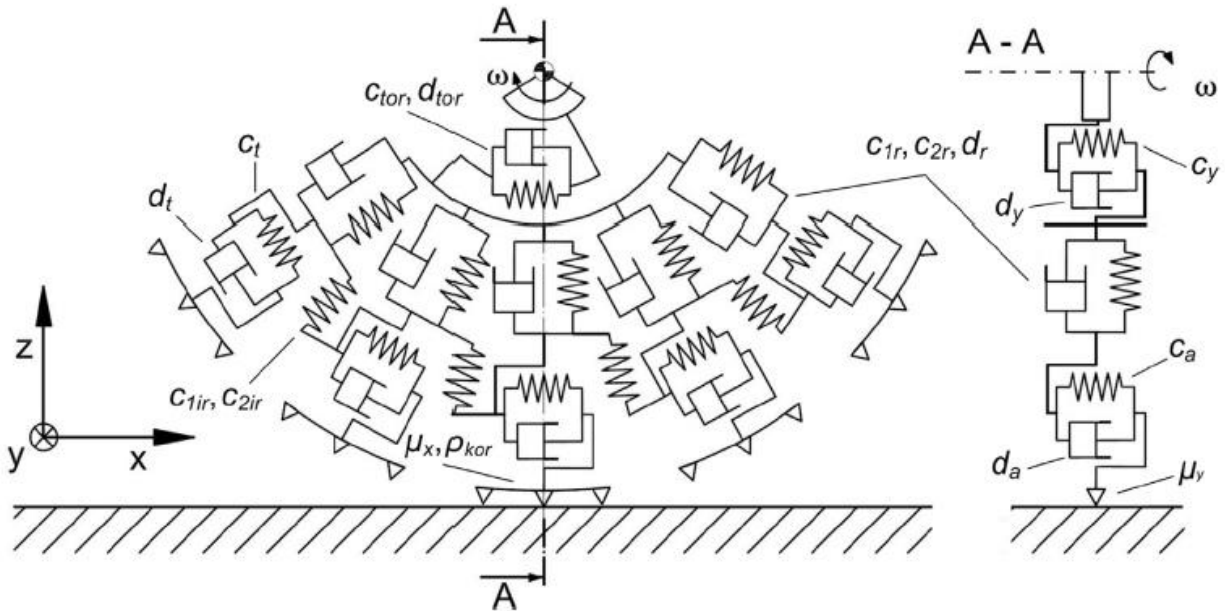
Figure 4: Hohenheim tyre model structure, (Witzel, 2018).

A flat track test rig is used to obtain the required vertical and damping tyre parameters together with a single wheel tester used to obtain lateral and longitudinal tyre parameters. An instrumented test tractor is used to validate the tyre model, as described by Witzel (2018).

The FTire model is a physics-based flexible structure tyre model developed by cosin scientific software (2017). The model can be used for handling and ride comfort simulations on rough terrain. The FTire model can be parameterized at two inflation pressures with the use of static tests to obtain vertical stiffness (on flat surface and cleats), lateral stiffness and longitudinal stiffness together with footprints and tyre geometry. Modal analysis will contribute to model parameterisation but it is not an essential

requirement. Damping over cleats and dynamic tests in the form of lateral force vs. slip angle and longitudinal force vs. % longitudinal slip are used for validation. The required tests can be conducted on a flat track or drum tester. The FTire is a very flexible/adjustable tyre model and enables the user to adjust the amount of tread on the belt and inflation pressure amongst other parameters. The parameterisation of a FTire model does require huge amounts of data and a very large parameterisation effort.

Finite element tyre models are physics-based models and typically require detailed carcass construction information, non-linear material properties and accurate tyre geometry, with damping, vertical, lateral and longitudinal stiffness data used for validation. It is challenging to get all the required parameterisation data for large tyres. Stallmann (2018) developed a model parameterisation approach for large off-road tyres. Although it seems that finite element models require the least amount of information, the data is not always easy to obtain. The difficulty with finite element models is the boundary conditions and interaction between the different materials used in the tyre (Stallmann, 2018). Finite element models also tend to be computationally very expensive in simulation terms. Many studies have been conducted on static tyre loading and single tyre simulations, however a rolling tyre over rough terrain remains a huge challenge with extremely high computational costs, making it infeasible for incorporating into a multibody dynamics model.

Table 1 gives a short summary of the basic requirements for different tyre models. Some measurements are required for model parameterisation and others can be used for model validation. These data sets are not always easy to obtain. Many tyre parameterisation test rigs are available for the parameterisation of passenger car tyres, however

parameterisation test rigs for larger tyres are very limited and for some large tyre not available. On very large tyres only limited parameterisation tests can be completed, these may even be limited to static tests only.

In conclusion all tyre models require some form of experimental data in order to parameterise a representative tyre model. Different tyre models are to be used for different simulation analysis. All tyre models require static stiffnesses at multiple vertical loads, damping characteristics and some tyre geometry. Some tyre models require additional information in the form of modal analysis, contact areas, static loading at camber angles, static stiffness over cleats, stiffness at multiple inflation pressures and/or material properties.

Table 1:Measurements required for parameterisation of tyre models.

Tyre Model	Tests Data Required	
Magic Formula+ single point contact	Lateral force vs. slip angle at three vertical loads	
	Longitudinal force vs. % longitudinal slip at three vertical loads	
	Vertical stiffness and damping at three vertical loads	
PAC'89 +3D Equivalent Volume Contact Model	Lateral force vs. slip angle at three vertical loads	
	Longitudinal force vs. % longitudinal slip at three vertical loads	
	Vertical stiffness and damping at three vertical loads	
	Tyre Geometry – used for contact model	
HSSTM	Tyre Geometry	Rolling radius
	Modal Analysis	Mode shapes
		Natural Frequencies
		Damping
	Vertical Stiffness	0 kPa and Inflated
		0, 3 and 6 degree camber
		Cleat @ 0, 45 and 90 degrees
		Footprints – contact area
	Tangential Stiffness	Inflated
	Lateral Stiffness	Inflated
Hohenheim Tyre Model	Tyre Geometry	Rolling radius
	Vertical Stiffness	Use lookup tables for Fz vs. Displacement
		Vertical stiffness over cleats
	Damping	Response over cleats or obstacles
	Axial stiffness	Lateral force vs. slip angle
	Tangential Stiffness	Longitudinal force vs. % longitudinal slip
	Contact	Multi spoke with radial runout connected to spoke length
FTire	Tyre geometry	Carcass profile
	Static Stiffness	On flat plate
		Over Cleats (Lateral and Longitudinal orientation)
		Various camber angles
		Various inflation pressures
	Foot prints	On flat plate
		At various camber angles
		Various inflation pressures
	Damping	Dynamic cleat tests
	Lateral force vs. slip angle	
	Longitudinal force vs. % longitudinal slip	
Finite Element	Tyre Geometry	
	Static stiffness	
	Material properties (depending on model used)	

2.2.   Tyre Parameterisation Test Methods

Tyre characteristics can be measured by multiple methods. Each method has different constraints and has its own advantages and drawbacks. This is the case for passenger car, motorsport, motorcycle, commercial truck, heavy duty truck, agricultural and construction vehicle types. Many test laboratories are spread worldwide and most have the capability to parameterise relatively small tyres (truck tyres up to 50kN vertical load, (fka, 2021)). Larger tyres present challenges as one needs large amounts of driving power and infrastructure to test these tyres at the designed loads. Only a few examples of test equipment are referenced in this document. Typical indoor laboratory test rigs include drum test rigs or flat track rigs (MTS, 2021). Some test rigs can only be used for traction or braking characterisation, where other test rigs can conduct lateral force vs. slip angle tests, motion resistance measurements or even simulate track racing conditions.

The University of Hohenheim has multiple agricultural tyre test rigs in the form of a flat belt test stand, single wheel test trailer and an instrumented test tractor (Witzel, 2018). These test rigs can be used to measure damping, longitudinal forces, lateral forces and motion resistance on larger agricultural tyres. Other single wheel test trailers have been built for agricultural tyres, used and upgraded from the early 1960's to present. These trailers were mainly designed for Terramechanics research and can be used on any terrain. Billington (1973) introduced the NIAE MkII single wheel tester in 1973. Crolla and El-Razaz (1987) presented some results measured on deformable terrain. Ambruster and Kutzbach (1989), developed a single wheel tester which tests a driven wheel at pre-set slip angles. Shmuleviuch et al., (1996) presented a new field single wheel tester. It is

unknown if all these single wheel testers are still in service. Currently the University of Hohenheim's single wheel tester can test tyres with diameters up to 2000 mm at vertical loads up to 40kN, (Witzel, 2018). Mardani et al., (2010) from the Faculty of Agriculture at the Urmia University, Iran, uses a single wheel tester in a soil bin to determine the motion resistance and traction with variation in dynamic loading, ballasting, travel speeds and tyre inflation pressures.

Previous studies by Misiewicz et al., (2016) that compared methods for estimating the carcass stiffness of agricultural tyres (600/55-26.5 implement tyre) on hard surfaces indicated that the tread on an agricultural tyre has an effect on the vertical deflection, however it has no effect on the slope of the load vs. deflection characteristics. This study further investigated the contact pressure change for different tyre inflation pressures on a treaded and a smooth tyre. It was concluded that the tyre vertical load and inflation pressure has a significant effect on the mean and maximum surface contact pressure on a smooth tyre compared to a treaded tyre where only the inflation pressure had an influence on the resulting contact pressure. These findings agreed with studies by Karafiath and Nowatzki (1978). Misiewicz et al., (2016) concluded that the carcass stiffness of the treaded implement tyre was significantly greater compared to the carcass stiffness of the smooth tyre. Misiewicz (2010) observed that tyres maintain a near constant contact area, when the tyres are loaded with the recommended inflation pressure as specified by the tyre manufacturers. This is expected and the reason why tyre manufacturers supply the user with recommended inflation pressures of specific load applications. Murphy and Lines (1991) conducted a comprehensive study on the stiffness of agricultural tractor tyres and found the inflation pressure, rolling speed, tyre size and

tyre age have the largest effect on the vertical stiffness where the tyre lug length and the type of surface does have some influence. Murphy and Lines (1991) also proposed the vertical stiffness to be estimated from the tyre size, inflation pressure and age using eq. (1)

$$K_{Fz} = 172 - 1.77D_{rim} + 5.6A_{year} + 0.34W_{rim}D_{rim}P_{bar} \qquad \text{eq. (1)}$$

where K_{Fz} is the vertical stiffness (kN/m), W_{rim} and D_{rim} are the tyre section width and rim diameter, respectively, in inches. A_{year} is the tyre age in years with P_{bar} the inflation pressure in bar.

Limited assessments of the longitudinal/ tractional stiffness and lateral stiffnesses have been conducted in previous studies at different tyre wear conditions. These stiffnesses are the important factors when considering the loads on the driveline and handling characteristics of the vehicles. Measuring tyre characteristics on any tyre is not a trivial exercise. The logistics, setup time and costs increase with tyre size.

New novel techniques that are available to characterise tyres, but not utilized in this study include Digital Image Correlation (DIC) techniques and the Tyre-Terrain Camera (T2CAM) system. The T2CAM system measures the tyre deformation from inside the tyre, (Guthrie et al., 2017) and Pegram et al., 2020). This is done with the use of cameras mounted such that images of the contact patch are continuously captured as the wheel rotates. DIC techniques are then used to measure the tyre deformation form the captured images as described by Botha and Els (2015). Cameras can also be mounted on the outside of the tyre to measure the tyre deformation or profile the terrain with the use of DIC.

Vehicle OEMs use tyre characteristics parameters during the design phase of a vehicle to evaluate the ride comfort, handling, efficiency and performance of the vehicles. These parameters are most of the time only available for new tyres with 100% tread on them. The effect of wear on tyres, especially on agricultural tyres, has not been investigated as much in the past. These tyres have large tapered lugs that may change the tyre characteristics as the tyre wears, due to the increase in the amount of rubber in contact with the road as the tyre wears. This indicates that it is required to investigate the effect tyre wear has on the change in tyre characteristics.

Stallmann (2013), investigated the verification of tyre models over off-road terrain on large off-road tyres. These tyres had large, almost square shaped lugs and it was found that the tread pattern had very little effect on the main characteristics of the tyre due to the higher inflation pressures, however the position at which these large lugs came into contact with the cleats during a rolling test did have an effect on the measured damping characteristic. These lugs were wide with small gaps between the lugs compared to the lugs on agricultural tyres where the gaps are much larger compared to the size of the lugs in the tread pattern as shown in Figure 5. The large gaps on agricultural tyres facilitate a self-cleaning effect which prevents mud from building-up in the tread and thus supplies the vehicle with improved traction on deformable terrain. The large gaps between the tread blocks also induce vibration into the vehicle. The distance between the tread blocks can be estimated from vibration measurement tests at constant speeds, Becker and Els (2015).
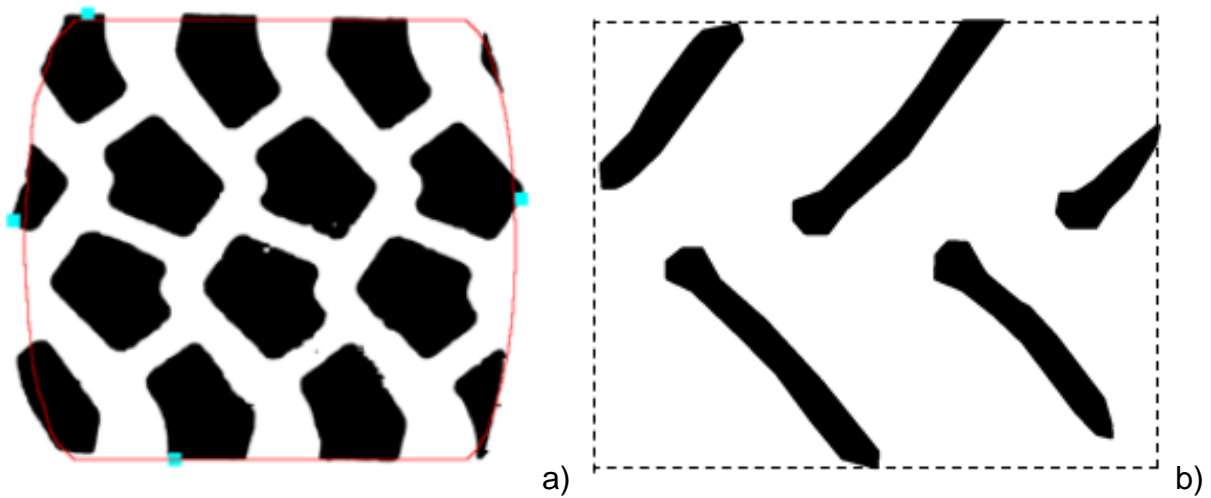
Figure 5: Footprints of a) Military off-road tyre vs. b) Agricultural tyre.

Literature has indicated that a number of parameters control the characteristics of the tyre. These parameters are controlled by either the tyre OEM or the End User/Test Laboratory. Table 2 summarises the parameters that affect tyre characteristics and separated the parameters that are controlled by the tyre OEM and the End User/Test Laboratory.

Table 2: Tyre Parameters Controlled by OEM vs. End User/ Test Laboratory

Controlled Parameters that Affect Tyre Characteristics	
OEM	**End User/ Test Laboratory**
• **Load rating** (Design for a specific vertical load condition)	• **Applied vertical load** (under-load vs. optimal load vs. overload on tyre)

• **Carcass construction**
 	
➢ Material used:
 	
  ▪ Rubber (different compounds)
 	
  ▪ Steel
 	
  ▪ Kevlar vs. Canvas
 	
➢ Amount of layers
 	
➢ Direction of reinforcement material
 	
  ▪ Radial vs. Cross ply
 	
  ▪ Driven wheel vs. non-driven wheels
	• **Inflation pressure**

• **Speed rating**	• **Testing speeds**
• **Tread pattern** (Dependent on application example mining vs. construction vs. earth moving vs. agriculture)	• **Wear**
• **Temperature** (Designed for specific ambient operating temperature)	• **Temperature** (Ambient conditions used in)
• **Age** (Additives in rubber composition to reduce aging effect)	• **Age** (Time period that the tyres are used)
• **Terrain** (Tyre designed for specific terrain application)	• **Terrain/Test Surface Characteristics**: ➢ Roughness ➢ Friction ➢ Non-deformable vs. deformable

2.3.   Motion resistance

Wong (1993) indicated that the complex relationships between the design and operational parameters of the tyre and motion resistance make it extremely difficult, if not impossible, to develop analytic methods for predicting the motion resistance of a tyre. The determination of the motion resistance, therefore, relies almost entirely on experimental measurements. From these experimental measurements empirical formulas can be proposed for the calculation of motion resistance values of a tyre on hard terrain. On soft soil, Wismer and Luth (1974) used a purely empirical based method to predict the motion resistance with the use of a single soil parameter known as the cone index. The cone index is obtained by measuring the force required to push a cone penetrometer into the soil. Bekker (1956) assumed that the wheel was equivalent to a plate continuously being pressed into the soil to a depth equal to the depth of the rut produced by the tyre. The current study focused on the methods of measuring the motion resistance on hard terrain, thus the soft soil methods were not considered.

Vehicle OEMs use coast down and towed vehicle tests to determine the motion resistance of tyres used as the OEMs does not always have access to dedicated test rigs. Drum test rigs and motion resistance test trailers can also be used to determine motion resistance, Witzel (2018). Most research on motion resistance to date have been conducted on passenger car tyres with on-road truck tyres coming into focus, Macmillan (2002). Motion resistance studies on agricultural tyres traversing over deformable terrain have been conducted in the past, Shmuleviuch et al., (1996). However as more off-road

vehicles are being used on-road, more off-road vehicle OEMs are investing in motion resistance measurements on non-deformable terrain, TüV SüD (2021).

The motion resistance of the tyres contributes continuously to the operating costs of the vehicle together with the efficiency of the vehicle drivetrain. These vehicles also operate at different vertical loads (between un-laden and laden conditions) and large variations of tyre pressures for different terrains and loads. All of this adds to the complexity of the vehicles' behaviour and changes the contribution of the motion resistance in the operating cost and efficiency of the vehicle. The vehicle OEMs drive the design for improved drivetrain efficiency and the tyre manufacturer drives improved tyre design for lower motion resistance and improved traction. Vehicle OEMs frequently use towed vehicle and coast down tests to determine the motion resistance of tyres which enables them to decide on which tyre to use on their vehicles to run at the highest efficiency on deformable and non-deformable terrain. Tyre manufacturers mostly use drum test rigs to determine the motion resistance of their tyres at indoor laboratories. Research and test procedures are well established for passenger car tyres, but very limited for large tyres, especially with off-road construction and large lugs/high lug profile or large tread blocks. With the limitation of test equipment capable to test large tyres, OEMs of agricultural, construction and mining vehicles have internal test procedures/specifications to measure motion resistance, which do not always result in the same results obtained during independent third-party vehicle evaluation testing.

Motion resistance is a very difficult measurement as the longitudinal force on a free rolling tyre is very small compared to the applied vertical load on the tyre, especially on non-deformable terrain. The motion resistance on passenger vehicles traveling on non-

deformable terrain and at high tyre inflation pressures can be as low as 0.5% (Gillespie, 1992 and Wong 1993), which places a lot of emphasis on the accuracy of the measurement systems used during these tests. Due to the very low longitudinal load compared to the large vertical load measured on the axle when driving on non-deformable terrain, Wheel Force Transducers (WFT) in general are not suitable for this specific application as the motion resistance measurements are within the noise band of the sensors. In the passenger car and commercial semi-truck industries a large variety of tyre parameterisation test rigs, mostly external drums, are available. Many test laboratories are spread worldwide and most have the capability to parameterise these relatively small tyres.

The MIRIAM project, an acronym for "Models for motion resistance In Road Infrastructure Asset Management systems" is a project with twelve partners from Europe and USA. This project focused on reducing the energy consumption due to the tyre/road interaction, by selection of pavement with lower motion resistance. In this project, Sandberg (2011) performed a comprehensive study of all possible methods for measuring motion resistance ranging from inner and outer drums, with different surface textures, to a motion resistance trailer and coast down tests on passenger and commercial semi-trucks. However, the MIRIAM project was unable to directly compare different techniques on the same tyre.

The literature indicates that measuring the motion resistance coefficient of a tyre has many contributing factors from ambient temperature, tyre operating temperature, tyre operating pressure, tyre diameter, test speed, test vehicle efficiency, tyre rubber compounds, tyre tread patterns, terrain surface texture, and terrain unevenness to terrain

stiffness (Wong, 1993). Different methods used to determine the motion resistance includes tests such as drum tests, coast down tests, towed vehicle tests and trailer tests. Some of these methods will be discussed in the following sections.

2.3.1. Drum Tests

Laboratories conducting motion resistance tests using drum test rigs, test according to ISO 28580:2009 and calibrates/aligns their test equipment relative to a master laboratory and reference tyre. This allows one to be able to compare results between different test laboratories. This indicates the possible variance in motion resistance coefficients, C_r, that can be obtained even between testing laboratories.

The laboratory alignment procedure in ISO 28580, which, for passenger tyres uses two alignment tyres to calibrate a test laboratory to a master laboratory, states that it will compensate for differences induced from tests conducted using different options under the test standard. These options include the use of one of four measurement methods (force, torque, power, or deceleration), textured or smooth drum surface, correction of data to a 25°C reference temperature, and correction of data from tests conducted on a test drum of less than 2.0m in diameter to a 2.0m test drum. The ISO test standard strives to be functional with the various technical capabilities. In ISO 28580, Section 10.2.2: "The reference machine laboratory control tyre monitoring must occur at a maximum interval of one month. Monitoring must include a minimum of 3 separate measurements sometime during this one-month period. The average of the 3 measurements made during a one-month interval shall be evaluated for drift from one monthly evaluation to another." Per

ISO 28580, Section 10.5.5: "The alignment process must be repeated at least every second year and always after any significant machine change or any drift in candidate machine control tyre monitoring data."

2.3.2. Coast Down

Coast down tests are typically conducted with the use of the ISO 28580:2009 or SAE J2263-1996 standards to determine the motion resistance value of tyres. Any vehicle can be used during a coast down test as these tests can be conducted with only the use of a Global Positioning System (GPS). Ambient conditions need to be noted and sometimes measured, depending on the standard used for the motion resistance calculations. These tests are dependent on the gradient of the test surface and the texture of the test surface. Tests are conducted in opposite directions to eliminate wind direction and gradient effect. The inertia of the test vehicle's drivetrain can have an effect on the test results, however if the same vehicle is used to compare different tyres, this can be neglected to an extent depending on the context in which the motion resistance is used.

2.3.3. Towed Vehicle

The early work of McKibben and Davidson, (1940), measured motion resistance by equating it to the towing force required to move different types of wheels across different surfaces, e.g. road (hard/non-deformable), stubble (firm), cultivated (soft) etc. Macmillan

(2002) points out that a major aspect of understanding and predicting vehicle performance is in measuring the motion resistance of a wheel as it is towed over the terrain without slip. Reece (1965) indicated that determining the motion resistance of a driving wheel, when slip is present, is more complex. This will not be considered in this study.

Towed vehicle tests can be used to evaluate multiple vehicle parameters by changing the orientation of the test vehicle relative to the loading vehicle in the form of traction performance, braking performance, cooling capacity or even motion resistance measurements. During motion resistance tests, the test vehicle is towed by another vehicle at a constant speed with a loadcell mounted between the towing point and the towing bar or rope. The force measured at the towing point at a constant speed will be the combined motion resistance force from all the tyres, driveline resistance and aerodynamic drag, (Gillespie, 1992). Conducting the motion resistance tests at a lower speed eliminates the aerodynamic drag. This is a valid approximation for tyres with very low speed ratings, such as construction, earthmoving, mining and agricultural equipment. When testing tyres with high speed ratings (e.g. passenger car tyres), the vehicle would preferably have to be enclosed to eliminate the aerodynamic drag and the driveline disconnected. This is not always feasible, thus the need to measure motion resistance with the use of other methods.

2.4.   Surface Roughness and Friction

Laboratory tests are often performed on test surfaces that include metal (e.g. steel or aluminium drums and continuous stainless-steel belt flat tracks (MTS, 2021) as well as abrasive surfaces (often P80 or P120, fka 2021, also known as safety walk surfaces). Multiple studies have been conducted in measuring the friction coefficient of tyres and measuring the surface roughness of a specific terrain. Persson (2001), conducted tests on rubber blocks with the same compound as tyres and has indicated that different testing velocities result in different friction coefficients. Higher velocities result in a lower friction coefficient and flash temperature has a significant effect on the friction coefficient. These variables can be controlled to a degree between laboratory tests and field tests. Methods such as the grease sample, sand patch, outflow meters, British Pendulum and circular track meters are methods used to gauge the texture and friction coefficient of a terrain. Salehi et al., (2019), performed a comprehensive study to determine the rubber friction on multiple grain sizes corundum surfaces on a Laboratory Abrasion Tester and found that a corundum disc with disc designation 180 correlated to friction coefficient measurement on a test track in Europe. The surface roughness of the European test track was unfortunately not stated.

The basic friction mechanism of dry relative motion between the tyre and the road is generated by a combination of adhesion and hysteresis effects, as described by Gillespie (1992) and Salehi et al., (2019). The total longitudinal friction force can be written as per eq. (2):

$$F_x = F_{adhesion} + F_{hysteresis} \qquad \text{eq. (2)}$$

The adhesion occurs in the real contact area, particularly the fine-scale texture below 0.5mm on self-affine fractal microtexture surfaces (Persson, 2001). It is generally noted that the softer the rubber compound and higher the vertical force, F_z, on the tyre, the larger the effect of adhesion as a larger effective contact area is achieved due to the rubber deforming around the terrain. The smoother the terrain the larger the adhesion component is in the total friction force. The hysteretic component results from the internal friction of the rubber. During sliding, the asperities of the rough terrain exert oscillating forces on the rubber surface, leading to cyclic deformations of the rubber, and to energy dissipation via the internal damping of the rubber. Because of its low elastic modulus, rubber often exhibits elastic instabilities during sliding. This involves the compressed rubber surface in front of the contact area undergoing a buckling which produces detachment waves which propagate from the front-end to the back-end of the contact area. These are the so called Schallamach waves, (Persson 2001), and is the cause of the stick-slip phenomena predominantly seen on smoother surfaces.

Pavement textures can be described in multiple forms and range from microtexture, macrotexture to megatexture as described by the International Organization for Standardization, ISO 13473-1:1997 and the Permanent International Association of Road Congresses, PIARC, 1995 as shown in Figure 6.

The megatexture of a terrain generally effects the ride comfort dynamics of a vehicle and covers wavelengths from 50mm to 500mm. The surface texture characteristics of a pavement has a direct relation to the friction properties. These surface texture characteristics are known as macrotexture and microtexture. The macrotexture is

associated with the roughness of the road surface that affects the water drainage from the tyre footprint, where the surface deviations have wavelengths from 0.5mm to 50mm. The microtexture varies from harsh to polished and affects the friction coefficient at low speeds where the adhesion effects are dominant. These surface deviations have wavelengths less than 0.5mm and are measured at a micron scale (Ergun et al., 2005).
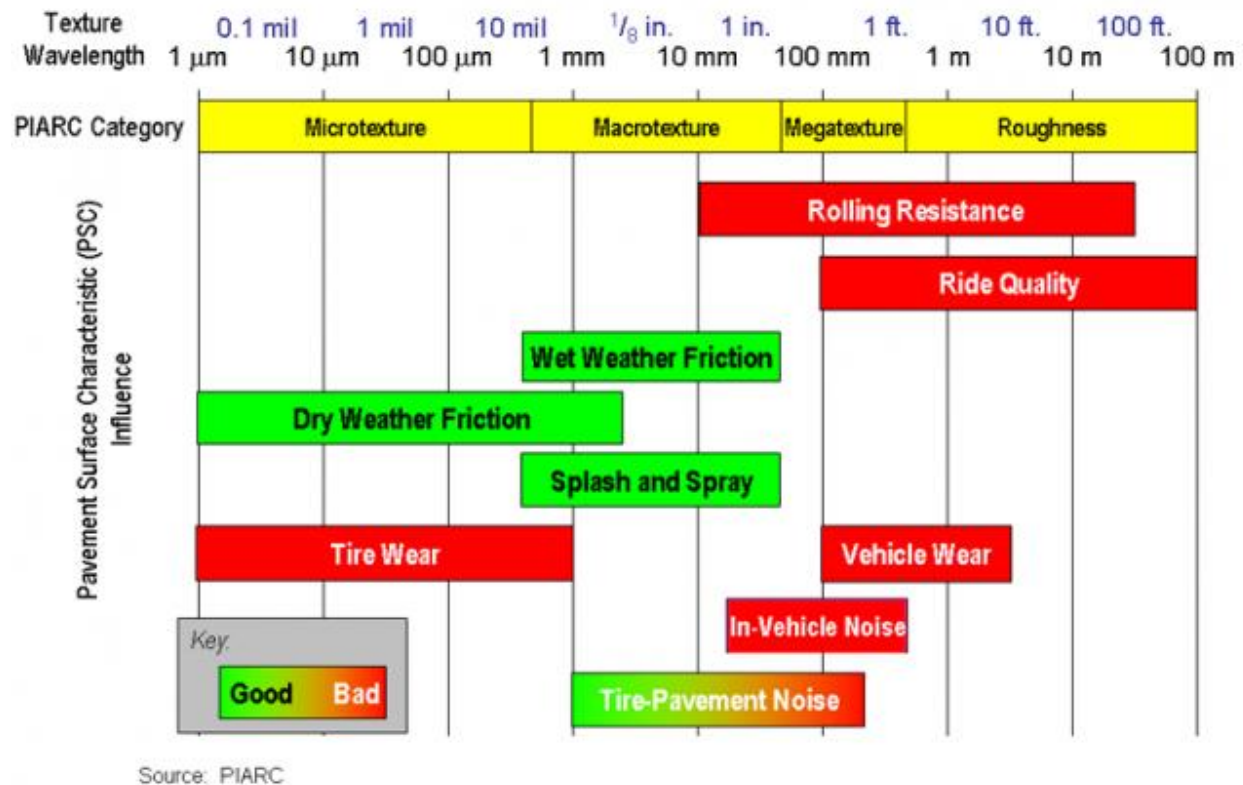
Figure 6: Pavement texture wavelength range, (The Transtec Group, 2021).

The roughness of a surface with a profile sample length (l) can be specified using several parameters ranging from the average roughness (R_a), the maximum peak height (R_p), the mean square value (R_q), the maximum profile valley depth (R_v), the maximum height (R_z), etc. as described in the International Organization for Standardization ISO 4287:1997 and shown in Figure 7. Additional roughness parameters can be the Root Mean Square

elevation (RMS) in the spatial domain or a Displacement Spectral Density (DSD) in the spatial frequency domain (Gorsich et al., 2003).
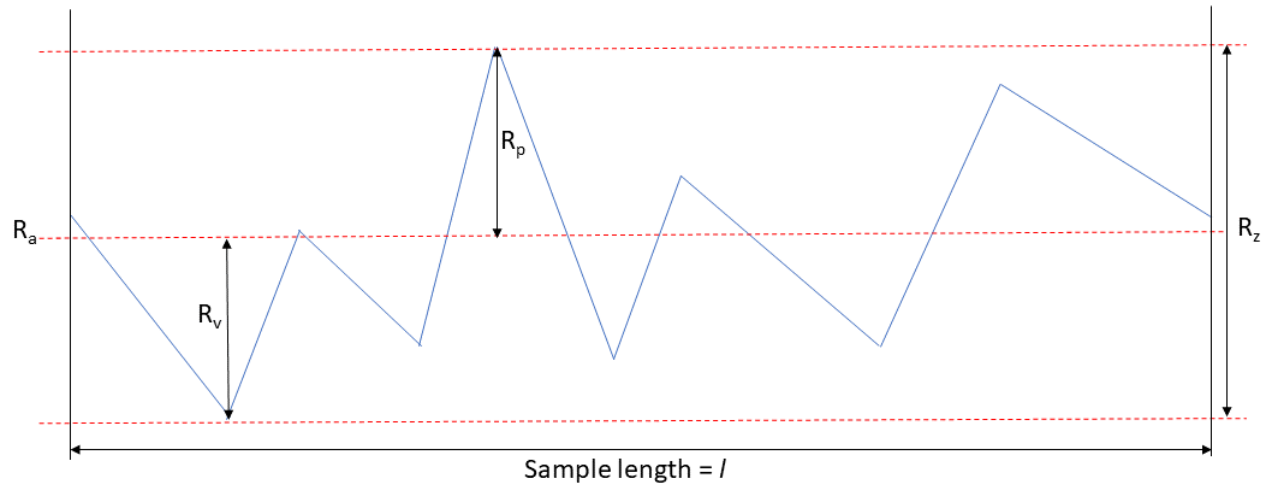
Figure 7: Surface roughness parameters.

The megatexture roughness of a terrain is characterized according to ISO 8608:1995. The RMS of the vertical displacement of the profile and the square root of the area under the displacement spectral density should result in the same value. The Power Spectral Density (PSD) of a signal generally describes how the power of a signal or a time series is distributed in the frequency domain. The same can be done for the displacement; consequently, the DSD of a signal describes how the displacement of a signal or a spatial series is distributed in the spatial frequency domain. The DSD can also be used to compare the roughness of multiple macro- and microtexture profiles of different terrains.

The ISO 8608:1995 specifies a uniform method of reporting measured vertical road profile data for either one-track or multiple-track measurements. It applies to the reporting of measured vertical profile data measured on roads, streets and highways and on off-road terrain. The standard provides general guidance for the use of road profile statistical data

for simulation studies and for related studies such as evaluation of comfort, suspensions and road profiles. The ISO standard defines different road classifications. These classifications are supplied in the form of class limits for the DSD for different classes of roads. The classes range from a class-A road which is a smooth road to a class-H road which is a very rough road. The DSD of a random road, plotted on a log-log scale, forms a straight line and may be described by the power function as shown in eq. (3).

$$S_z = A_r \varphi^{-n_{RI}} \qquad\qquad \text{eq. (3)}$$

Where S_z is the vertical DSD, n_{RI} is the road index, A_r is the roughness coefficient at a spatial frequency of 1cycle/m and φ is the spatial frequency measured in cycles/m. The road index parameter is calculated with a spatial frequency window from 0.05 to 10 cycles/m as this is the window in which ride comfort is most affected by. The ISO 8608:1995 specifies that for off-road profiles the reported spatial frequency range for φ should be from 0.05 cycles/m (wavelength = 20 m) to 10 cycles/m (wavelength = 0.1 m) as the tyre creates an enveloping effect that filters the road vibration input. Profiles including wavelengths below 0.1m may be used to investigate suspension vibration with noise investigations requiring wavelengths as low as 1mm or 1000 cycles/m. This straight line describing the megatexture, on a log-log scale, extends to the macrotexture, however the gradient for the microtexture increases and can be referred to as the surface index. The surface index will be described more in section 4.2.

Another method for calculating the DSD was described by Zaayman (1988). In this method the DSD $S_{xx}(\delta)$ of the road was calculated by dividing the squared Fast Fourier

Transform (FFT) X_δ of the road profile $x(d)$ by twice the step-in frequency ΔF as shown in eq. (4):

$$S_{xx}(F) = \frac{\left|X_\delta(F)\right|^2}{2\Delta F}$$ eq. (4)

The squared FFT is equivalent to the FFT of the road profile X_δ multiplied with the complex conjugate of X_δ.

$$\left|X_\delta(F)\right|^2 = X_\delta X_\delta^*$$ eq. (5)

This method is used by Becker and Els, (2014), for calculating the DSD of the measured profiles of the test tracks at Gerotek Test Facilities. The tracks were profiled with the use of the Can-Can machine, which is described in section 3.6.1.

Scholtz and Els (2020) showed that the Heinrich/ Klüppel friction model, (Heinrich and Klüppel, 2008), can be used to estimate the friction coefficient for both smooth and rough concrete surfaces. This model was compared to measured friction coefficient using the Da Vinci method (American Institute of Physics, 2015), where the friction coefficient is determined mathematically by dividing the longitudinal force by the normal force as shown in eq. (6):

$$\mu = \frac{Longitudinal\ Force}{Normal\ Force} = \frac{F_x}{F_z}$$ eq. (6)

The same Belgian paving concrete tests section as tested by Scholtz and Els (2020) is also used in this study. For simplicity, in this study friction coefficient is calculated from measured longitudinal force and vertical/normal force as described in eq. (6).

2.5.   Postulates

The literature review in this chapter has shed some light on the complex problem commonly known to man as, the tyre. A few observations are made from the literature review and is summarised as follows:

Many studies have been conducted in the past with regard to tyres, however the older findings are not always applicable to the current technology used in tyre carcass construction and rubber compounds, which has a large effect on the tyre characteristics. The lack of accurate tyre characteristic data will have a negative effect on simulation results. This is especially the case for agricultural tyres, as the tyre carcass construction is not the same as for passenger car tyres and the amount of rubber in the tread is a lot more. This means that designers cannot use old tyre data with 100% confidence in the simulation results, when input data from old tyres are used. Tyre footprints are incorporated into only a few tyre models and only FTire has the functionality to adjust the tyre wear when modelling the tyre for simulation purposes. Agricultural farms are growing in size and farmers travel on public road over longer distances on non-deformable terrain from one field to the next. This accelerates the wear on agricultural tyres and more often agricultural vehicles are being operated on tyres with very little tread left. This changes the handling characteristics of the agricultural vehicle and may even transform the vehicle from a vehicle, that is prone to slide to a vehicle that will roll-over before it slides during an evasive manoeuvre. Very limited literature is available where the same tyre with different tread wear conditions were characterised. If tyre models are parameterised with

data from new tyres and one is able to change the wear condition in the simulation model, how representative are the simulation results when the tread is worn away. It has been noted that the surface roughness on different laboratory test rigs are not the same, the effect this has on the measured tyre stiffness characteristics and sliding friction coefficients could not be found in literature. Tests have been conducted where the friction coefficient of a rubber sample was determined on different surface roughness, but does this represent the response of a tyre carcass. It is noted that the tread pattern can affect the response of a tyre as it rolls over a cleat. FTire parameterisation data sets require stiffness measurements for different cleat orientations, thus the change in stiffness characteristics for different cleat orientations are important. This is an important aspect that needs to be investigated on agriculture tyres, with large gaps between the lugs, as the cleat position and orientation can cause the cleat to be in contact with only one or multiple tread blocks, which will have an effect on the stiffness characteristics of the tyre. The majority of tyre models use stiffness parameters from a rolling tyre to parameterise the tyre model, some physics-based tyre models use static tyre stiffness data sets for parameterisation and rolling for validation purposes. This raises the question of how the stiffness of a tyre change from a static tyre to a rolling tyre and is it possible to compare the two conditions directly if the tyre is rolling at a low speed as the operating speeds of agricultural vehicles are low. It has been seen that the measured damping characteristics is also influenced by the position of the cleat relative to the tread pattern as the tyre rolls over the cleat. As these tests are usually conducted with new tyres, does this continue to be the case when the tread wears down. Multiple methods are available to measure or calculate the motion resistance, however it could not be determined how these methods compare when the same tyre is used. Studies have been conducted to measure the

motion resistance at different inflation pressures however this was again always done with new tyres, thus the question of how much change can be expected in the motion resistance values during the life of the tyre as the tyre wears down.

The following postulates are formulated from the literature review and are investigated in this study on an agricultural tyre used on non-deformable on-roads:

I.   The tyre footprint of an agricultural tyre is affected by a change in tread depth

II.   A change in surface roughness affects the sliding friction coefficient on an agricultural tyre

III.   A change in surface roughness does not affect the longitudinal tyre stiffness characteristics of an agricultural tyre, only the peak friction value

IV.   The tyre stiffness characteristics of an agricultural tyre change due to the change in tread depth

V.   The sliding friction coefficient value changes for different tread depths on an agricultural tyre

VI.   The vertical tyre stiffness characteristics of an agricultural tyre are affected by the cleat orientation

VII.   Asymmetric longitudinal and lateral stiffness characteristics are caused by the lugs on an agricultural tyre

VIII.   Static/non-rolling tyre characteristics can be used to predict dynamic/rolling tyre characteristics on an agricultural tyre

IX.   Tyre damping correlates to inflation pressure and not to tread condition on an agricultural tyre

X.   Motion resistance measurement on an agricultural tyre is dependent on the method used

XI.   Inflation pressure has a larger effect on motion resistance compared to tread wear condition on an agricultural tyre.

These aspects will be investigated in-depth by performing a large range of tests on an agricultural tyre with large lugs. The rest of the document will describe the test equipment used, followed by discussions on the results, conclusions and recommendations as well as some proposed future work.

3. Test Equipment

In order to prove/disprove the postulates set in Chapter 2, extensive testing is required to obtain tyre characteristics. To obtain these tyre characteristics suitable test equipment is required. Over the last decade the Vehicle Dynamics Group (VDG) in the Department of Mechanical and Aeronautical Engineering at the University of Pretoria in South Africa, has developed test equipment specifically aimed at testing large tyres over different on- and off-road terrains. This equipment is essential for obtaining tyre characteristics that can be used to develop and validate tyre and multibody vehicle simulation models. The development of the test equipment, described in this section, forms an integral part of this study.

3.1.   Wheel Force Transducers (WFT)

VDG has designed and manufactured a family of WFTs. These WFTs range in size to fit rim diameters from 10 inches up to 29 inches, with dynamic load ratings from 0.8kN to 300kN, as shown in Table 3. The WFTs are designed for a dynamic load rating of up to four times static load, which makes them robust and ideal for off-road use. The rim diameter specified in Table 3 is the minimum rim diameter on which the WFT can fit. The WFT can also be used on larger rims with the use of custom-made adaptors.

Table 3: Wheel Force Transducers developed by VDG.

Rim Size Load rating Maximum operating speed	Vehicle Dynamics Group Wheel Force Transducers
10-inch rim 0.8kN maximum dynamic load 50km/h maximum speed	
16-inch rim 30kN maximum load 100km/h maximum speed	
20-inch rim 180kN maximum load 50km/h maximum speed	
29-inch rim 300kN maximum load 50km/h maximum speed	

The 16 inch to 29 inch WFTs are designed to be used in conjunction with all of VDG's test equipment described in this section. The current study used the 16 inch WFT of which the development is described by Els (2012). The WFT consists of two aluminium rings with one mounted to the rim and the second mounted to the wheel hub. The two aluminium rings are connected to each other via six individual loadcells of which three are mounted in an axial direction and three are mounted in the tangential direction as shown in Figure 8.
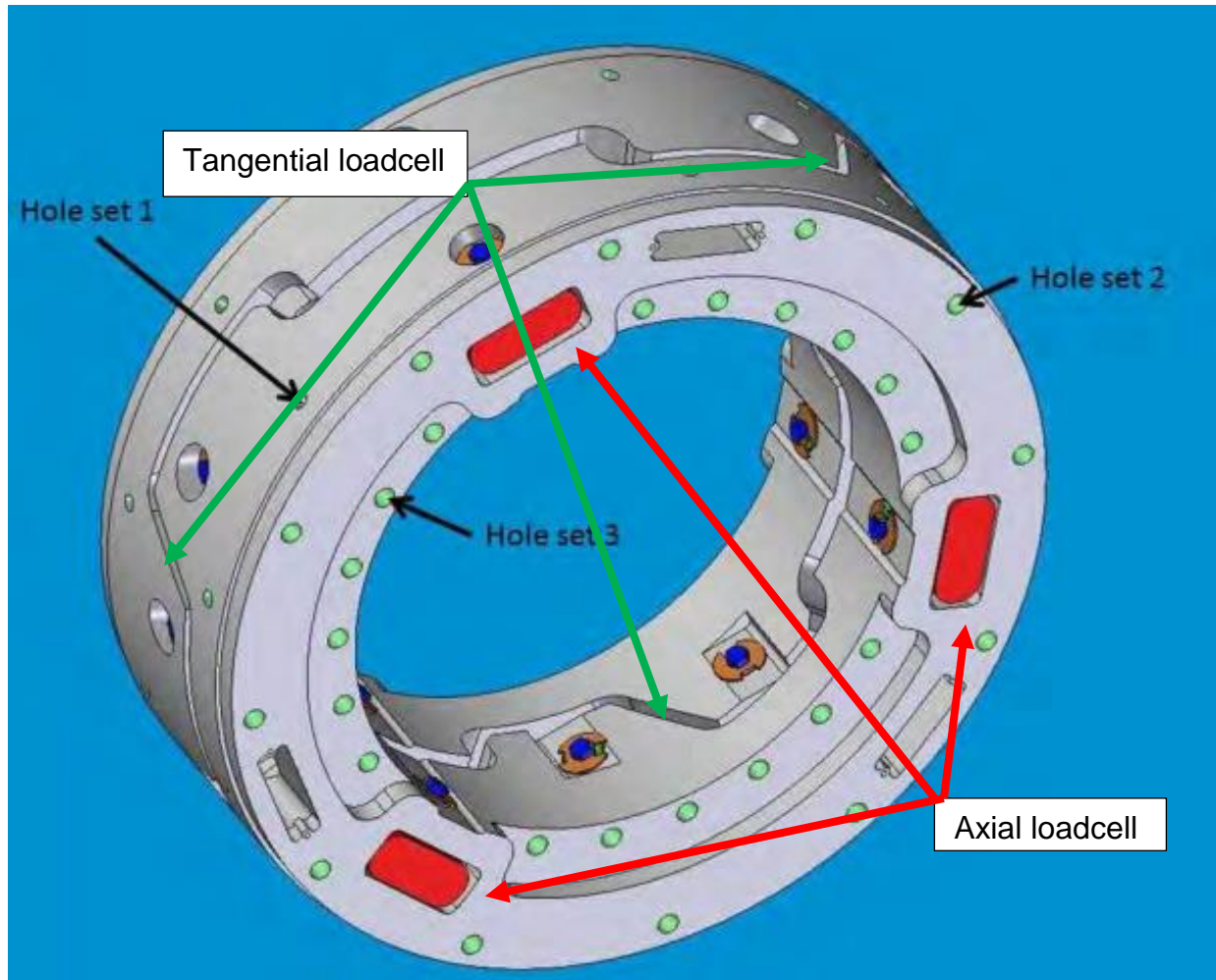
Figure 8: 16 inch VDG Wheel Force Transducer (Els, 2012).

The six individual loadcells are 350 Ohm full bridge strain gauges arranged in a tension and compression configuration with a sensitivity of 1.6mV/V. Each loadcell can be calibrated individually up to a load of 50kN. The WFT operates in conjunction with a VDG developed signal conditioning and data acquisitioning system (based on a Diamond Systems Helios PC/104 computer) used to record the measurements at 16-bit resolution at 1000Hz. This system is mounted on the wheel and is also equipped with an encoder, which measures the wheel rotation continuously during a test. The data is stored onboard and downloaded via WiFi. The applied forces and moments at the wheel hub are

calculated in postprocessing from the measured individual loadcell forces and wheel rotation angle. These WFTs form an essential part of VDG's vehicle dynamic research. The WFTs are interchangeable with all of VDG's test rigs and can be used on vehicles. This allows test engineers to use the same equipment on all of the test rigs, which eliminates uncertainties in measurements between test rigs.

3.2.   Static Tyre Test Rig (STTR)

The Static Tyre Test Rig (STTR), as described by Becker and Els (2018) was developed by VDG to obtain quasi-static tyre deformation characteristics. The STTR can measure the static force vs. displacement characteristics of a tyre in the lateral and longitudinal direction at pre-set camber angles and predetermined vertical load as shown in Figure 9.
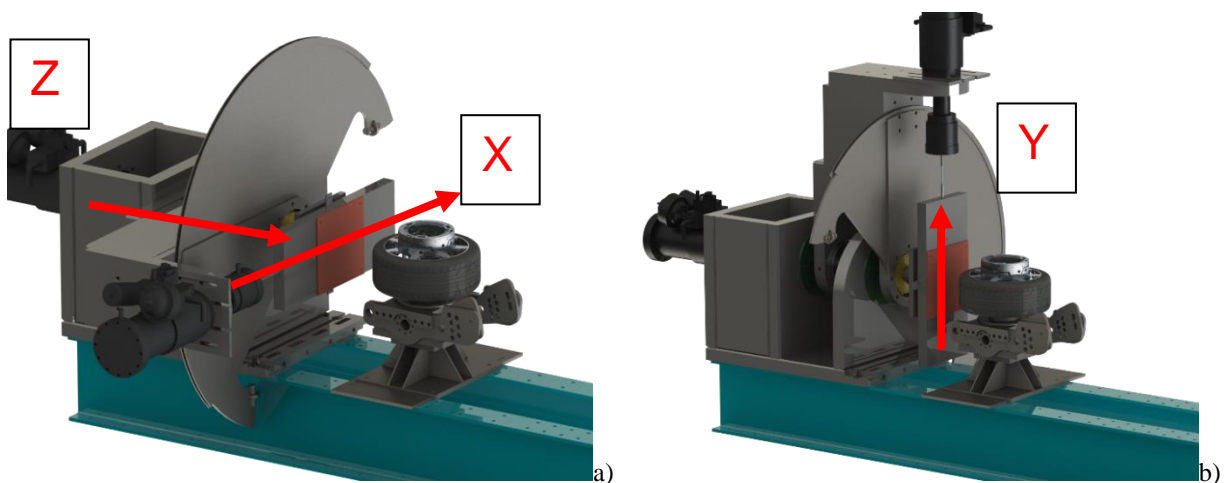
Figure 9: a) STTR Longitudinal and b) Lateral characterization test setup, respectively, Wright et.al. (2019).

The STTR is equipped with 1MN actuators and can accommodate tyres up to 4000mm in diameter and 1100mm wide. The actuators can move at speeds up to 33mm/s. The

STTR is fitted with an in-house developed six component loadcell that uses high-quality low profile ULP-G loadcells (Loadcell Services, 2021) with a combined error in linearity and hysteresis of 0.03%. These loadcells can be calibrated individually or a reference calibration can be done in-situ on the road plate. The VDG developed WFTs can be used in conjunction with the STTR and data sets are synchronised and sampled at 1000Hz. The road plate, that is in contact with the tyre, can be exchanged with plates of different materials, surface roughness, or obstacles, such as cleats, as well as road surface samples such as a Belgian paving block as indicated by the red dash squares in Figure 10.

The following tests can be conducted with the use of the STTR:

- Vertical force vs. vertical displacement characteristics
- Lateral force vs. lateral displacement at a predetermined vertical load
- Longitudinal force vs. longitudinal displacement at a predetermined vertical load
- Footprints (paint on paper) and contact pressure (with a Tekscan system) at a predetermined vertical load
- Self-aligning moment at a predetermined vertical load
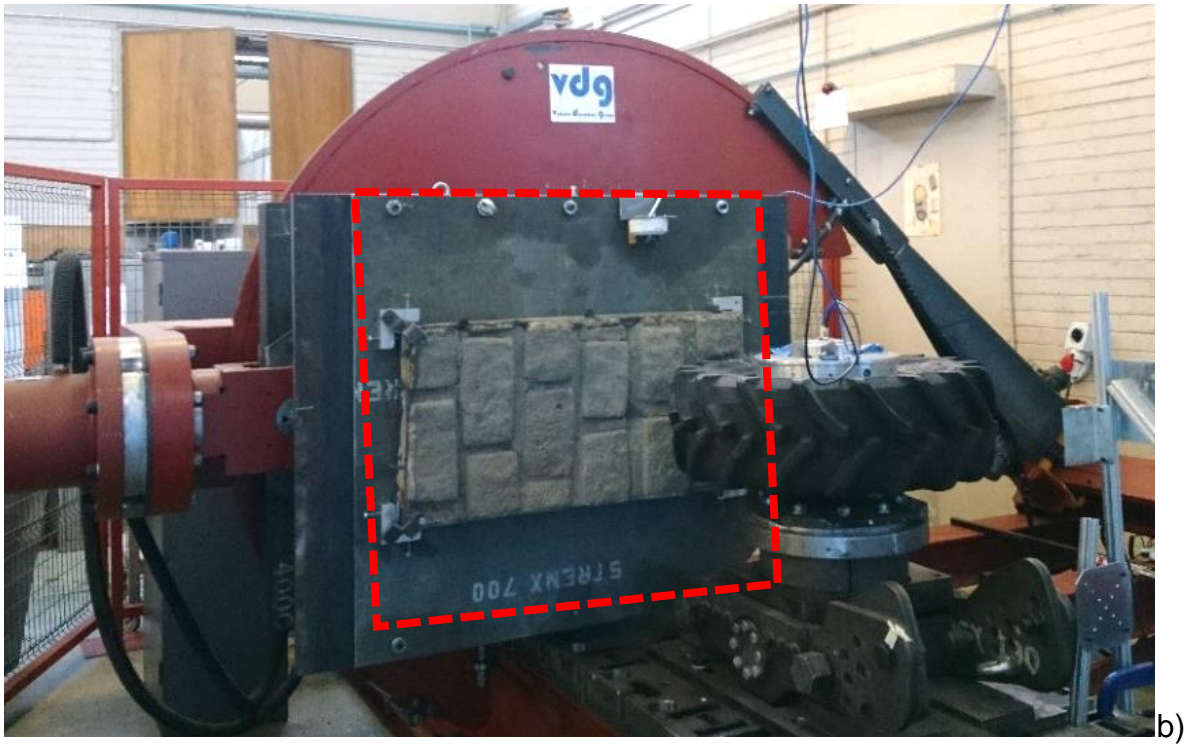
Figure 10: Static Tyre Test Rig from the Vehicle Dynamics Group at the University of Pretoria fitted with a) P80 grit sandpaper and b) Belgian paving block on the road plate.

The tyre is mounted on a mechanism that allows the camber angle to be changed from zero to five degrees in one-degree increments. Actuator movements are programmed with G-code and can be customised for specific tests. The STTR's control system and data acquisitioning is done with a Diamond Systems Helios PC/104 computer and is synchronized with the data acquisitioning system on the WFT if used. The general testing procedure is as follows:

- The test wheel is mounted on a non-rotating hub/pedestal at the required camber angle and inflation pressure.

- Vertical load is applied to the wheel with a pre-specified surface texture fixed to the road plate.

- Depending on test setup, the road plate is displaced in a longitudinal or lateral direction for up to 450mm.

- The vertical load is removed to relax/reset the tyre and vertical load is re-applied.

- The road plate is then displaced in the opposite longitudinal or lateral direction.

- Vertical load is removed.

This sequence is performed for multiple vertical loads, different tyre inflation pressures, different surfaces on the road plate and different camber angles (as required).

3.3.   Dynamic Tyre Test Trailer (DTTT)

VDG developed a Dynamic Tyre Test Trailer (DTTT), Figure 11, as presented by Becker and Els (2018). The DTTT is fitted with two axles with the rear axle for stabilisation purposes only. On the testing axle, located in the middle of the DTTT, two of the same tyres are characterised simultaneously in opposed lateral slip directions. A maximum load of 50kN per wheel can be applied and wheel diameters of between 800mm and 2000mm can be fitted. The DTTT's control and data acquisitioning is performed with a Diamond Systems Helios PC/104 computer and is synchronized with the data acquisitioning system on the VDG developed WFTs. Data sets are synchronised and sampled at 1000Hz. The tyre forces and moments are recorded during lateral force vs. slip angle measurements, longitudinal force vs. % longitudinal slip measurements as well as combined lateral and longitudinal force measurements during braking at pre-determined lateral slip angles. The DTTT's measurement axle can continuously vary the slip angle from -1 to 18 degrees at a maximum rate of 1.5 degrees/s. The measurement axle is fitted with a braking system that induces longitudinal slip and can induce a braking torque of up to 20kNm. No driving torque can be applied on the measurement axle as the power requirements to add driving torque are extremely high on large diameter tyres. This is a limitation of the DTTT, however by testing the tyres in the opposite rotation direction to the normal rotation direction, a good estimate can be obtained of the traction characteristics of the tyre (mostly necessary for directional tyres). The STTR is able to obtain longitudinal force vs. positive and negative longitudinal displacement characteristics at different vertical loads for a static tyre. These STTR measurements can

be used in conjunction with the DTTT braking tests (in the normal tyre rotation direction) to estimate the traction characteristics of the tyre. The trailer can be towed over different test surfaces which is dependent/limited by the tow vehicle used.
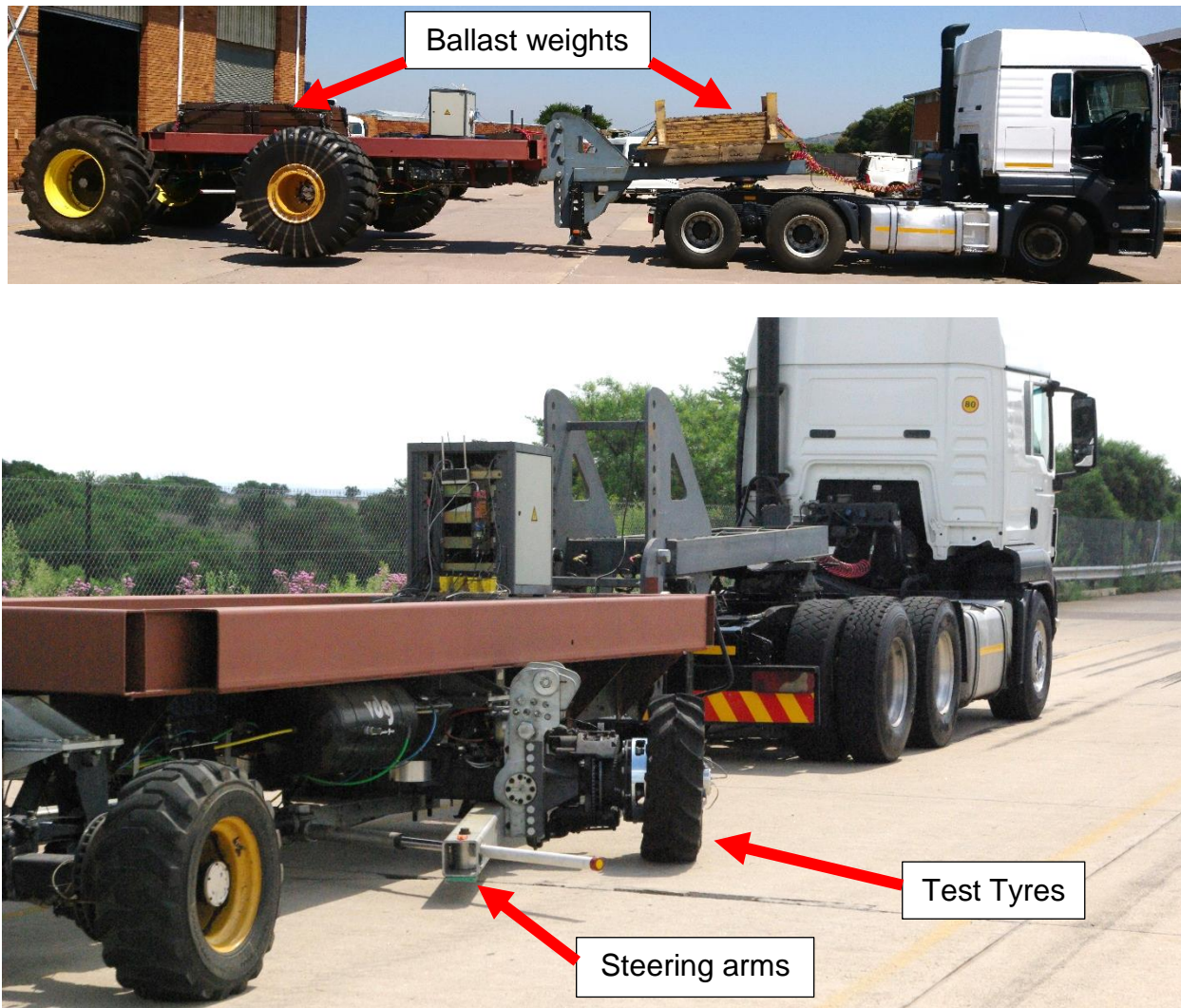
Figure 11: Dynamic Tyre Test Trailer from the Vehicle Dynamics Group at the University of Pretoria.

Dynamic tyre characterisation tests are usually conducted on the High Speed Test Track at the Gerotek Test Facilities, (Gerotek Test Facilities, 2021), to the west of Pretoria, South Africa.

The test procedure involves three different approaches to determine the longitudinal and lateral forces, and the force envelope (or friction circle). The longitudinal force test procedure involves accelerating the DTTT up to the desired constant test speed. The brake pressure on the measurement axle is then gradually increased. The brake application rate is adjusted for each test setup, as it is dependent on the test speed, applied vertical load and brake temperature. When the highest possible longitudinal load is reached the brakes are released and the wheels are allowed to accelerate back up to the free-rolling speed. The procedure is repeated several times during the same test run. The lateral force test procedure involves accelerating the DTTT up to speed and then changing the tyre slip angles on the measurement axle continuously, sweeping from -1° slip to 18° slip at a constant rate. The force envelope tests involve changing the slip angle in discrete increments with the actuators and then increasing the brake pressure until the maximum longitudinal load is reached while the slip angle is held constant. The brake pressure is in turn released and the slip angle is changed to the next increment. The brake pressure is increased again and the process repeats up to the maximum lateral slip angle. Tests can be conducted at camber angles from -5 to 5 degrees in 1-degree increments. Test speeds of up to 80km/h can be achieved, but speeds are usually kept low due to excessive tyre wear and heat build-up during high speed testing. On large off-road and agricultural tyres, the test speeds are limited by the tyre's speed rating.

3.4. Damping Test Trailer (DTT)

The Damping Test Trailer (DTT) is another important part of VDG's collection of tyre test rigs, as shown in Figure 12. This trailer has no suspension fitted and can be loaded with ballast weight to have a vertical load on each tyre up to 50kN. The longitudinal position of the axle can be adjusted to move the longitudinal center of mass of the loaded trailer over the axle. The trailer is fitted with WFTs which are interchangeable with the STTR and DTTT. In general, the trailer is used for tyre damping measurements on level roads, where the trailer is towed over a cleat or trapezoidal bump with the vertical response of the trailer measured with either force, acceleration and/or laser displacement measurements. The trailer has a height-adjustable tow hitch so that a large variety of tyre sizes can be tested with the trailer remaining in a horizontal position.

Figure 12: Damping Test Trailer from the Vehicle Dynamics Group at the University of Pretoria.

The DTT is instrumented with three laser displacement sensors, one mounted close to the tow hitch and two mounted on the axle. The laser displacement sensors are used to measure the vertical translation of three points on the trailer. Using these displacement measurements, the vertical motion of the rigid body at any location can be determined. Two 10g tri-axial accelerometers are mounted on the axle, close to the hubs. A 4g tri-axial accelerometer is mounted close to the tow hitch. A Racelogic VBOX 3i Global Positioning System (GPS) with a single antenna is mounted on the trailer to accurately measure the trailer speed. The GPS samples at 100Hz with a velocity accuracy of 0.1km/h (averaged over 4 samples) and resolution of 0.01km/h (Racelogic, 2018a). The two WFT data acquisitioning systems start sampling at 1000Hz when they are triggered by an external trigger supplied by a third data acquisitioning system mounted on the DTT.

The third data acquisitioning system is used to record the laser displacement sensors, the accelerometers, velocity and the trigger signal for data set synchronization.

3.4.1. Damping Test Setup

The damping characteristics of tyres are determined by towing the DTT at a constant speed over discrete obstacles while measuring the wheel forces and moments with the WFTs. The wheel base of the DTT is much wider than that of the tow vehicle. This enables the tow vehicle to avoid the obstacles so that only the tyres on the DTT come in contact with the obstacles. The damping test setup used in this study is shown in Figure 13. The acceleration measurements and the laser displacement measurements can also be used to determine the dynamic damping of the tyres. Since the axle is rigidly connected to the chassis and assuming the trailer is a rigid body, the only damping in the system is that of the tyres and the friction at the tow hitch. Assuming that the tow hitch friction is negligible allows one to determine the vertical damping of the rolling tyres at a constant speed. The discrete obstacle used can be a square cleat or trapezoidal bump. A 28x28mm square cleat was used as excitation obstacle during these damping tests. The damping tests over the cleat are usually conducted at a low speed due to the tread block excitation and road input which becomes a forced excitation at higher speeds (as the trailer is not fitted with a suspension or dampers, it starts to bounce at higher test speeds). The inflation pressure also contributes to the speed limit at which a test can be conducted as lower tyre inflation pressures adds some damping to the system.

Figure 13: Damping Test Trailer fitted with TM700-280/70R16 tyres.

The system, consisting of the DTT, the ballast weights and the tyres are considered to be a rigid body system with a single degree-of-freedom that pivots about the tow hitch in the pitch direction. The inertia of the DTT, the load and the tyres about the tow hitch is known, and the system may be approximated as shown in Figure 14. The tyre vertical force and displacement is measured. The tyre is usually approximated as a linear spring and damper, but a non-linear spring damper analysis could also be assumed.
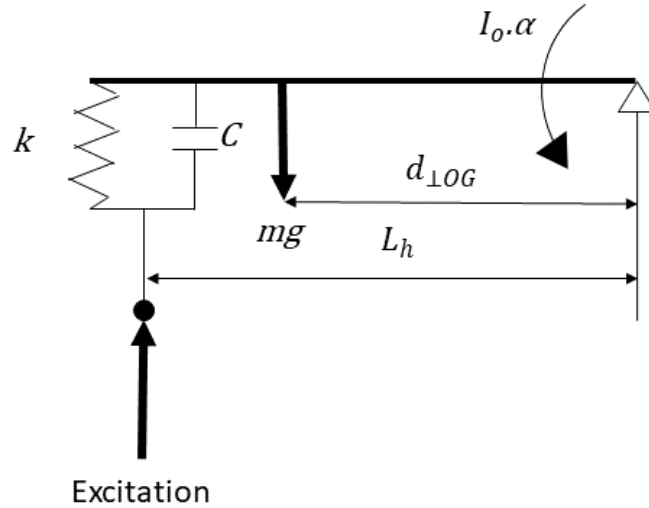
Figure 14: Single degree-of-freedom approximation of DTT.

The dynamic damping of the tyre is determined with the use of the logarithmic decrement of the vertical response when the DTT is towed over the cleat. This method of determining the viscous damping of the tyres relies on the assumption that the vertical excitation of the system is a case of underdamped free vibration and that the tyre is a linear spring-damper system. The vertical acceleration of the DTT is measured with two 10g accelerometers placed on the axle, as close to the hubs as possible. To compensate for the nonlinear characteristics of the tyre in real life, the average logarithmic decrement of the vertical response is determined over four complete cycles. Two peaks are selected that indicate the beginning and end of four complete, consecutive cycles. Since the amplitude of the oscillation is described with eq (7), the logarithmic decrement can be determined with eq. (8) and the damping ratio is determined with eq. (9). Eq. (7) describes the amplitude of underdamped free vibration at time instance t_i. (Meriam & Kraige, 1998; Rao, 2004).

$$x(t_i) = Ce^{-\zeta \omega_n t_i} \qquad\qquad\qquad \text{eq. (7)}$$

$$\delta = \frac{\ln(x_0/x_n)}{n}$$ eq. (8)

$$\zeta = \frac{\delta}{\sqrt{\delta^2 + (2\pi)^2}}$$ eq. (9)

where $n = 4$, the number of consecutive cycles, used throughout this project. The undamped period of the system, τ, is calculated using the damping ratio and the mean damped period of oscillation, τ_d, between the selected peaks. Eq (10) is used to determine the undamped period of the system and eq (11) is used to determine the linear viscous damping coefficient of the tyre averaged over the number of consecutive cycles.

$$\tau = \sqrt{1 - \zeta^2}\left(\frac{\tau_d}{n}\right)$$ eq. (10)

$$C = \frac{\zeta I_o 2\pi}{\tau L_h^2}$$ eq. (11)

where C is the linear viscous damping coefficient, I_o is the inertia of the system about the tow hitch and L_h is the distance from the tow hitch to the center of the tyres. The pitch inertia of the trailer and the tow hitch is 1009kg.m^2. The additional weight and inertia of the ballast weights is added to the inertia of the system using the parallel axis theorem as described in eq. (12). The inertia of the DTT was determined experimentally. The addition of ballast weights, wheels and WFTs to the DTT increases the inertia and results in different inertias for each load case. The ballast weights, wheels and WFTs were assumed to be point masses added at the axle at a known distance of 3.13m from the tow hitch for the test case used in this study.

$$I_O = I_G + md_{\perp OG}^2$$ eq. (12)

where I_O is the inertia about the hitch point, I_G is the inertia about the center of mass, m is the mass and $d_{\perp OG}$ is the perpendicular distance from the center of mass to the hitch point.

3.4.2. Motion Resistance Test Setup

A six component loadcell can be mounted on the tow hitch of the DTT, which allows for motion resistance measurements (Figure 15). The axle position is adjusted so that the vertical load on the six component loadcell is close to zero. The six component loadcell is fitted with sensitive loadcells so that small motion resistance forces in the longitudinal direction can be measured accurately. This requires extreme care during acceleration, braking and manoeuvring as not to overload these loadcells. Due to the flexibility of the DTT measurements can be conducted on a wide range of tyre sizes with static vertical loads up to 50kN per wheel. The DTT is towed at a constant speed on a flat test track with the tyre pressures and longitudinal force in the tow hitch monitored. Ambient conditions in the form of ambient temperature, wind speed and direction are noted.

Figure 15: Motion resistance test setup for large tyres at high loads.

3.4.3. Static Longitudinal Friction Coefficient Test Setup

The DTT trailer can also be equipped with brakes in order to conduct static longitudinal stiffness tests on field surfaces. The locked wheels ensure 100% longitudinal slip during the static longitudinal stiffness field tests. The tests are conducted with the brakes on the trailer applied. The tow vehicle pulls the trailer as slow as possible in a straight line for up to 150mm longitudinal displacement. The longitudinal displacement of the non-rolling tyre is measured with a horizontally mounted displacement laser with a grounded reference perpendicular to the direction of travel. As the tyre deforms during the longitudinal displacement test, the longitudinal and normal force on the tyre is measured with the use of the WFTs. With these forces known, the longitudinal stiffness and sliding friction coefficient can be calculated and compared to the results obtained from the laboratory tests on the STTR on multiple surfaces.

3.5.   VDG Test vehicle

The VDG test vehicle (Figure 16) used during the motion resistance coast down and towed vehicle tests is a 1997 Land Rover Defender 110 vehicle fitted with the tyre of interest for this study as defined in section 3.8. The Land Rover Defender was used as the research team did not have access to a tractor. Using this vehicle enabled the required research to be conducted at reduced logistical and operating costs on a tyre applicable to the research questions. As the test vehicle is part of VDG's test equipment any required modifications needed to be made to the vehicle could be done with ease.

Figure 16: Vehicle setup used for motion risistance testing.

3.6.   Terrain profilers

Tyre characteristics change for different terrains. In order to classify and compare different terrains the terrain profile needs to be measured. Due to the large difference in amplitudes and wavelengths in the terrain roughness spectrums, multiple profilers are used to measure the terrain in order to characterise the following:

- Megatexture –> 50mm to 500mm (20 to 2 cycles/m)

- Macrotexture –> 0.5mm to 50mm (2000 to 20 cycles/m)

- Microtexture –> smaller than 0.5mm (from 2000 cycles/m)

This following section describe these measurements.

3.6.1. Megatexture Measurements

The megatexture covers the wavelengths from 50mm to 500mm in a profile. Terrain profiles covering this spectrum of wave lengths can be profiled with the use of Can-Can machine, (Becker and Els, 2014). The Can-Can machine is a mechanical profilometer, developed by VDG, which is towed behind a vehicle at a slow walking pace and produce profiles of rough terrains quickly and efficiently (Figure 17). The profilometer is equipped with multiple profiling arms on the rear beam of the profiler. The vertical displacements are calculated from the rotation angle as the arms travels over the terrain. The global orientation and location of the profiler can be measured with the use of a VBOX 3i RTK with Inertial Measurement Unit, with dual antenna and base station setup, (Racelogic,

2018b) or with a Novatel Inertial Measurement Unit. The profile of the terrain can be produced in a grid with a 6mm longitudinal spacing and 36mm lateral spacing with a 1mm vertical resolution.

Figure 17: Can-Can machine profiling the rough track at Gerotek.

The Displacement Spectral Densities (DSD) of each of the profiled terrains at Gerotek Test Facilities provided information about the mega texture of the terrains in the form of the Roughness Coefficient as well as the dominant spatial frequencies. The spatial frequency range covered from 0.05 to 10cycles/m.

3.6.2. Macrotexture Measurements

During this study an XY table fitted with an AR700 Acuity road profiling laser (Acuity, 2015), was used to measure the macrotexture of the surfaces, as shown in Figure 18, by scanning 10 longitudinal lines equally spaced in the lateral direction as indicated by the red lines in Figure 18b).
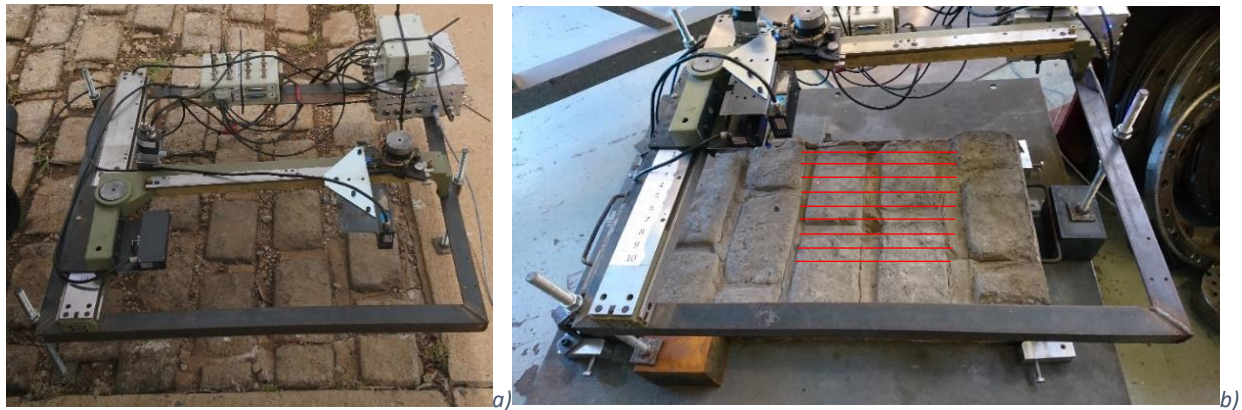
Figure 18: Macroprofiler measuring on a) Outdoor Belgian paving section b) Laboratory casting of Belgian Paving.

The average DSD is calculated and compared. The smallest wavelength is limited by the diameter of the dot size of the laser which is 120µm. The longest wavelength was defined by the travel of the XY table which was 200mm. The XY table used to measure the macrotexture is fully mobile and was used to measure the macrotextures of all the field and laboratory test surfaces used in this study. The spatial frequency range covered by the XY table was from 5 to 8333 cycles/m.

3.6.3. Microtexture Measurements

The microtexture of multiple test surfaces were measured with an engineering stylus in the form of a Mitutoyo SJ-210 portable surface roughness tester (Mitutoyo, 2021), as

shown in Figure 19, that is able to measure the surface roughness according to the International Organization for Standardization ISO 4287:1997.
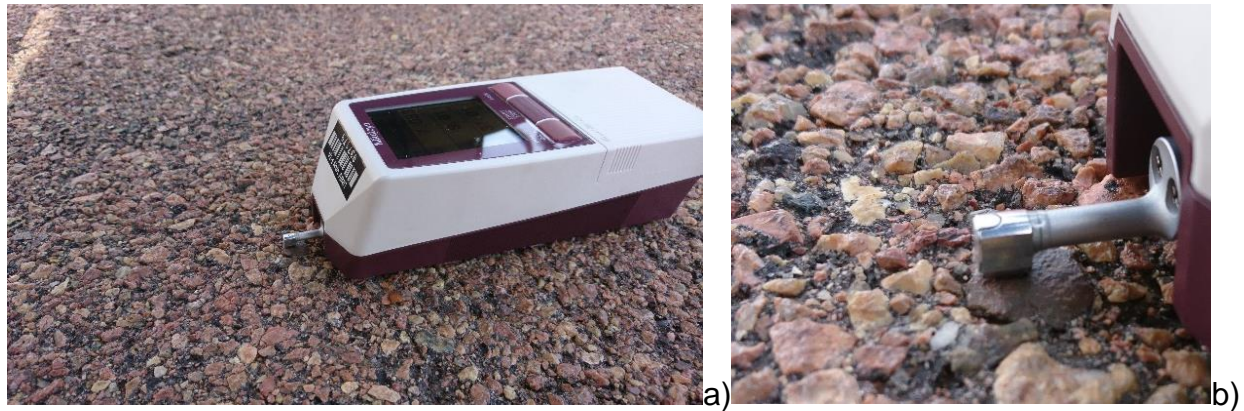
Figure 19: Micro profiler a) On Asphalt surface macrotexture scale b) Close-up for microtexture scale.

The sample length of these microtexture profiles are 4mm with an average pitch/increment of 0.5 µm. This covers the spatial frequency range of 250 to 2 000 000cycles/m. The output from the surface roughness tester is a profile of the test section and values for R_a, the average roughness, R_q, the mean square value and R_z, the maximum height in the measurement, all noted in µm as described in section 2.4 and shown in Figure 7.

3.7.   Test Surfaces

Multiple test surfaces were used during this study for different sections of the study. All of these test sections were profiled using the equipment described in section 3.6. These surfaces are listed in the following sections.

3.7.1. Gerotek Test Tracks

The Gerotek Test Facilities, (Gerotek Test Facilities, 2021), to the west of Pretoria, South Africa, have multiple test tracks cast in concrete. The Gerotek Test Facilities was established in the 1970s to satisfy an urgent need for an all-encompassing test facility at which vehicle design and development could be monitored in a typical South African environment. This world-class test facility offers unique heat and altitude test conditions. Figure 20 shows an aerial photograph of Gerotek (Google Earth, 2018) with selected sections (indicated with red lined) surveyed to obtain track gradients used during motion resistance tests.

Figure 20: Gerotek Test Facility (Google Earth, 2018).

The Suspension tracks at Gerotek (section K-L) is used to perform repeatable and comparative suspension tests under simulated conditions. These tracks are used to test the body structure, body mountings, suspension, axles, steering, chassis, driveline durability and ride comfort. The Belgian paving (located on the Suspension track section at Gerotek) is mainly used for testing ride comfort and durability of a vehicle. A 1m x 0.5m mould was made from a section of the Belgian paving as shown in Figure 18. This enabled the VDG team to cast this Belgian paving section in concrete and use it on the STTR for static tests. Long flat sections of concrete are also located between the suspension tracks, these flat sections were used during the motion resistance part of this study. The High Speed Track at Gerotek, (sections A-B and C-D) were also used during parts of this study. The survey results of the selected sections shown in Figure 20 are tabulated in Table 4.

Table 4: Gerotek Track Survey Data.

Section	Track description	Path Length:	Azimuth:	Slope
A-B	Northern section of High Speed Track	425.38 m	82° 54' 11.9" (B to A)	-0.03°
C-D	Southern section of High Speed Track	228.05	89° 43' 29.4" (C to D+	0.07°
E-F	Concrete section to Tank/ Rally Track	842.75 m	303° 37' 19.9" (F to E)	0.89°
G-H	Asphalt section towards Dynamic Handling Track	1.006 km	82° 29' 8.7" (G to H)	2.58°
I-J	Entrance to Dynamic Handling Track	180.6 m	181° 51' 38.8" (J to I)	0.26°
K-L	Concrete sections between Suspension Track	688.68 m	81° 15' 17.1" (K to L)	0.03°
M-N	Long Straight Track	896.32 m	81° 42' 11.9" (M to N)	0.00°

3.7.2. Static Test Surfaces

The test surfaces used on the STTR can be easily changed as described in section 3.2. The literature review indicated that different tyre test rigs had different surface textures. The surfaces used during the static tests included the following:

- Mild steel sheet

- Aluminium 6 series sheet

- Strenx 700 steel sheet

- Concrete

- Belgian paving casting

- Klingspor CY308 Y P80 grit sandpaper

- Klingspor CS 311 Y P180 grit sandpaper

- Klingspor CS 311 Y P220 grit sandpaper

- VSM RK700X P180 grit sandpaper

These surfaces used on the STTR were profiled with the macro- and micro-profiler and DSD compared during the surface roughness section of the study.

3.8.   Tyre of Interest

The literature review shows that limited tyre characteristics, used for tyre modelling, are available on agricultural tyres. The tyre of interest in this study is a Trelleborg TM700-280/70R16 agricultural tyre with large lugs, a load index of 112 (1120kg or 10 987.2N) and speed rating of A8 (40km/h). This tyre was selected as it is possible to mount these tyres on the test vehicle (Figure 16) used for the motion resistance part of this study and due to the load limitations on the test drum used for motion resistance tests as described in section 4.7.1. Tests were conducted on non-deformable on-road terrain. It is important to note that although the selected tyre is relatively small compared to the average agricultural tyre, the effects investigated in this study are expected to be present on small and large agricultural tyres.

In this study the tyre characteristic tests were conducted at two inflation pressures, three tread wear cases and a single vertical load case of 5.68kN. The load case corresponds to the wheel load on the test vehicle used during the motion resistance tests on non-deformable terrain. The different tread conditions were as follows:

- 100% Tread – New tyre, run-in, static tests conducted post motion resistance tests, (Becker and Els, 2020), where no traction or braking was applied to the tyre. Tread depth at 30mm.

- 50% Tread – 15mm of tread shaved with tyre regrooving tool with surface buffed post shaving.

- 0% Tread – Additional 15mm of tread shaved and tyre buffed post shaving.

The inflation pressures of 80kPa and 200kPa were based on the specified Trelleborg load limitation of 640kg per wheel at 80kPa and 1000kg per wheel at 200kPa. The wheel load of the test vehicle was at 80% of the specified load at 80kPa as prescribed by the tyre manufacturer (Trelleborg TM700 brochure, 2018). The highest rated operating inflation pressure of 300kPa was not selected as the test vehicle's vertical wheel loading would be too low. The large lugs would induce too much forced vibrations at these high inflation pressures.

A single load case was selected to be able to investigate the effect the wear on a tyre will have during the life of the tyre when mounted on a vehicle. Figure 21 shows the condition of the tyres used during this study.

The mass of the tyre for the different tread wear conditions is noted in Table 5. The change in tyre mass due to the tread wear is significant and the tyre loses 7.5kg or 31% of its mass.

Table 5: Mass of test tyre and rim for different tread wear conditions.

Tread wear condition	Tyre mass [kg]	% Change in tyre mass
100% Tread	24	-
50% Tread	22	8%
0% Tread	16.5	31%

The Shore A hardness of the rubber at different locations on the tyre was measured at the different tread wear conditions. Measurements were conducted with the use of a Bondetec BS-392A Portable Shore A Hardness Tester (Bondetec, 2021). These values are tabulated in Table 6 and correspond to the positions indicated in Figure 21.
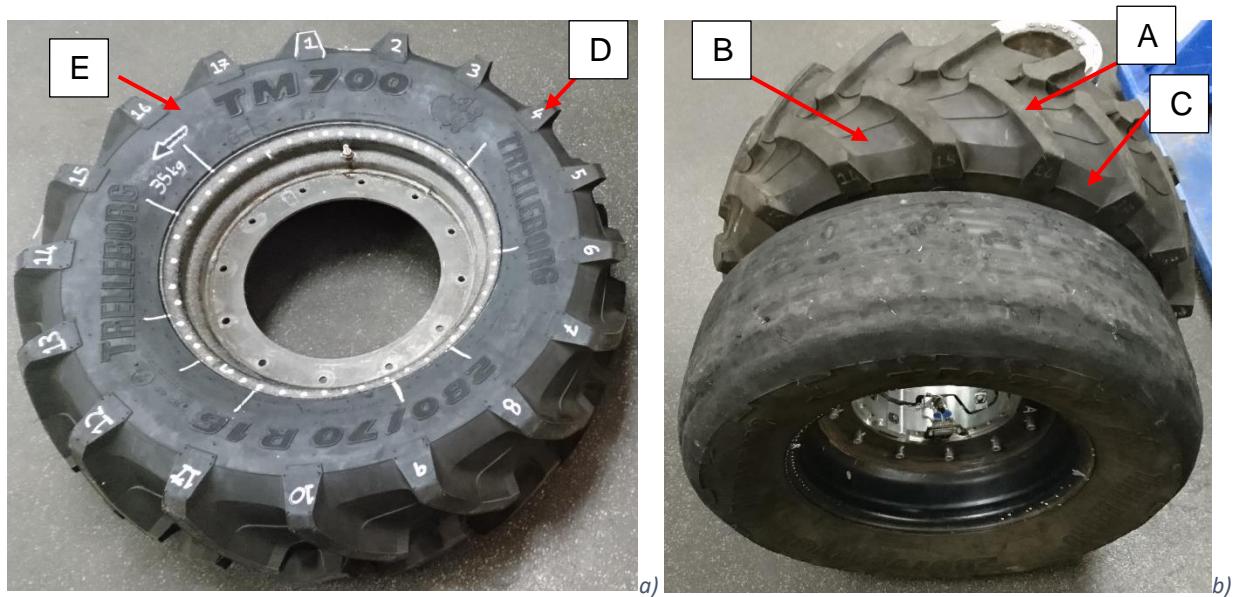
Figure 21: a) Trelleborg TM700-280/70R16 tyre with 100% tread, b) Trelleborg TM700-280/70R16 tyre with 50% and 0% tread respectively, with indicated positions where the Shore Hardness A measurements were taken.

The results form table 6 indicate that the increase in Shore A Hardness values at 0% tread, may be caused due to the reduced rubber layer above to canvas of the tyre carcass. This can result in a higher value measured due to the increased hardness of the canvas below the thin layer of rubber.

Table 6: Shore A Hardness Measurements.

Tread wear condition/ Location	100% Tread	50% Tread	0% Tread
Top of Tread block (A)	61.8	61.4	70.4
Carcass ring between tread blocks (B)	67.9	69.5	65
Partly sidewall between tread blocks (C)	67.9	68.6	67
Side of tread block on sidewall (D)	62.4	62.7	66.2
Sidewall (E)	62.4	62.7	65.4

4. Results and Discussions

In the following sections, results are presented from tests conducted on the tyre of interest.

4.1. Contact Area

Postulate:

I.   The tyre footprint of an agricultural tyre is affected by a change in tread depth

The size of the tyre contact patch was captured by painting the tyre and applying the 5.68kN vertical load, for this purpose, a sheet of white paper was used between the tyre and a smooth steel test surface on the STTR for each inflation pressure and tread wear condition. The footprints for each tread wear condition at 80kPa and 200kPa are shown in Figure 22, with the red line a reference indicator of 10mm x 100mm. The thin dashed line shows the change in contact patch perimeter between tread conditions. The contact area was determined by taking the sum of the black paint print within the perimeter of the footprint.
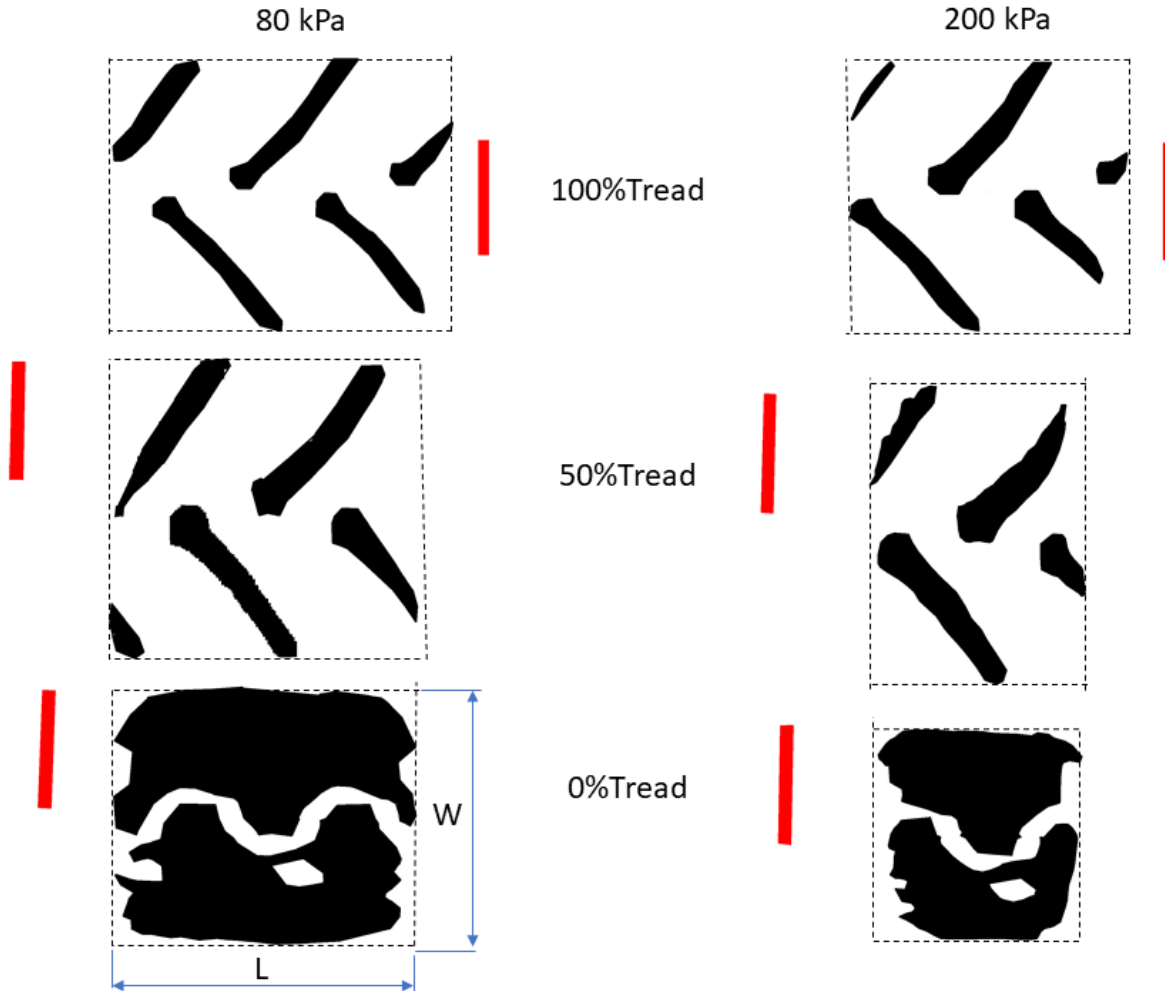
Figure 22: Footprints at different tread conditions and two inflation pressures, with the 10x100mm red line as reference indicator.

The pressure distribution of the three tread conditions on a hard flat surface at 200kPa was measured with the use of a TireScan system from Tekscan (2021), connected to an 8001-pressure sensor, mounted on the STTR. The three pressure maps for an inflation pressure of 200kPa are shown in Figure 23, with the colour scale ranging from blue representing low pressure, green - medium pressure and red - high pressure.
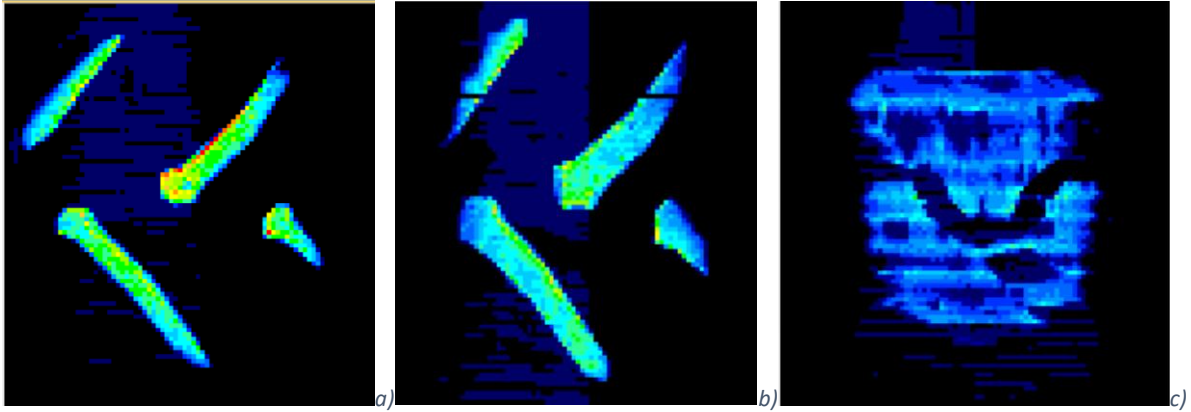
Figure 23: TM700-280/70R16 Pressure distribution at 200kPa for a)100% Tread, b) 50% Tread and c) 0% Tread, respectively.

From the footprints and pressure maps it is noticed that the 100% tread condition has a longer footprint compared to the 50% tread condition which has an overall wider footprint and wider tread blocks. The wider tread blocks are due to the taper shape of the tread block. The 0% tread condition has the smallest perimeter measurements; however, this condition has the highest rubber contact areas of the three conditions, thus it has the lowest contact pressure. The tread contact pressure was estimated with the use of eq. (13):

$$\text{Pressure} = \frac{\text{Force}}{\text{Area}} \qquad \text{eq. (13)}$$

The different contact pressures in the footprint due to the change in footprint size/tread wear condition is presented in Table 7, along with the area of actual rubber in contact area and the perimeter of the contact patch.

Table 7: Estimated average tread contact pressure as a function of tread wear and inflation pressure, with rubber in contact area and perimeter dimensions.

Tread wear condition	Constant vertical load of 5.68kN					
	200kPa	80kPa	200kPa	80kPa	200kPa	80kPa
	Average Tread Contact Pressure [kPa]		Rubber in Tread Contact Area [mm^2]		Perimeter of Contact Patch, L x W [mm]	
100% tread	669	476	8490	11909	240x235	300x240
50% Tread	657	492	8642	11534	180x250	265x250
0% Tread	270	157	21021	35993	165x180	265x220

It can be seen in that the contact pressure slightly increases at the lower inflation pressure of 80kPa as the tread wears from 100% to 50%. A 60 to 66% contact pressure drop is noted at 0% tread condition due the increase in actual rubber in contact with the test surface. The contact area, for 0% tread condition and an inflation pressure of 80kPa, increases by 202% compared to the 100% tread condition at 80kPa. The contact area for 0% tread condition for an inflation pressure of 200kPa increase by 147% compared to the 100% tread condition at 200kPa.

Postulate conclusion:

I.   *As expected, the contact area changes significantly with wear. This is an important variable for all tyre models as the contact area/ length and width should be accounted for especially in for example volume contact models, FTire models, etc. It is even important in a point-follower model, because with point-follower models the road input is often filtered with half the contact patch length, thus it will have a direct effect on the simulation results obtained.*

4.2.   Surface Roughness

Postulate:

II.   *A change in surface roughness affects the sliding friction coefficient on an agricultural tyre.*

To investigate this postulate, it is important that the surface roughness measurements are conducted systematically on all test surfaces. To ensure that macro- and microtexture of the same surface are profiled over which the friction coefficient measurements were conducted, a template was made with 21 measuring points that replicated the contact patch of the new tyre as shown in Figure 24. This template was placed in the same location as the contact patch on all STTR test surface as shown by Figure 25.
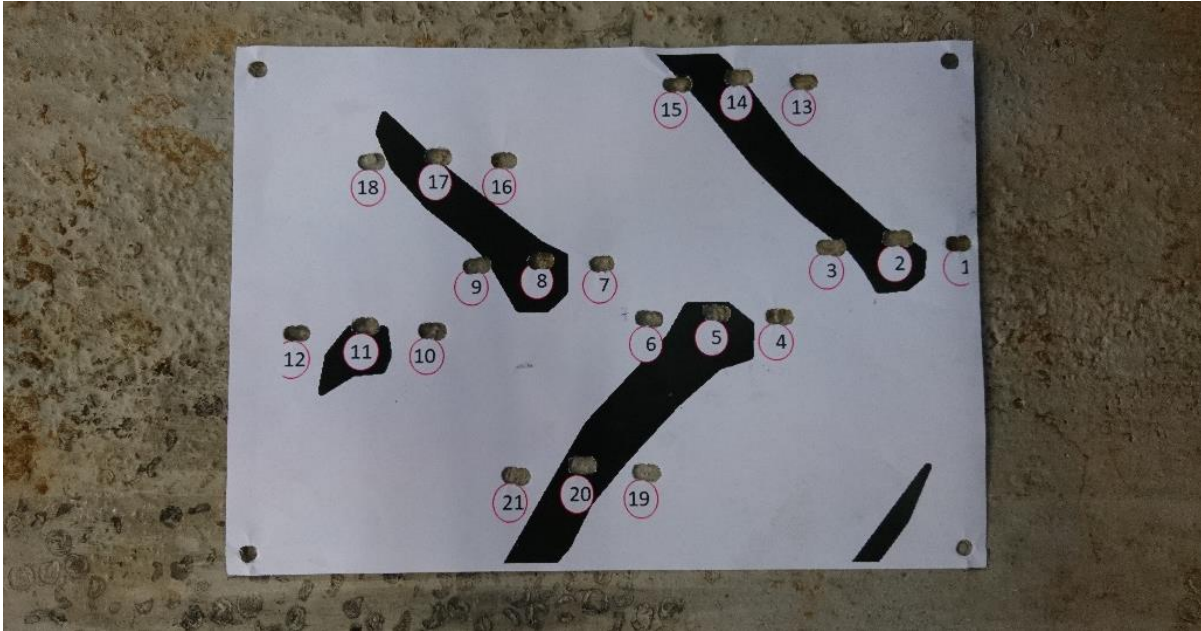
Figure 24: Microtexture profiling location template.

Figure 25: Microtexture profiling location template on STTR fitted with concrete test surface.

The longitudinal friction coefficient was determined on multiple surfaces in a laboratory

and on multiple surfaces at the outdoor test tracks at Gerotek Test Facilities. The list of

test surfaces used is highlighted in bold in Table 8 with the average of the 21 measurements within the contact patch noted. The Mild Steel sheet (construction steel, 300MPa yield strength), Aluminium 6 Series sheet (240-270MPa yield strength) and Strenx Steel sheet (700MPa yield strength) are standard off the shelf materials available in South Africa. The only preparation done on these test surfaces was sanding of the Mild Steel sheet with P80 grit sandpaper (to remove mill slag), all other surfaces were used as delivered from the supplier. All surfaces were cleaned with acetone to ensure that the surface was clean and oil free.

The microtexture surface roughness measurement of sample surfaces are shown in Table 8, with R_a the average roughness, R_q the mean square value and R_z. the maximum height in the measurement, all noted in μm.

Table 8: Microtexture Surface Roughness Measurements

Roughness Measurements	Condition Standard =ISO 4287:1997 Filter=GAUSS Lc=0.8mm Ls=2.5µm N=5 Pre_Length=OFF Speed=0.5mm/s Range=AUTO Average Pitch=0.5µm		
Surface measured	R_a [µm]	R_q [µm]	R_z[µm]
Mitutoyo Calibration Surface	**2.94**	**3.275**	**10.079**
Cell phone screen protector	0.009	0.012	0.087
Glass	0.014	0.018	0.128
Aluminium 6 Series sheet	0.493	0.6	2.602
Mild Steel_P80 conditioned	1.05	1.251	5.797
Mild Steel sheet	1.227	1.607	7.397
Shaved Tyre	1.293	1.71	8.019
New Tyre	2.58-2.71	3.17-3.45	14-17
paper	2.843	3.382	15.027
Strenx steel sheet	3.06	3.835	17.177
Concrete block STTR	4.983	6.329	27.077
Gerotek High speed concrete track	7.404	8.801	41.508
Asphalt	8-12	10-14	41-51
Used Tyre	10.343	12.895	54.391
New tyre post P80 test	10.782	13.074	50.899
Gerotek concrete	11.367	14.289	64.743
P180 grit sandpaper VSM RK700X	11.526	15.361	71.739
TM700 buffed tyre	11.853	14.671	59.57
P220 grit sandpaper Klingspor CS311Y	14.607	17.486	70.330
Belgian block	15.148	18.234	72.397
P180 grit sandpaper Klingspor CS311Y	18.245	21.988	88.167
P120 grit sandpaper	18.906	23.174	85.028
P100 grit sandpaper	26.209	31.717	123.52
P80 grit sandpaper Klingspor CS308Y	27.772	33.019	118.66

The microtexture profiles and DSD of some of the surfaces in Table 8 are shown in Figure 26 and Figure 27 respectively. The microtexture surface profiles give a visual indication of the roughness of the surface. The black lines in both Figure 26 and Figure 27 are

measured from the calibration surface of the Mitutoyo SJ-210 portable surface roughness tester. The calibration surface profile is a continuous sinusoidal wave with a constant amplitude and wave length of 10μm. This is clearly shown by the black DSD line in Figure 27, as it has a distinct peak at 10^4 cycles/m indicating that the profile is not random. When comparing the DSDs of the other surfaces it is clear that most surfaces have random amplitudes generally following a straight-line trend.
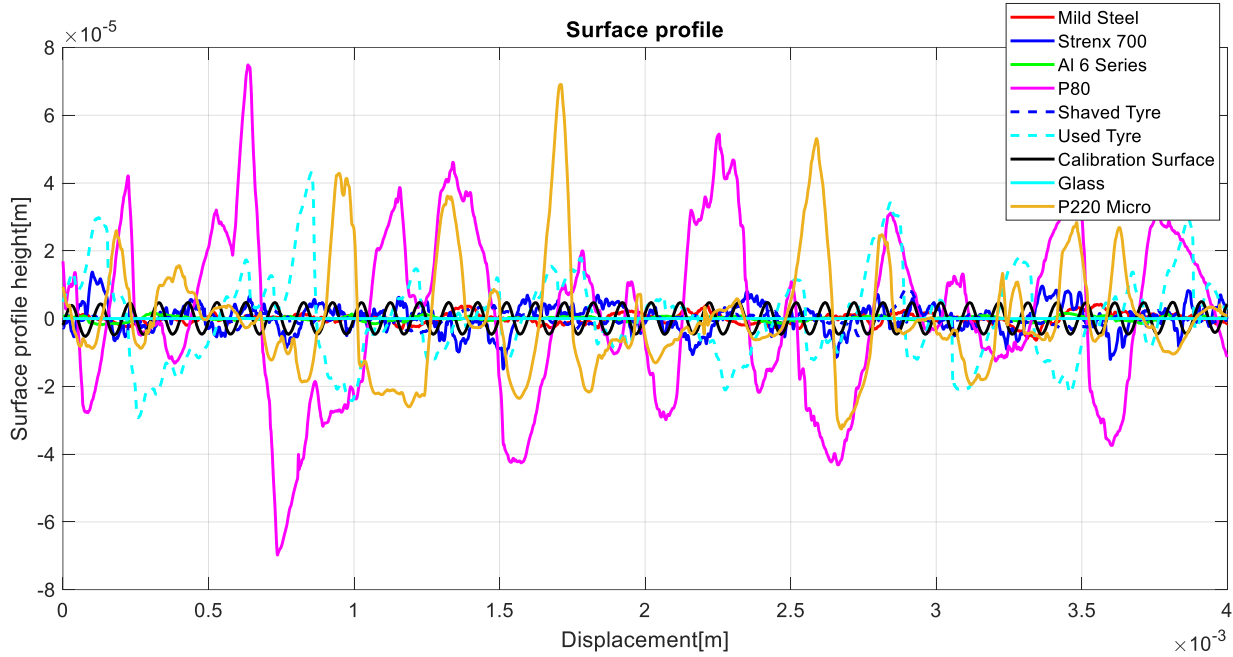
Figure 26: Microtexture profile of sample surfaces.
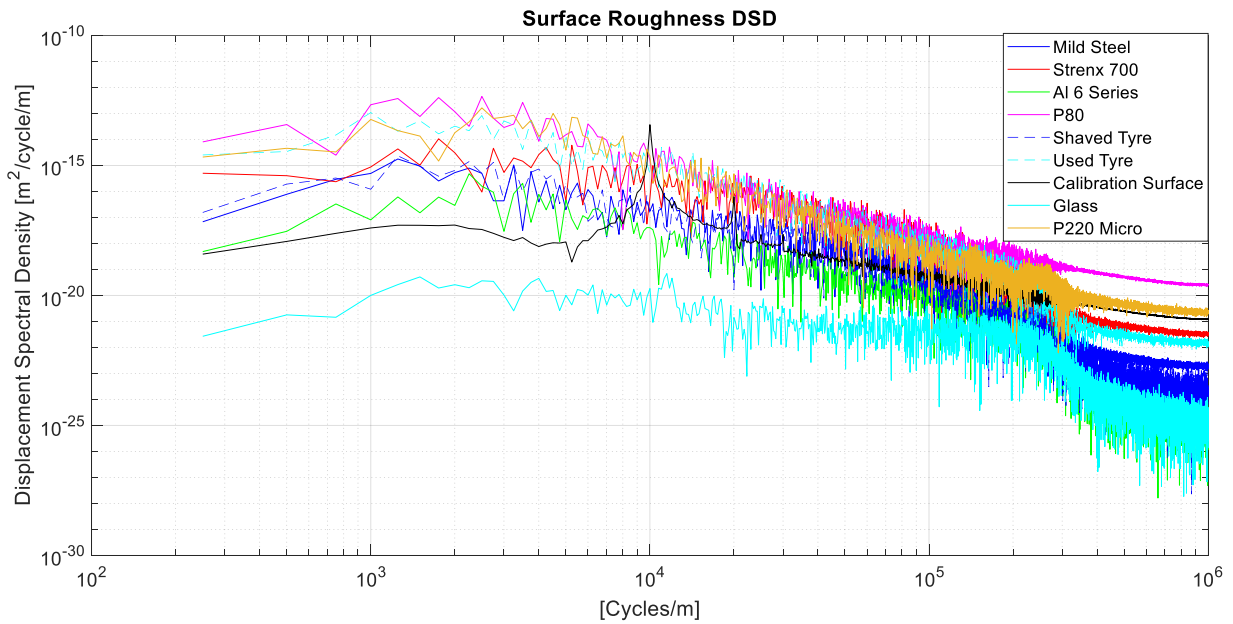
Figure 27: DSD of microtexture profiles of sample surfaces.

Some of the test surface microtexture profiles used on the STTR and at the Gerotek Test

Facilities, are presented in Figure 28 with the corresponding DSDs shown in Figure 29.
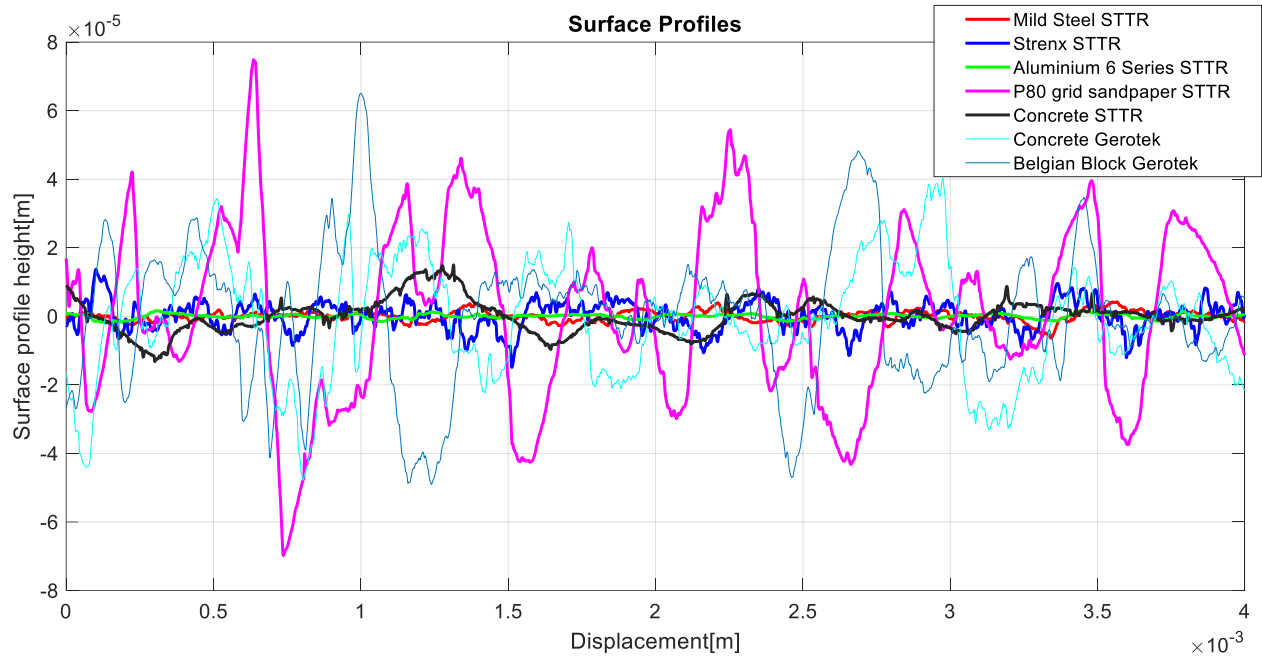
Figure 28: Microtexture profile of test surfaces.

To put the profiles in perspective, the different road class indicators for class A,D and H roads, as per ISO 8608, are added to the DSD plot in Figure 29, as well as some of the profiles of the concrete tracks and Belgian paving track at the Gerotek Test Facilities as presented by Becker and Els (2014).
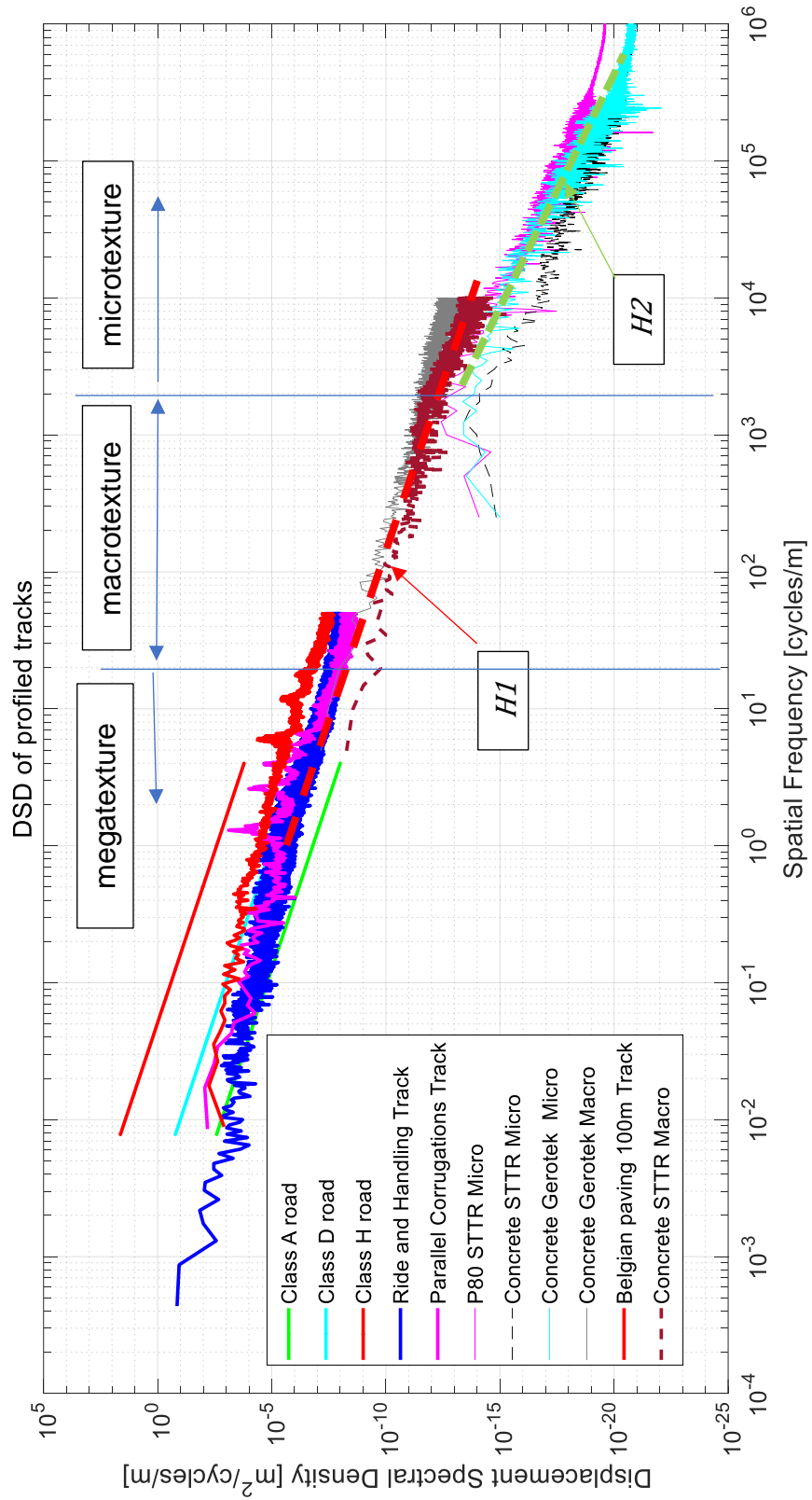
Figure 29: DSD of test surfaces.

It can be seen from Figure 29 that the gradient of the DSD of the megatexture (wavelengths exceeding 50mm) measurements on the Gerotek concrete tracks, Ride and Handling track and Parallel Corrugations track, correspond to the macrotexture measurements on the concrete surface as used on the STTR, as shown in Figure 25, between spatial frequencies 10^1 to 10^4 cycles/m. The change in gradient of red dashed line, *H1*, to the green dotted line, *H2*, corresponds to the Hurst exponent of macrotextures and microtextures respectively as described by Le Gal et al., (2008). As described in section 2.4, the gradient of *H1* is referred to as the road index as this section of the rod profile affects the ride comfort of the vehicle. The gradient of *H2* can be referred to as the surface index as this is a very important parameter to have when selecting the representative test surface in a laboratory as it has a direct impact on the measured friction coefficient and needs to match that of the surface used during field testing.

Postulate conclusion:

II.   *From the surface roughness measurements, it can be seen that each surface has different characteristics, which can indicate that the sliding friction coefficient of a tyre should be dependent on the surface roughness. In general, the rubber compound of each tyre differs which will also have an effect on the sliding friction coefficient of each tyre on the same surface as the rubber deforms over the surface. To eliminate this effect the same tyre is used during experimental tests. This postulate will be investigated further during the experimental tests which is discussed in the following section.*

4.3.   Effect of Surface Roughness on Stiffness and Friction Coefficient

Postulate:

II.   *A change in surface roughness affects the sliding friction coefficient on an agricultural tyre*

III.   *A change in surface roughness does not affect the longitudinal tyre stiffness characteristics of an agricultural tyre, only the peak friction value*

IV.   *The tyre stiffness characteristics of an agricultural tyre change due to the change in tread depth*

V.   *The sliding friction coefficient value changes for different tread depths on an agricultural tyre.*

These postulates can only be validated with the use of experimental testing. The typical spread of longitudinal friction coefficient measurements is shown in Figure 30. The same tyre is tested on different surfaces in a laboratory, with the use of the STTR at different inflation pressures. All the measured data was left unfiltered to ensure all the surface roughness effects are kept in the data sets and not filtered out. Figure 30 shows that the longitudinal stiffness of the tyre, at displacement less than 20mm, is captured well by using any of the surfaces, however the maximum longitudinal friction coefficient generated by the tyre varies significantly. Persson (2001), confirmed that the friction of rubber on smooth surfaces are due to interfacial adhesion and has the largest effect for

surfaces with a surface roughness value R_a<1µm. When R_a.> 1µm the adhesion should have little to no effect on the friction coefficient.
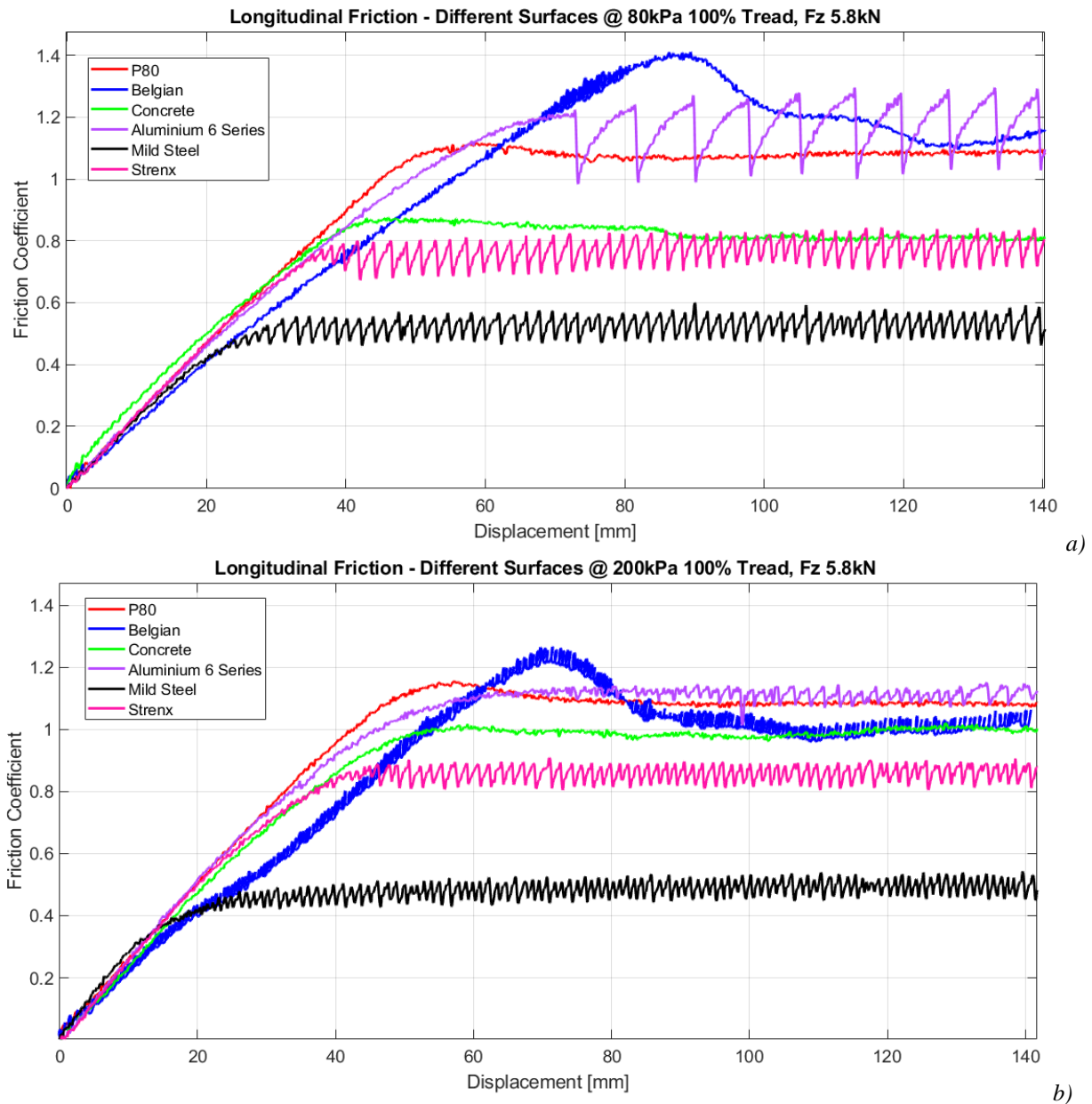
Figure 30: Longitudinal friction coefficient measurements on different surfaces for a) 80kPa and b) 200kPa inflation pressure, respectively.

Figure 30 illustrates the contribution of the adhesion, as the measured friction coefficient on the Alumunium sheet is larger than 1, with a surface roughness of R_a=0.493µm, as shown in Table 8. Compared to the Mild Steel sheet on which the friction coefficient is 0.5 with a surface roughness of R_a=1.227µm. Note the "sawtooth" response due to the stick-slip phenomena in Figure 30. This stick-slip phenomena will be disccused later. The measured DSD of the microtexture on test surfaces were shown in Figure 27. The DSD of the Alumimium sheet and Mild Steel sheet only differs at the higher spatial frequencies > 10^5 cycle/m. This is where the adhesion contribution is the highest as the DSD of the Aluminium sheet is lower. It can be seen that the concrete surfaces are in mid range when compared to the DSD of P80 sandpaper and Mild Steel sheets. From these graphs it can be seen that the higher the DSD the higher the measured friction coefficient, with the exception of the Mild Steel and Aluminium sheets.

Although the main focus of this study was on testing a tyre at a single vertical load, additional tests were conducted to illustrate how tyre characteristics change with different vertical loads on P80 sandpaper. It is an important aspect to understand when conducting vehicle simulations at vertical tyre loads for which the tyre models were not validated. Different vertical loads on the same tyre on the same contact surface yield different longitudinal stiffness and friction coefficients values as shown in Figure 31 and Figure 32. For different vertical loads, the longitudinal stiffness of the tyre in question can vary by

64% and the sliding friction coefficient can vary by 10% on the same surface and the same tyre tread wear condition.
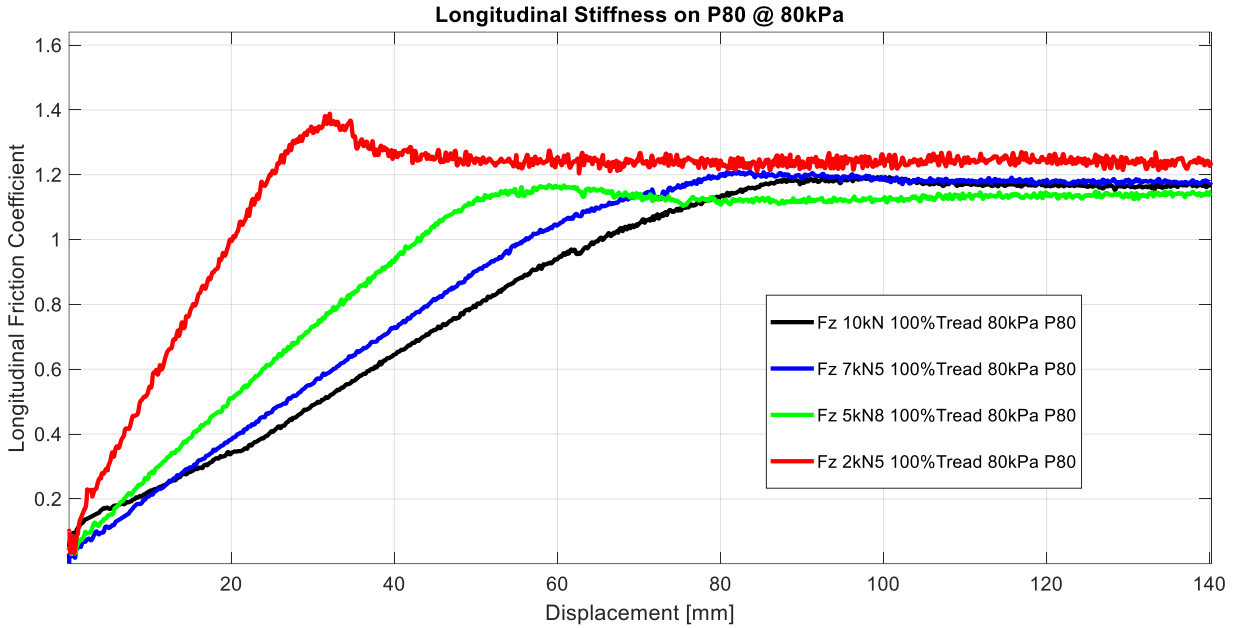
Figure 31: Longitudinal friction coefficient at multiple normal loads for 200kPa inflation pressure and 100% tread condition.
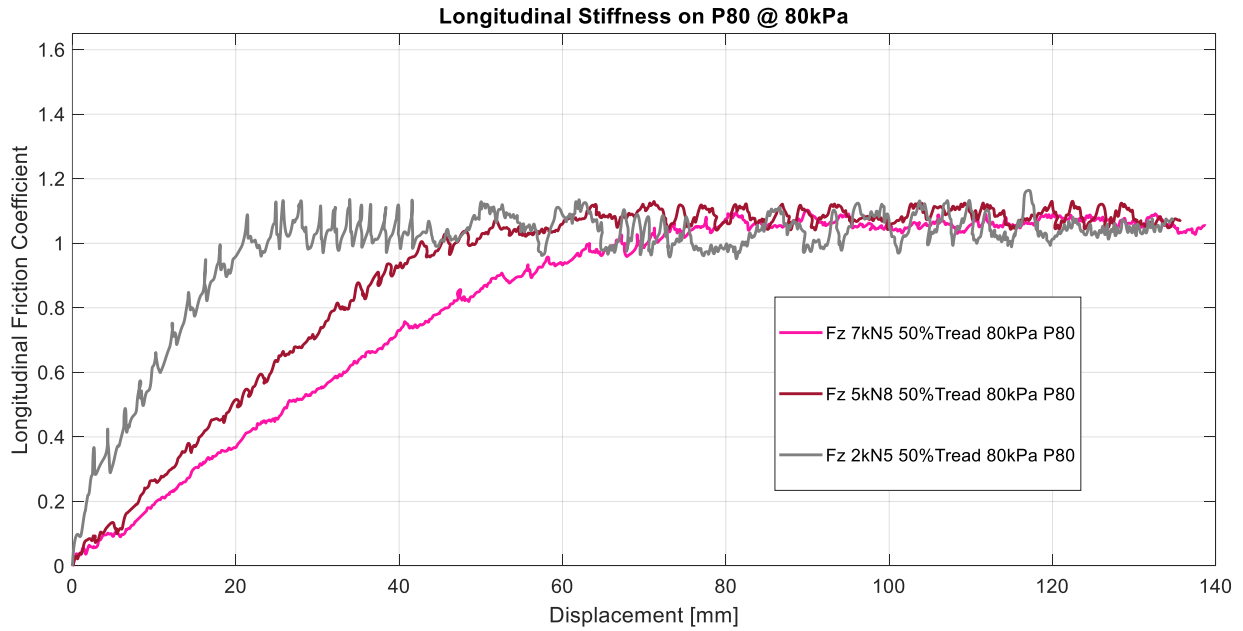
Figure 32: Longitudinal friction coefficient at multiple normal loads for 80kPa inflation pressure and 50% tread condition.

The same variation in longitudinal stiffness is noticed when the vertical load is varied and the tread wear condition is kept constant at 50% tread wear at a lower inflation pressure, as shown in Figure 32. This supports the argument that it is very important to validate the tyre model for the application it will be used for and that large simulation errors will be made if a tyre model is used outside the validation scope.

When the vertical load, surface roughness and inflation pressure are kept constant, the effect of the tread on the longitudinal stiffness and friction coefficient becomes apparent as shown in Figure 33. From Figure 33 it is clear that the tread wear condition results in less than 10% variation on the longitudinal stiffness and friction coefficient when the tread condition is 50% to 100%. The higher longitudinal stiffness at 0% tread condition is due to the removal of the deformation of lugs in the tread, thus only the inflated carcass stiffness is measured which is 21% higher. This indicates that the lugs decrease the longitudinal stiffness of the tyre. The large change of 50% in friction coefficient between 50% tread to 0% tread, is due to the significant increase in the actual amount of rubber in contact with the test surface (in the order of 200% increase in rubber contact), as shown in Figure 22. These findings are summarised in Table 9.
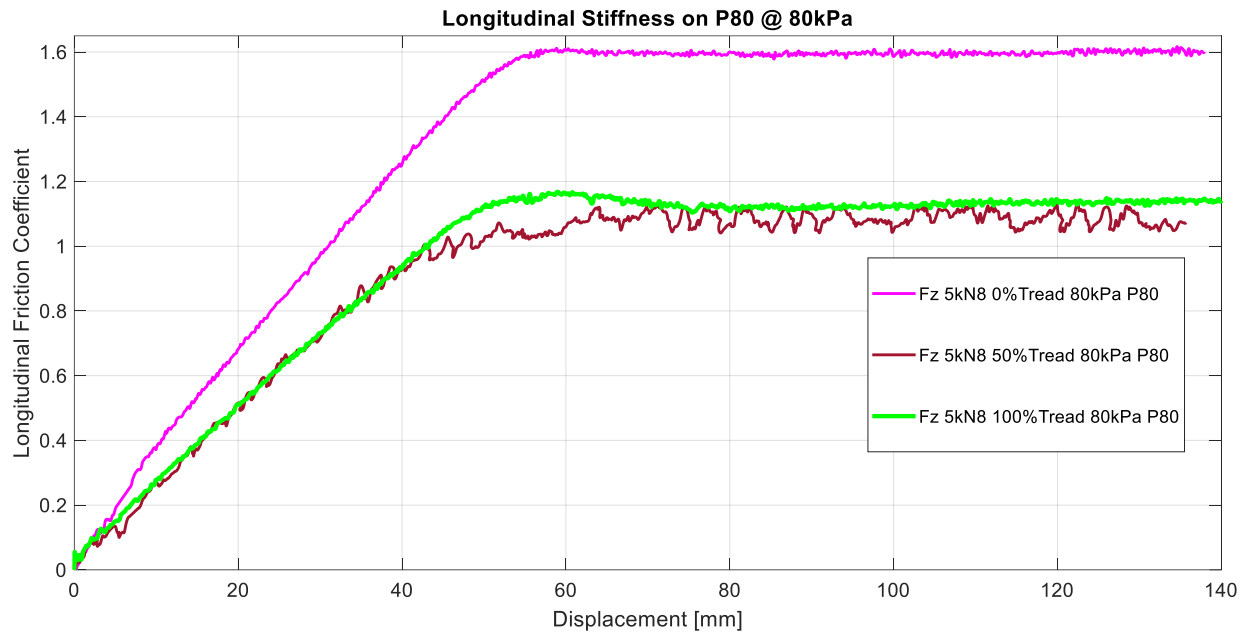
Figure 33: Longitudinal friction coefficient at constant load and inflation pressure with change in tread condition.

Table 9: Tyre characteristic change due to change in tread condition at 80kPa.

Tread Condition	Contact Area [mm²]	Difference in Contact Area	Change in Longitudinal Stiffness	Sliding Friction Coefficient	Change in Sliding Friction Coefficient
100%	11909	-	-	1.15	-
50%	11535	-3%	< 10%	1.1	-4%
0%	35993	202%	21%	1.6	40%

Due to the size and shape of the lugs in the tread, for the agricultural tyre of interest, the bending/deformation of the lug can be modelled as a cantilever beam with the longitudinal force applied at the tip of the lug in the contact patch as shown in Figure 34.

The deformation of the lug can thus be described by eq. (14) which is the calculated bending of a cantilever beam, as presented by Shigley (1986).

$$\delta_{lug} = \frac{F_x * l_{tread}^3}{3EI_{lug}}$$

eq. (14)
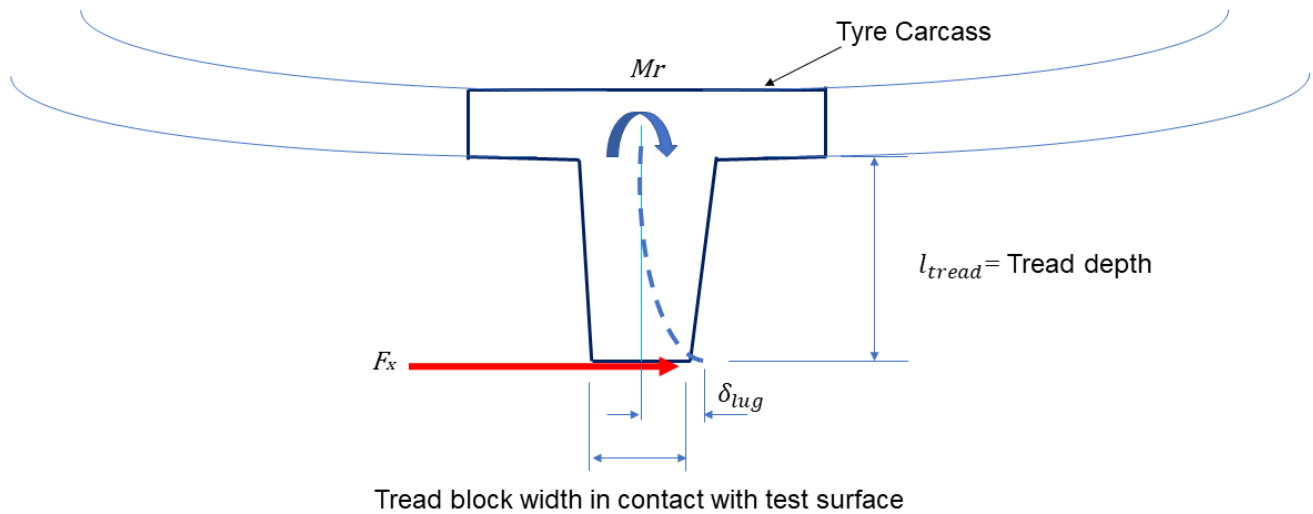
Figure 34: Longitudinal deformation of tread lug simplified to a cantilever beam.

The displacement, δ_{lug}, is directly proportional to the tread depth, l_{tread}. In this case the height of the tread block, is 30mm at 100% tread and 15mm at 50% tread. The reactive bending moment, Mr, at the clamped side of the beam (the tyre carcass and belt) is related to the inflation pressure as the belt and carcass stiffness is strongly dependent on the inflation pressure. This reactive bending moment needs to counter the bending moment generated by the longitudinal force which is proportional to the height of the lug as shown in eq. (15):

$$Mr = F_x l_{tread}$$

eq. (15)

The longitudinal deformation of the lugs in the tyre tread is shown in Figure 35 for 100% tread and 50% tread, respectively, at an inflation pressure of 80kPa. None of the commercially available tyre models are able to capture this effect of the lugs deforming and detatching from the surface. At this point the front face of the lug is in contact with the terrain and no current tyre model can capture this in simulation. It is suspected that the stick-slip that is seen on multiple smooth surfaces at only 100% tread condition, as shown in Figure 30, is due to the longitudinal deformation and the bending stiffness of the lugs. At 100% tread condition the lug deforms and increases the applied bending moment on the tyre carcass. It is suspected that the reactive bending moment in the tyre belt, supplied by the inflation pressure in the carcass, is just not enough to counter the applied bending moment. As a result the lug deforms more and as soon as the leading edge detaches from the surface a detachment wave is produced which propagates from the front-end to the back-end of the contact area. This results in the stick-slip phenomena. At some point, as the lugs wear down, the applied bending moment becomes lower than the bending moment the tyrecarcass can support, which in turn holds the deformed lug in position and prevents the detachment waves from forming.
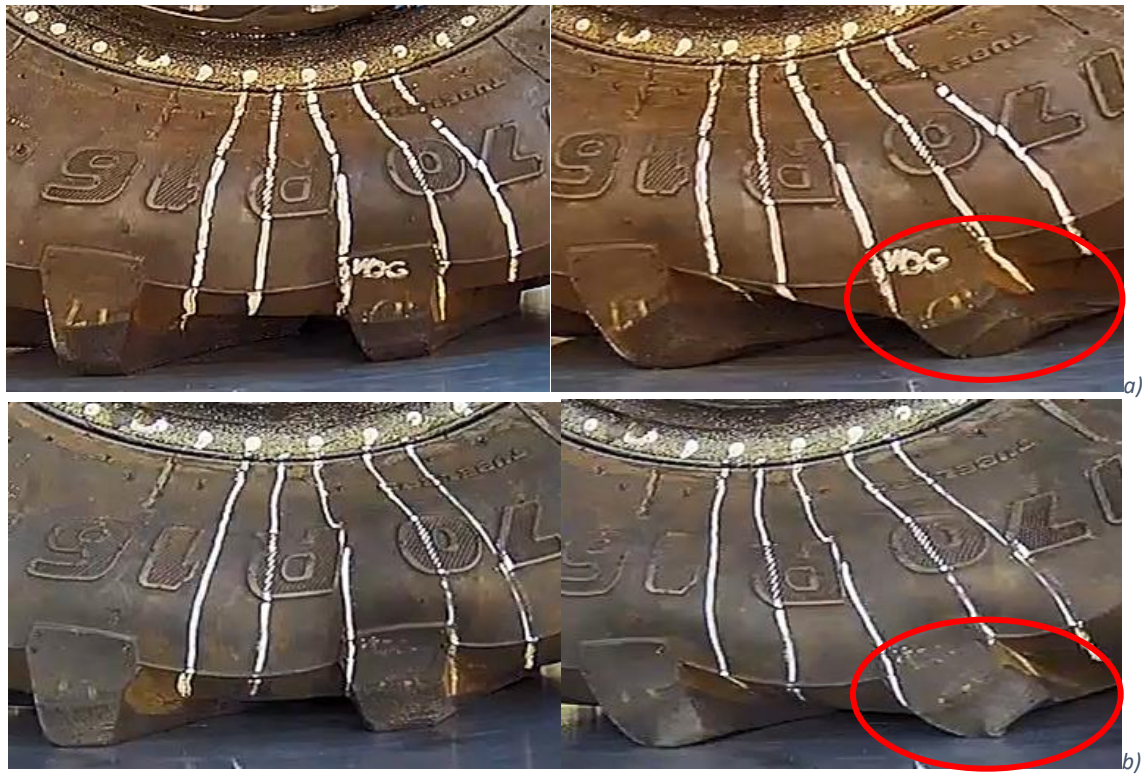
Figure 35: Longitudinal deformation of the tread lugs at 80kPa inflation pressure on an Aluminium sheet at a) 100% tread and b) 50% tread on an Aluminium surface where stick-slip is seen.

Stick-slip theory can be described as a mechanical system with a spring damper, where the damper element is linear and the friction force is decsribed by the Stribeck curve which is a discontinuous non-linear function, (Zuleeg, 2015). This mechanical stick-slip mechanism shows that, for a lower tangential stiffness in the carcass, the displacement oscilation frequency is high. When the carcass stiffness increases, as the inflation pressure is increased, the force displacement oscilations will be smaller, as shown in Figure 36. A very high friction coefficient is measured on the Aluminium sheet, with surface roughness R_a<1μm, where the adhesion component is very high. A slight change is seen in stick-slip frequency for surfaces with surface roughness values higher than

R_a>1µm (Mild Steel and Strenx). Note that as soon as the tread condition changes from 100%, no stick-slip is observed in the data. The stick-slip is not noticed during the tests conducted on concrete as shown in Figure 37, even at 100% tread, as the surface roughness of the concrete is higher compared to the surfaces in Figure 36. This is a motivation for using a more representative rough surface during laboratory tests.
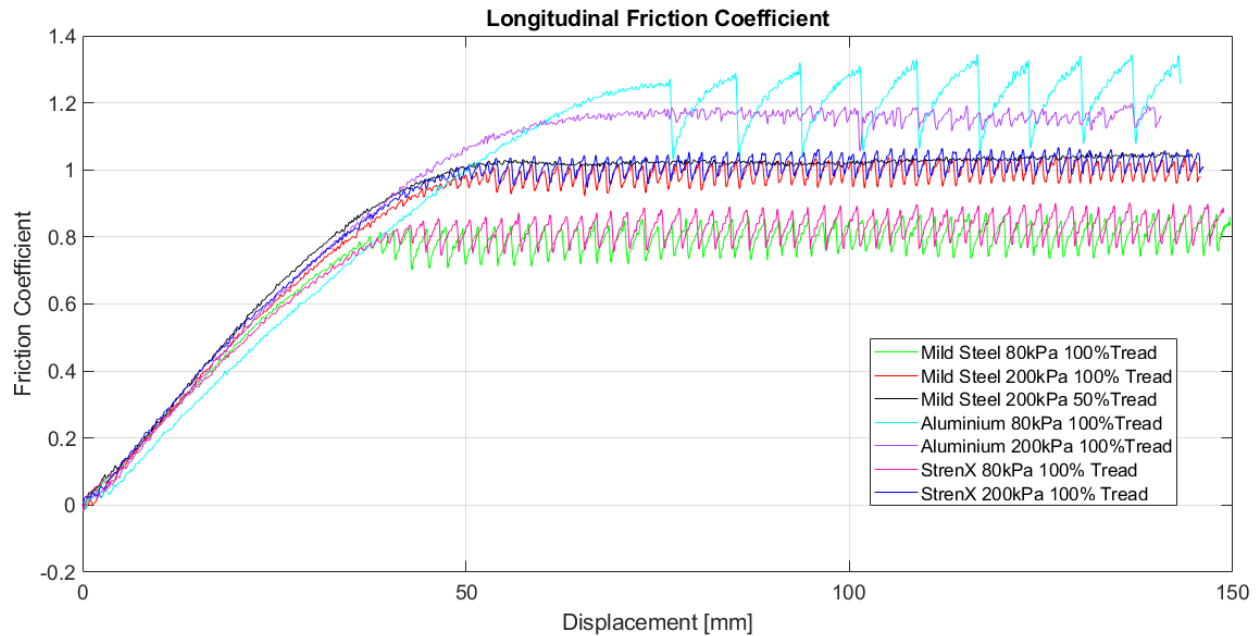
Figure 36: Stick-slip phenomena at different inflation pressures, on variety of surfaces at only 100% tread.

Figure 37 compares the different friction coefficients between the laboratory tests on the STTR fitted with a concrete surface and field tests at Gerotek on concrete.

Due to the ambient temperature of 25 degrees Celsius at Gerotek and slow longitudinal test speed, in the order of 8mm/s, the flash temperature and change in temperature of the rubber in the contact patch were deemed insignificant and were not taken into consideration.

The sliding friction coefficient measured during the laboratory tests indicated that the friction coefficient increases in the order of 10% between different tyre tread conditions due to the increase of rubber in the contact patch, where as the outdoor tests measured a more consistent sliding friction coefficient. It is suspected that this is due to the different ways in which the tyre is constrained between test methods. An average of 13% difference in sliding friction coefficent measurement was noted with 100% tread, where as the peak friction was within 3% to 5%. From these results, good correlation is observed between the laboratory tests on the concrete surface (as shown in Figure 25) and field test results as conducted with the DTT on the concrete tracks at the Gerotek Test Facilities (Figure 12). This concrete test surface can thus be used with confidence on the STTR to obtain accurate friction coefficient estimates for a tyre and will result in accurate model validated results on the concrete tracks at the Gerotek Test Facilities.
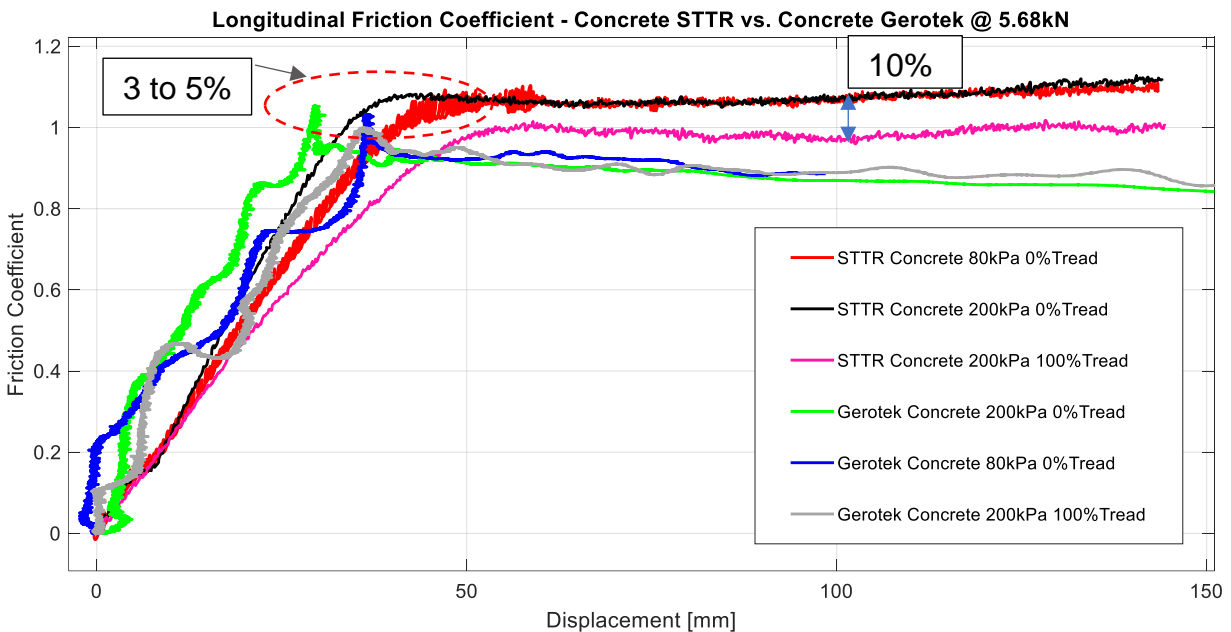
Figure 37: Friction coefficient measurement on concrete in laboratory tests and field tests.

It is noted that the friction coefficient is lower at a higher inflation pressure over the Belgian paving, as shown in Figure 38. The friction coefficient increases due to lug contact at 100% tread condition as the lugs slide into the cavities between the bricks in the Belgian paving. This also excites the vertical dynamics of the test trailer which cannot happen on the STTR due to the boundary conditions imposed by the test rig. The effect of the gaps between the Belgian blocks on the roughness of the track can also be seen in the DSD of the 100m Belgian profile in Figure 29, where the size of the bricks and gaps are represented by the peaks in the graph. To eliminate the effect of the lugs on the measurements, the friction coefficients at 0% tread condition are compared over the Belgian paving for both the STTR and Gerotek measurements. The same percentage difference to maximum sliding friction coefficient is noted between the static laboratory tests and the quasi-static field tests over the same section of the Belgian paving surface. The oscillations in the field tests are caused by the different boundary conditions on the tyre during the tests. For the field tests the tyre can move vertically, compared to the STTR where the tyre is constrained in the vertical direction. In general, the STTR and Gerotek test results correlate well when considering the different boundary conditions.
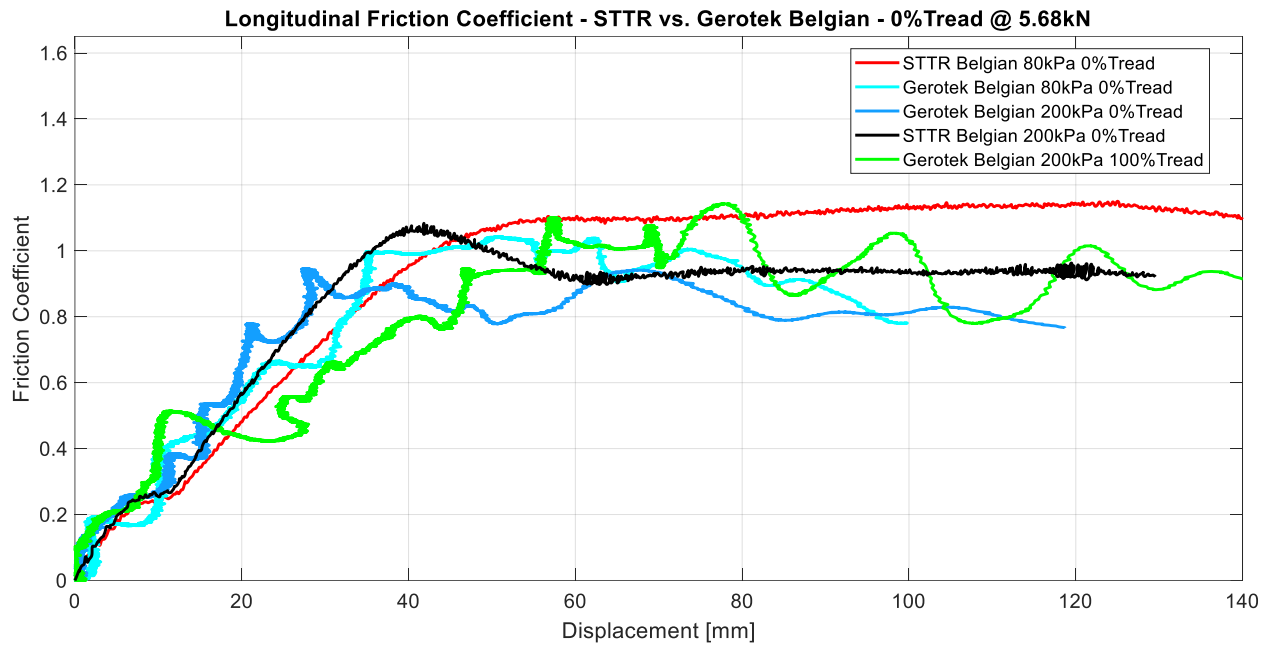
Figure 38: Belgian paving friction coefficient measurements in laboratory tests and field tests.

The change in longitudinal stiffness due to a lower inflation pressure and change in tread wear condition relative to a new tyre at 100% tread inflated to 200kPa, on concrete, is shown in Figure 39. Figure 39 indicates that the roughness of the test surface can have an increasing or decreasing effect on the measured longitudinal stiffness. Only the Mild Steel surface gave a consistent increase in longitudinal stiffness over the range of inflation and tread wear changes. Notice again the large jump when 0% tread is reached. If the 0% tread points are ignored, the longitudinal stiffness is reasonably independent of the surface roughness. This accentuates the complex interaction between the tyre carcass stiffness and friction coefficients.
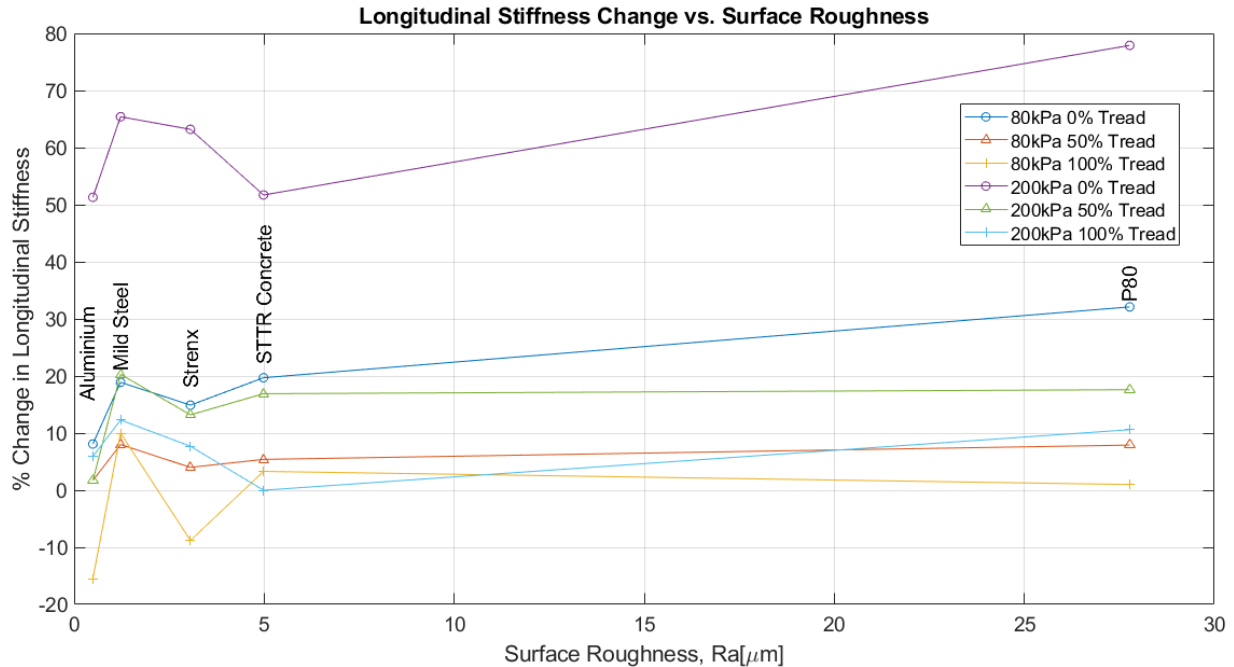
Figure 39: Change in longitudinal stiffness as a function of surface roughness, relative to 200kPa inflated tyre at 100% tread.

Figure 40 shows the effect of the surface roughness on the friction coefficient generated between the rubber and surfaces at different tread wear conditions. This shows that, in general, on very smooth or very rough surfaces one will measure a higher friction coefficient when testing tyres. This figure also shows that when testing on surfaces with 7µm<R_a<20µm a variation in friction coefficient in the order of 20%, for different tread wear conditions on the tyre, can be expected.
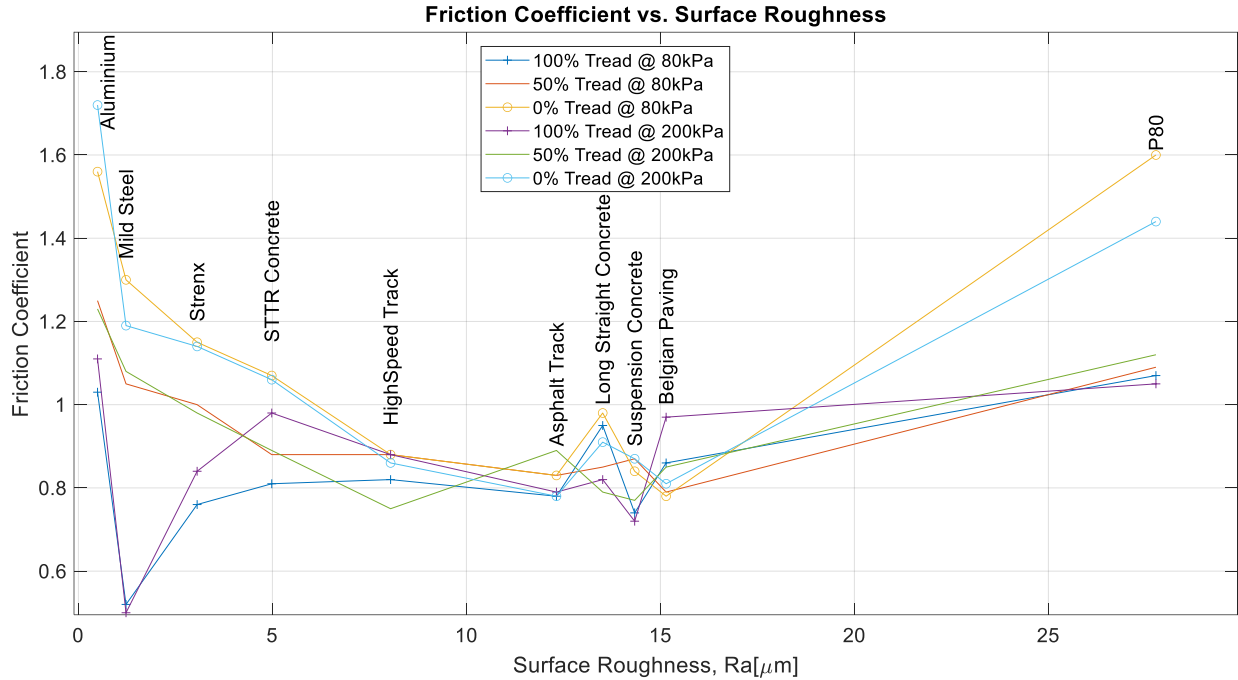
Figure 40: Friction coefficient vs. surface roughness for 80kPa and 200kPa inflation pressure at different tread conditions.

On agricultural tyres with large lugs the amount of rubber in contact with un-deformable terrain in the contact patch can be a little as 15%, as shown in Figure 22. Figure 41 shows the friction coefficient as function of the surface roughness R_a and percentage rubber in contact with the surface in the contact patch. It is observed that a more consistent friction coefficient is obtained on a surface with 7µm<R_a<20 µm and with a ratio of rubber in contact with un-deformable terrain in the contact patch of larger than 18%. It is clear that smooth surfaces (mild steel or aluminium surface) should not be used as it results in a large scatter in friction coefficient values ranging from 0.5 to 1.7. A large scatter in friction coefficient values are also noted for rough surfaces.
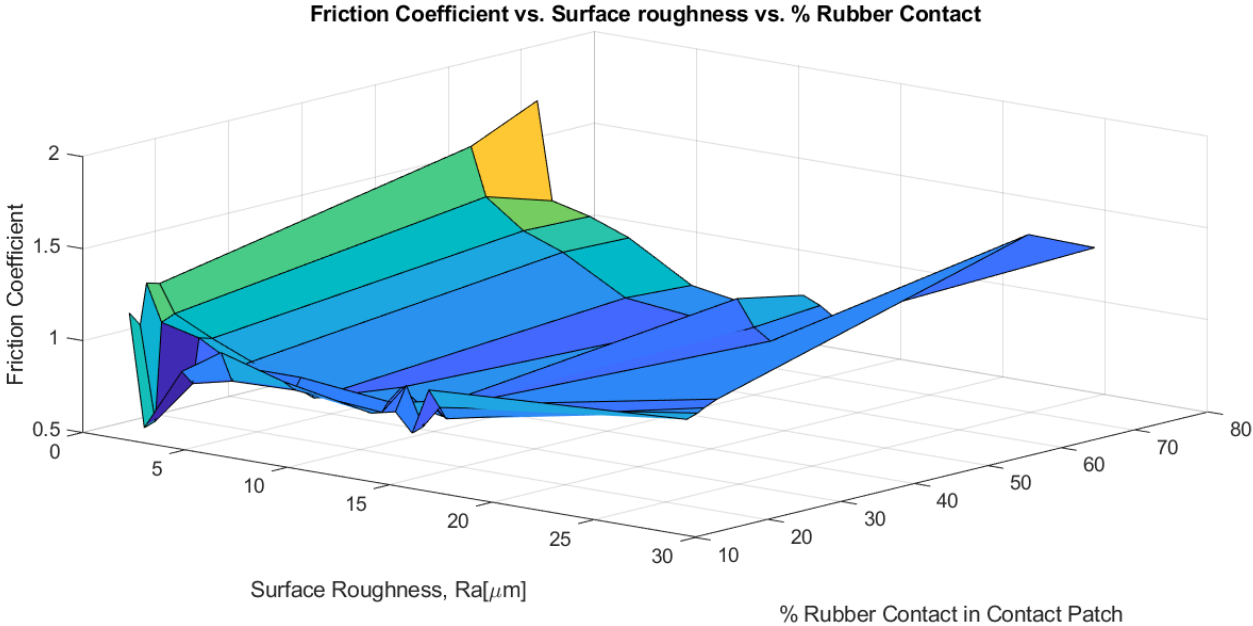
Figure 41: Friction coefficient vs. surface roughness as a function of rubber contact percentage.

The results show that the surface roughness and DSD should be used to determine which grit sandpaper or corundum tracks should be used in order to represent the outdoor environment during laboratory tests. It is seen in Figure 40 and Figure 41 that, for the concrete field test surfaces at Gerotek Test Facilities, the recommended laboratory test surface needs to have a surface roughness value, $10<R_a<15\mu m$. Table 8 indicated that this roughness is equivalent to a Klingspor CS 311 Y P180 or P220 grit sandpaper, (Klingspor, 2021b). The DSD of P80, P180, P220 grit sandpapers are shown in Figure 42. It can be seen that not all P180 grit sandpapers have the same DSD characteristics. Additional tests on P180 grit RK700X VSM, (VSM,2021) sandpaper resulted in a friction coefficient more representative of the Gerotek concrete surfaces at 0% Tread condition, as shown in Figure 43.
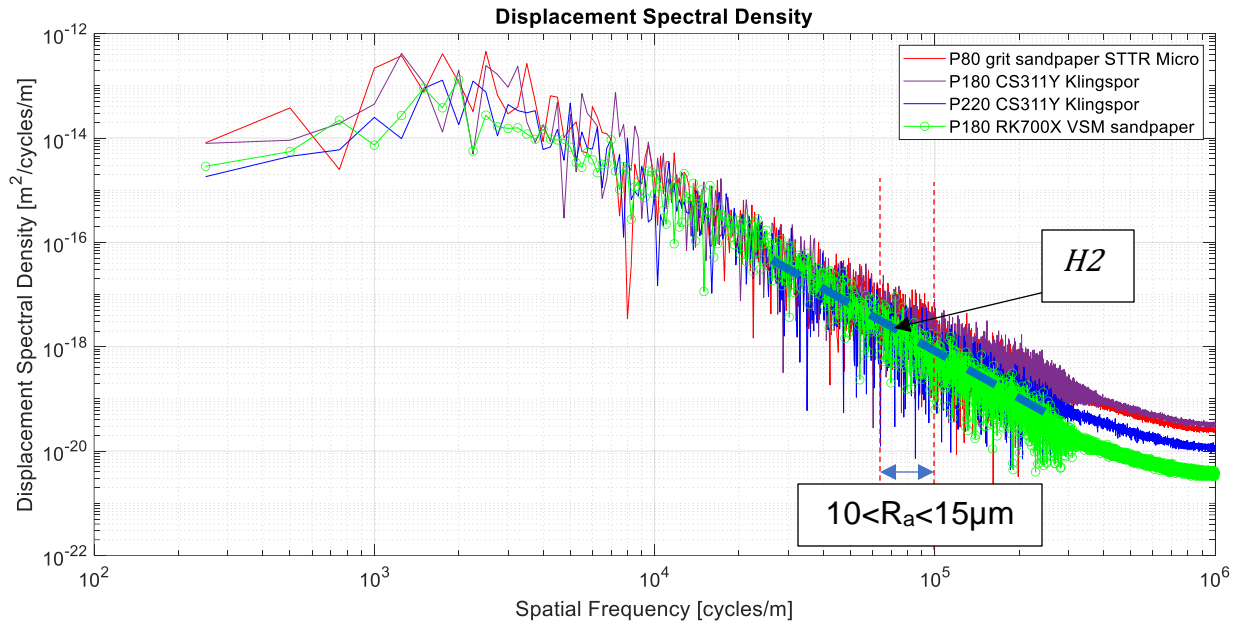
Figure 42: DSD comparison between the P80, P180, P220 grit sandpapers.
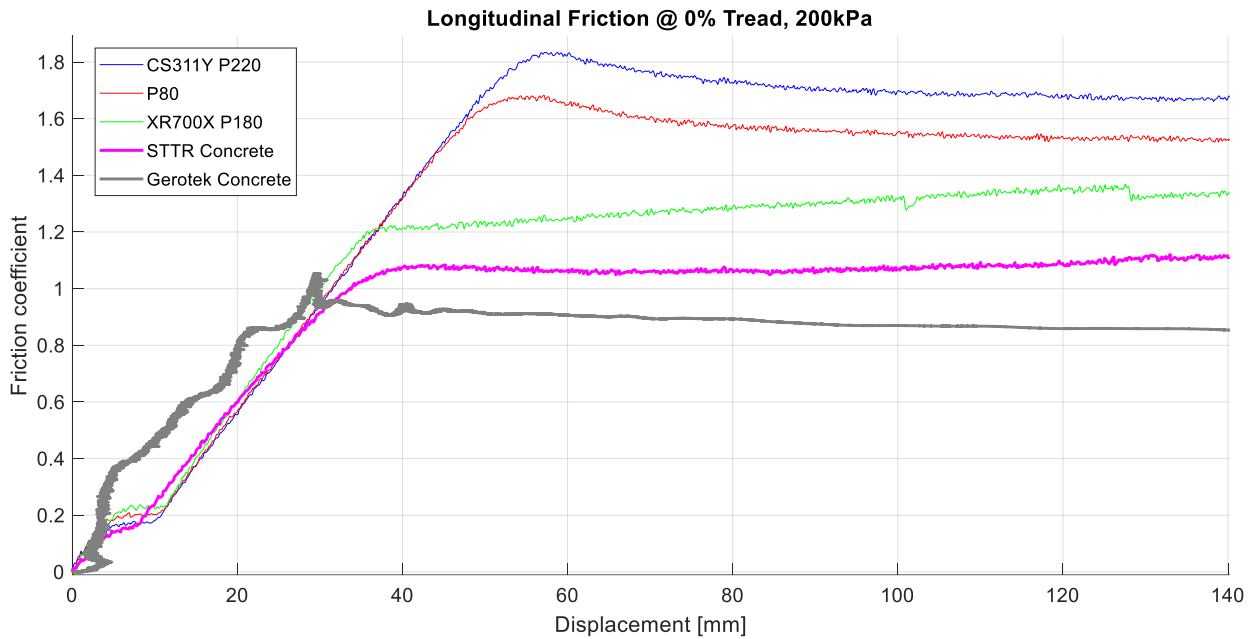
Figure 43: Longitudinal friction coefficient comparison between the Gerotek concrete surfaces and different grit sandpaper on a tyre with 0% tread.

Figure 43 shows that the P180 grit RK700X VSM sandpaper results in a 32% higher friction coefficient compared to an 80% higher friction coefficient should a P80 grit sandpaper be used. The concrete block used on the STTR was not 100% representative of the Gerotek concrete and resulted in a 17% increase in measured friction coefficient at 0% tread. The surface roughness value of $10<R_a<15\mu m$ correlates directly to the surface texture of the aggregate used in the concrete. This relates to a spatial frequency between 66 666 and 100 000 cycles/m, as indicated in Figure 42, with corresponding surface index, $H2$, and roughness coefficient at a spatial frequency of 75 000 cycles/m. In general, this surface index, $H2_{field}$ surface, represents the surface texture of the field/ validation test surface. The surface index of the surface used in the laboratory during tyre characterisation tests, $H2_{lab}$ surface, needs to match that of the field/ validation test surface in order to have a representative tyre characteristic for tyre modelling.

The majority of the road surface contains exposed aggregate (as shown in Figure 19), which is in direct contact with the rubber in the contact patch, and thus the dominating factor in friction generation. On new asphalt roads, a thin layer of tar is coated over the aggregate which will produce a higher friction coefficient. As the tar coating is worn away the aggregate is exposed, which then again becomes the factor in friction generation.

Postulate conclusion:

   II.   *The tests have shown that a rough surface such as P80 grit sandpaper does not guarantee a higher friction coefficient on agricultural tyres with a significant amount*

of tread on the tyre. The opposite is also seen for smooth surfaces, where a lower friction coefficient is not always observed.

III.   *The experimental tests have indicated that the surface roughness does not affect the longitudinal stiffness of the tyre, however it does have a major influence on the sliding friction coefficient.*

IV.   *The effect that the amount of tread, on an agricultural tyre, has on the tyre characteristics was demonstrated and confirmed. The amount of tread has a direct influence on the longitudinal stiffness of the tyre in the normal operating range.*

V.   *The experimental tests have highlighted the importance of measuring the surface roughness of the field test surfaces on which full vehicle tests are to be conducted for final model validation and testing purposes. This surface roughness should be used to identify a representative artificial test surface to be used for tyre characterisation in a laboratory. The friction coefficient of a tyre is highly dependent on the surface roughness together with the size and amount of rubber in the contact area which is a function of tread wear.*

4.4.   Quasi-Static Tyre Characteristics

Postulate:

V.   *The sliding friction coefficient value change for different tread depths on an*
      agricultural tyre

VI.   *The vertical tyre stiffness characteristics of an agricultural tyre is affected by the*
      cleat orientation

VII. *Asymmetric longitudinal and lateral stiffness characteristics are caused by the lugs*
      on an agricultural tyre

Static stiffness characteristic tests were conducted to measure the vertical, longitudinal and lateral stiffness at two inflation pressures of 80kPa and 200kPa. The vertical stiffness was measured and compared for the different inflation pressures and different tread percentage on the tyre on a flat surface covered with P80 grit sandpaper, a lateral 28x28mm cleat and a longitudinal 28x28mm cleat. While many tyre models only require the stiffness on a flat surface, some tyre models, such as FTire use stiffness over cleats to parameterise in- and out-of-plane bending stiffnesses of the tyre carcass. The results from the tests conducted with different tread wear conditions at 80kPa and 200kPa are discussed in the following sections. In order to maintain the highest integrity of the measurements, the measured data presented was unfiltered during post processing. The longitudinal and lateral tyre characteristics are also discussed in this section.

4.4.1. Vertical Static Stiffness on a Flat Surface

The vertical static stiffness was measured on a flat surface using the STTR with P80 grit sandpaper on the flat surface. These measurements are shown in Figure 44. Designers tend to use linear approximations for tyre characteristics should they have limited tyre data available. Most tyre models also only account for linear vertical stiffness. The linearized vertical stiffness around the vertical load of 5.68kN, for the tyre in question, is indicated by the dashed blue and dashed green lines for inflation pressures of 200kPa and 80kPa respectively. Figure 44 shows that the characteristics are significantly non-linear and a linear approximation may not be a good approximation when used in ride comfort simulations over uneven terrain where the vertical load on the tyre can vary between 0 load (wheel losing ground contact) and four times the static load (for a 4g axle load when vehicle lands on only 1 wheel). When driving over rough terrain at higher speeds, wheel lift-off occurs regularly and can result in up to 20% of the time not being in contact with the terrain. On the other extreme when a vehicle becomes airborne and lands on one wheel, the vertical wheel load can peak at four times the static load. Off-road military vehicles are designed for dynamic loads of between four and five times the static load. It can be seen that a linear approximation might be adequate when only used for static suspension deformation estimates or driving on smooth terrain. However, should one extrapolate the linear approximation lines (the dashed green and dashed blue lines in Figure 44), with the origin of the lines at zero displacement, a 16% to 21% error can be made in the estimated tyre deformation at the static load. On closer inspection it is clear that the vertical force vs. displacement characteristic is better represented by a parabolic

curve rather than a linear line, thus the importance of obtaining accurate tyre data for ride comfort vehicle simulation purposes. It can also be seen that the change in tread condition does not influence gradient of the vertical stiffness between 100% and 50% tread at the static load condition. As the tread nears 0% tread condition the vertical stiffness curve becomes more parabolic and has a larger influence on the vertical stiffness at lower loads. If the vertical load varies by 50% around the static position the vertical stiffness can decrease by up to 30% between 2kN and 3kN and increase by 40% between 9kN and 10kN. This indicates that linearization should always be applied with the use case of the model in mind. Tests on different surfaces have indicated that the surface roughness does not affect the vertical stiffness at all.
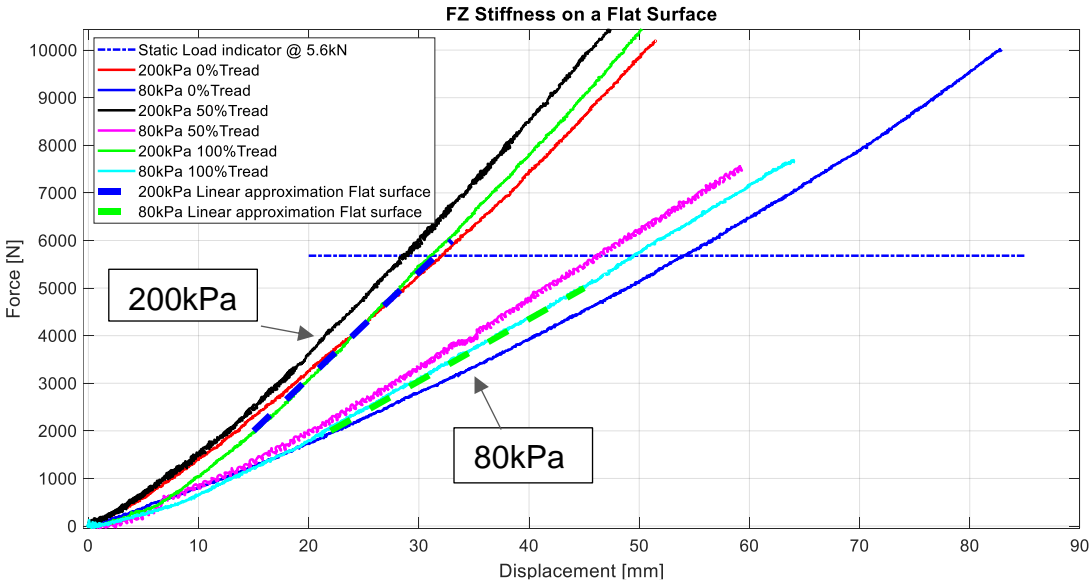
Figure 44: Vertical stiffness measurements for different tread conditions and inflation pressures on P80 grit sandpaper.

4.4.2. Vertical Static Stiffness on a Lateral Cleat

The vertical stiffness on a cleat was measured for three cleat positions. The lateral cleat was positioned perpendicular to the direction of travel at 50mm in front of the center line, in-line with the center line and 50mm behind the center line as shown in Figure 45 by the green, red and blue section respectively. The darker sections indicate the initial contact points, per cleat setup, about which the tyre deforms up to the point where the rest of the tyre is in contact with the flat surface. The grey shadow indicates the contact on a flat surface. Contact between the tyre and the cleat is therefore not distributed over the cleat as a line contact, but instead applied as discrete point loads to the tyre.
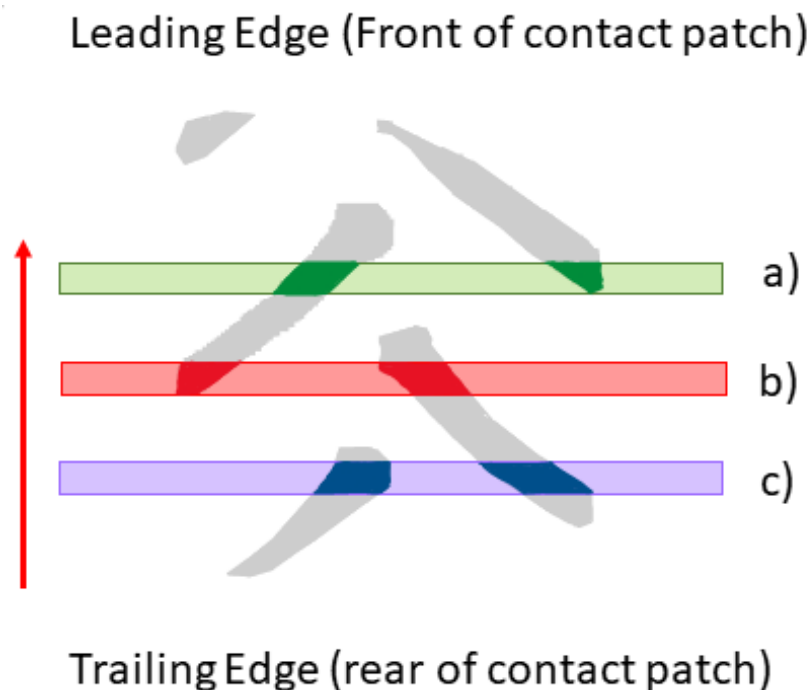
Figure 45: Lateral Cleat position: a) 50mm in front of center, b) in-line with center and c) 50mm behind center.

The effect of the tread wear condition and the position of the lateral cleat on the vertical stiffness is illustrated in Figure 46. The characteristic of the tyre becomes highly non-linear when the tyre travels over a cleat, as shown in Figure 46 for the lateral cleat orientation at 80kPa inflation pressure. Should a linear approximation be made for the vertical stiffness of the tyre one would have to consider a stage 1 stiffness, where the tyre starts to deform over the cleat and a stage 2 stiffness where the tyre comes into contact with the flat surface. Stage 1 can be described as the belt radial stiffness as it is mostly the belt deforming over the cleat. This is also noticed during the first 5 to 10mm vertical deformation on a flat surface where only the belt deforms to start forming the contact patch. Stage 2 can be described as the sidewall radial stiffness which is very dependent on the inflation pressure. On a cleat the transition point to stage 2 will be very dependent on the vertical load during this occurrence as well as the tread wear condition. The location of the transition from stage 1 to stage 2 stiffness over a cleat can change by up to 30mm as the tread wear condition changes, which is the maximum tread depth on the tyre in question. When comparing the linear approximation of the vertical stiffness on a flat surface, as shown by the dashed lines in Figure 44, with the stage 1 stiffness over a cleat as indicated by the red dashed lines in Figure 46, one can expect a decrease of 45 to 46% in the linear gradient between 80kPa and 200kPa inflation pressure respectively as shown in Figure 47.
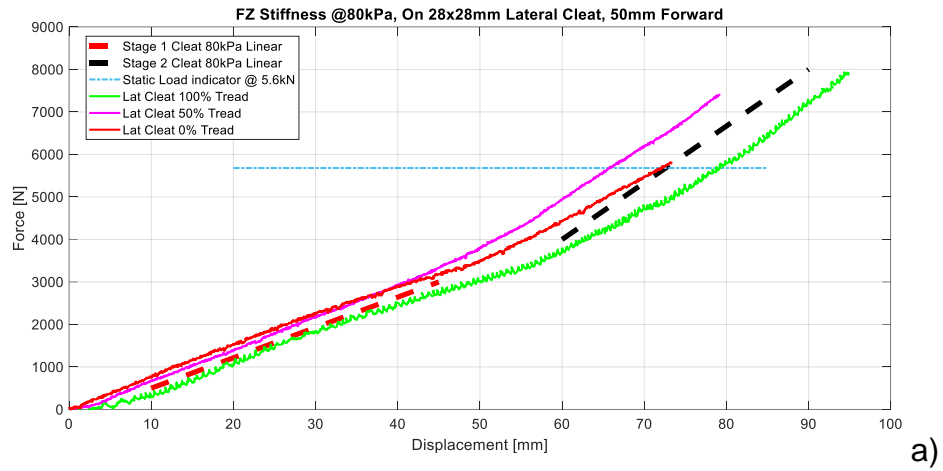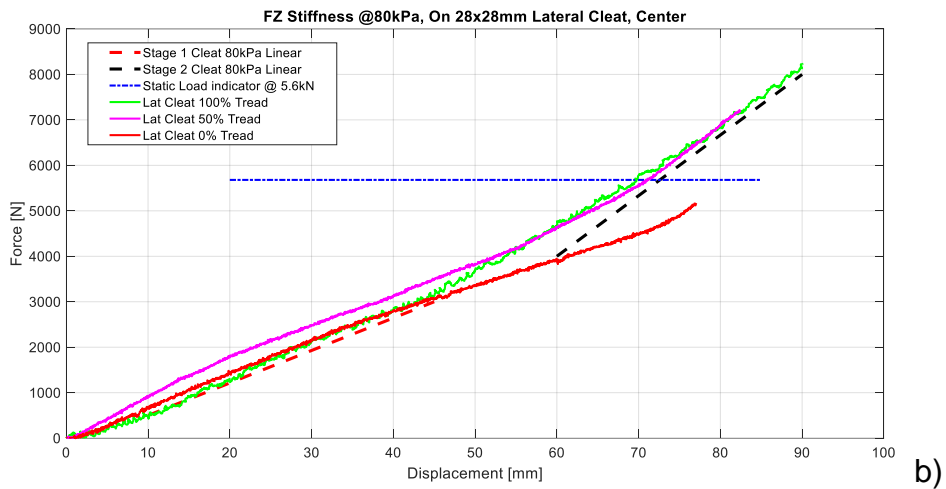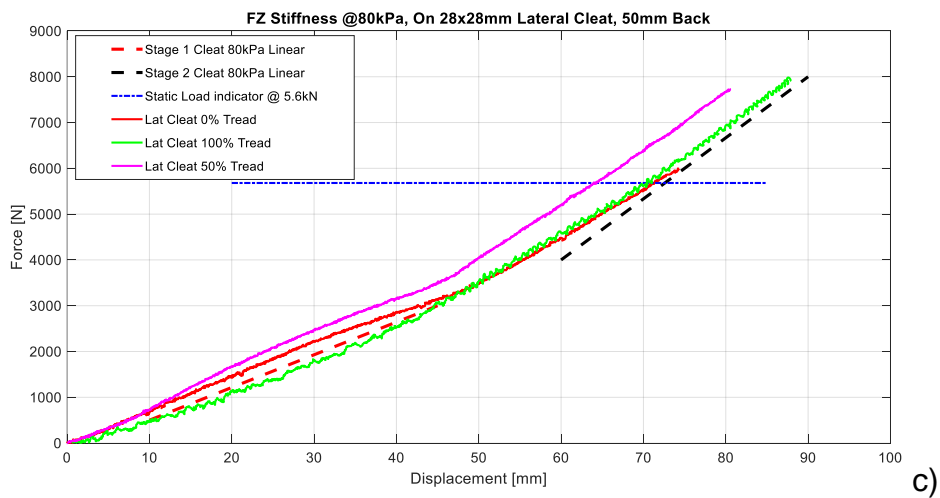
Figure 46: Vertical stiffness on a lateral cleat with different tread conditions for an inflation pressure of 80kPa at a) 50mm forward from the center, b) over the center and c) 50mm back from the center of the wheel, respectively.

This change in linear approximation is illustrated in Figure 47 where all the linear

approximations are shown compared to the measurements on a flat surface.
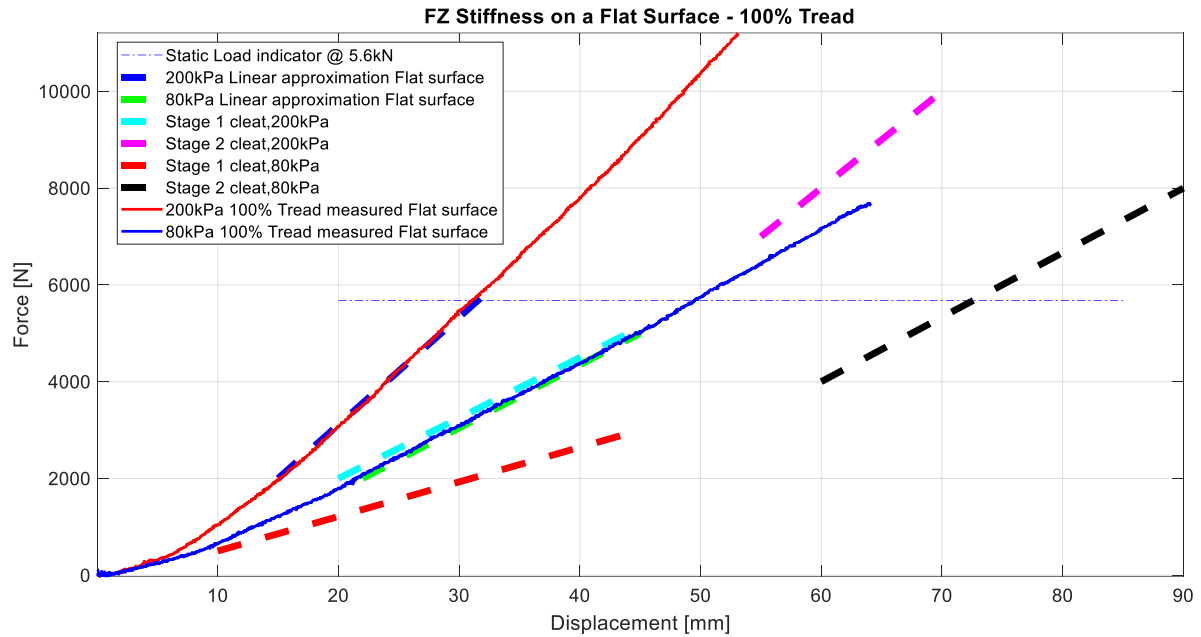
Figure 47: Change in linear approximations for vertical stiffness at 80kPa and 200kPa, with stage 1 and stage 2 over cleats.

The linear stiffness approximations are tabulated in Table 10:

Table 10: Linear vertical stiffness approximations.

	Fz Stiffness [N/mm]	Change in Stiffness [%]	% Change relative to
Flat surface contact			
200kPa	222	70	80kPa
80kPa	130		
Cleat contact			
200kPa Stage 1	120	-46	200kPa
200kPa Stage 2	200	-10	200kPa
80kPa Stage 1	71	-45	80kPa
80kPa Stage 2	133	2	80kPa

4.4.3. Vertical Static Stiffness on a Longitudinal Cleat

The longitudinal cleat was positioned in-line with the direction of travel with the cleat 50mm off set to the inside of the tyre, in-line with the center of the tyre and 50mm off set to the outside of the tyre, as shown in Figure 48 by the green, red and blue sections respectively. These positions were selected to investigate the contribution the stiffness of the lug in the tread makes to the vertical stiffness of the tyre. These positions had the longitudinal cleat in contact with the center of the lugs (inner and outer cleat position) or the edge of the lugs (in-line with the center of the tyre) as indicated by the darker section for cleat position a), c) and b), respectively. These points are also the initial contact points about which the tyre deforms up to where the rest of the tyre is in contact with the flat surface below the cleat.
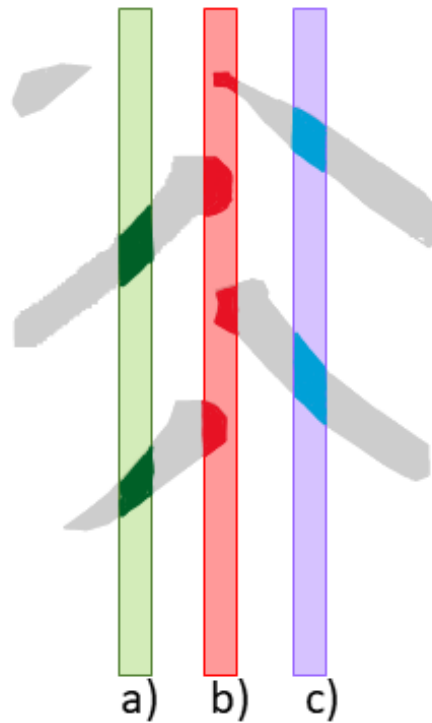
Figure 48: Longitudinal cleat positions in contact patch: a) 50mm off set in, b) in-line with center and c) 50mm off set out.

The change in vertical stiffness due to different inflation pressures, 80kPa and 200kPa, with different tread wear conditions for a longitudinal cleat in the center of the wheel is shown in Figure 49 a) and Figure 49 b), respectively. To illustrate the difference between lateral and longitudinal cleats the same stage 1 and stage 2 linear approximations are added to the graphs in Figure 49. It is seen that the vertical stiffness characteristic of the tyre does not change as much for different lateral positions of the longitudinal cleat when compared to the effect different tread wear conditions have at the center of the wheel.
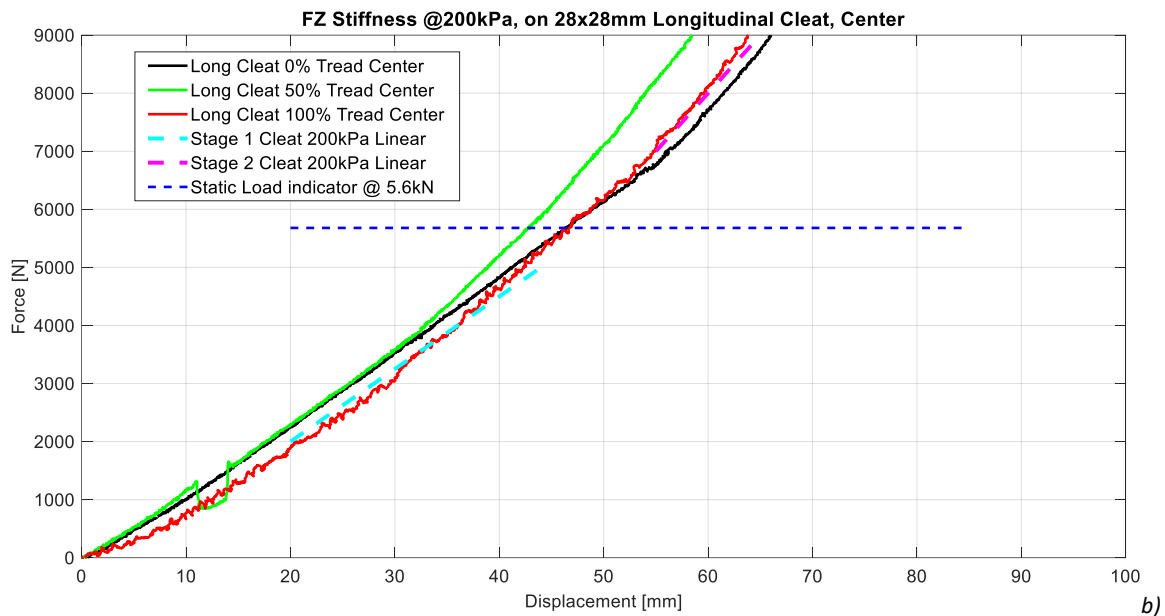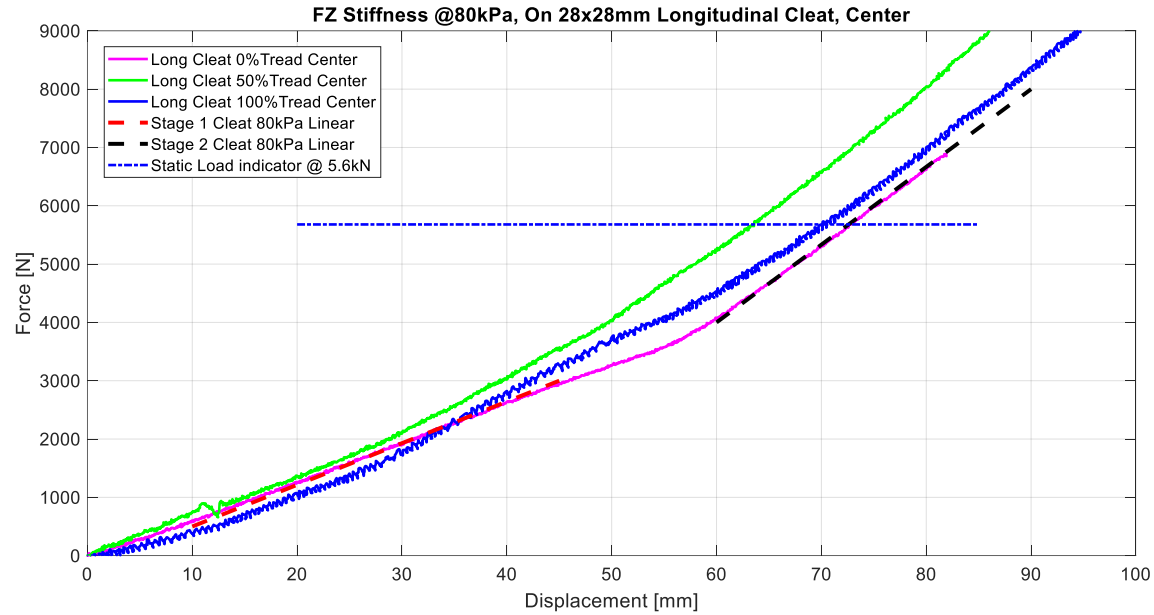
Figure 49: Vertical stiffness change due to a longitudinal cleat at different tread wear conditions, at 80kPa and 200kPa respectively.

Figure 50 is a very good representation of how the tyre will react over different cleat orientations for different tread wear conditions. The stage 1 and stage 2 linear stiffness approximations as described above are also shown in Figure 50 a), it can be seen that

for the same inflation pressure at 100% tread condition the tyre stiffness change is relatively small (in the order of 10% difference) for a lateral or longitudinal oriented cleat. This changes significantly as the tyre tread wear condition changes from 100% to 0% tread where the amount of tread on the belt directly affects the belt radial stiffness. This can be seen in Figure 50 b) and Figure 50 c), respectively. The stiffness transition point from stage 1 to stage 2 moves and requires more vertical displacement to take place with less tread on the tyre.

The figures in this section show that when a tyre travels over a cleat in the lateral or longitudinal orientation, one can expect up to a 46% decrease in vertical stiffness with up to a 10% change in stiffness during stage 2, depending on the tread wear condition, where the vertical stiffness returns to nearly the same stiffness as measured on a flat surface at high vertical loads. The combined tread block and belt radial stiffness contribute to lower vertical stiffness at lower vertical loads whereas at higher vertical loads the main contribution to the vertical stiffness is from the compression of the air volume inside the tyre which translates to the side wall radial stiffness. It is noted that the transition from stage 1 to stage 2 stiffness is tread wear dependent and independent of the inflation pressure as indicated by the vertical green dash lines in Figure 50 for the lateral cleat and the vertical green dash-dot lines for the longitudinal cleat.
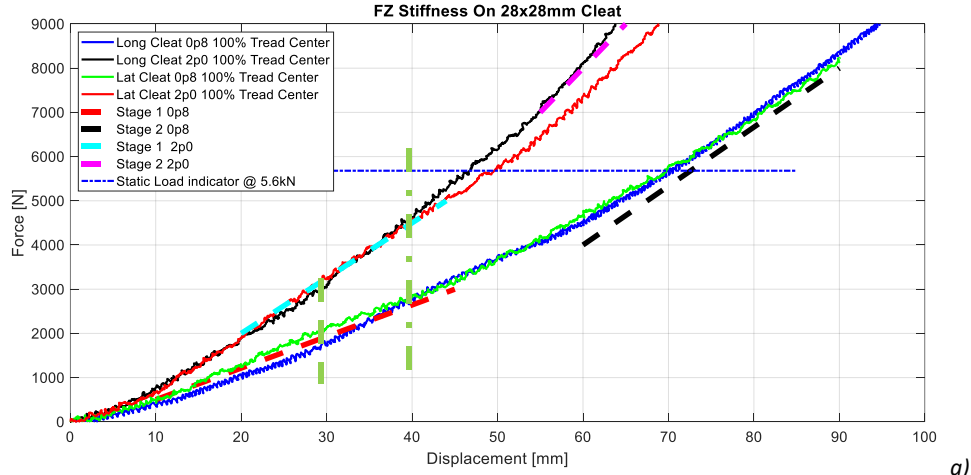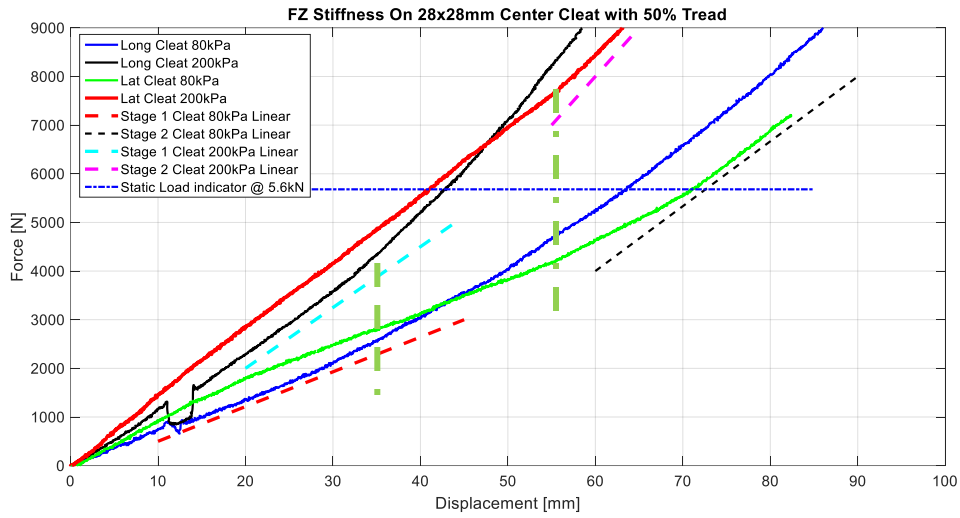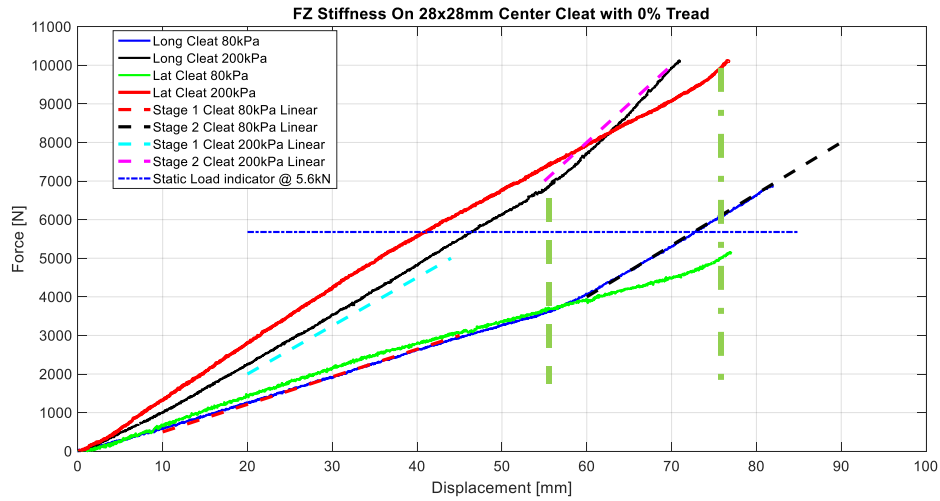
Figure 50: Vertical stiffness comparison over lateral and longitudinal cleats at 80kPa and 200kPa for different tread wear conditions, with transition from stage 1 to stage 2 stiffness indicated by the vertical green dash lines for the lateral cleat and the vertical green dash-dot lines for the longitudinal cleat.

The stiffness transition from stage 1 to stage 2 can be estimated by calculating the beam deflection of a simply supported beam, as described in eq. (16), (Shigley, 1986), for a single point contact at the center of the beam. The beam in this case is the lug and carcass of the tyre deforming about the cleat as shown in Figure 51. The assumption of a single point contact is made due to the size of the cleat, in the order of 10 to 20% relative to the dimensions of the contact patch and length of the lug/beam. The point contact approximation also eliminates the effect of the cleat-lug cross interaction which is in the order of 45 degrees for a lateral or longitudinal oriented cleat as shown in Figure 45 and Figure 48, respectively. This allows for a simplified 2-D analysis for both lateral and longitudinal cleat orientations.

$$\delta_{lugFz} = \frac{F_z \, l_{lug}^{\,3}}{48 \, E \, I_{tread}} \qquad\qquad \text{eq. (16)}$$
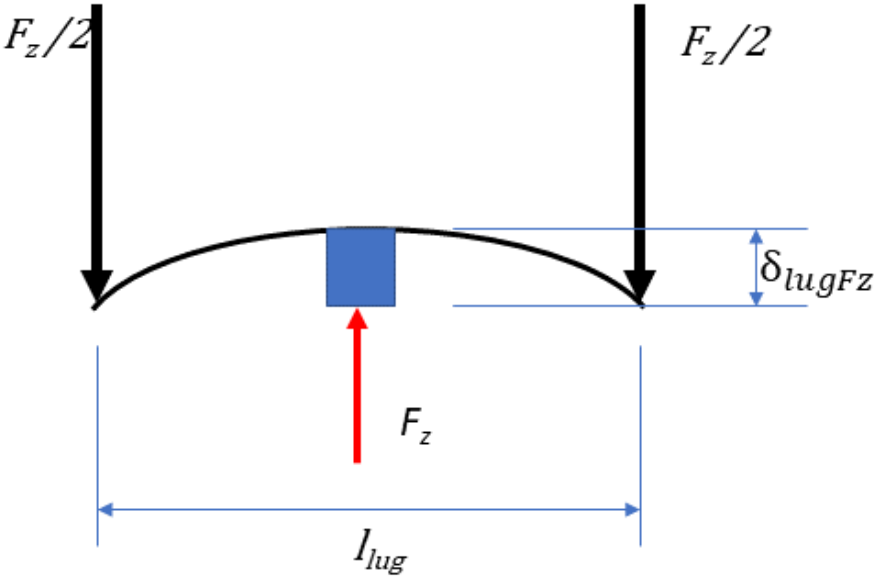
Figure 51: Deflection of lug around a cleat.

The applied force, F_z, is determined from measured results with 100% tread condition, where F_z is adjusted until the same deflection is calculated at the transition point, 30mm and 40mm as indicated by the green dash and dash-dot lines in Figure 50 a) for the longitudinal and lateral cleat orientation, respectively. The same force can then be used to estimate the deflection for different tread wear conditions. The force values used were $F_{static}/4$ and $F_{static}/3$ for the longitudinal and lateral cleats respectively. The length of the lug, l_{lug}, as measured on the tyre, is 165mm for the tyre in question. The Young's modulus for the rubber, E, was calculated with the use of eq. (17) (cosin scientific software, 2017), with the use of the Shore A Hardness value, s, of 65 for the tyre in question.

$$E = 218300(1.0482792^s) \qquad\qquad \text{eq. (17)}$$

The moment of inertia of the lug section, I_{tread}, is determined from the cross section of the lug and thickness of the carcass of the tyre as shown in Figure 52, with the base width the distance between 2 lugs on the tyre, which is 108mm for the tyre in question.
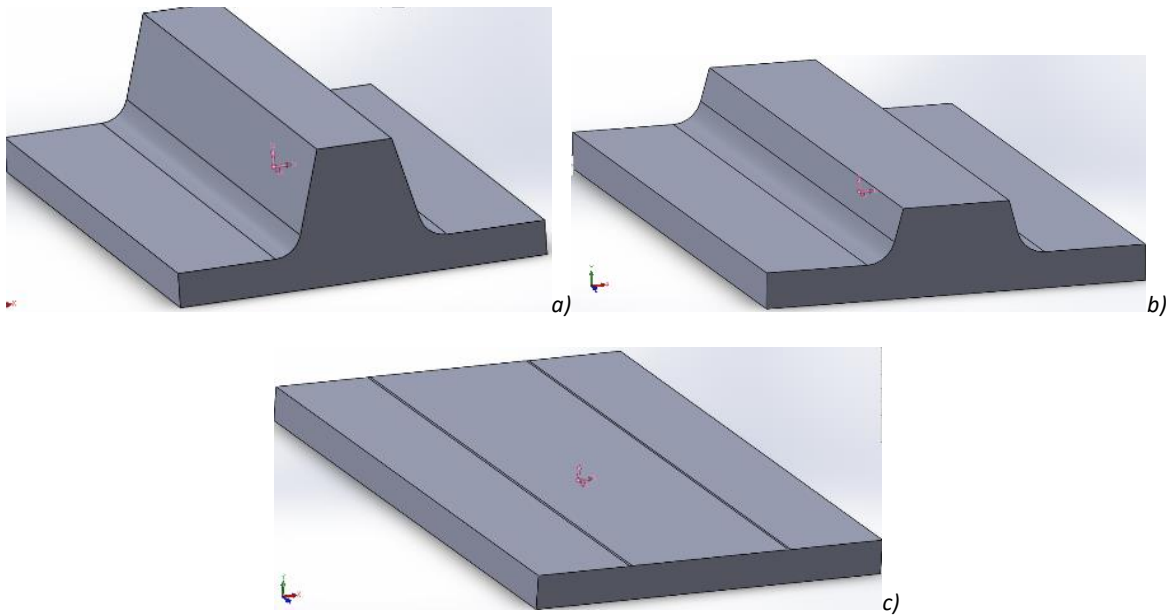
Figure 52: Cross section for a)100% Tread, b)50% tread and c)0% tread.

The results from the calculated and measured deflection, as indicated by the green dash and dash-dot lines in Figure 50, are tabulated in Table 11. When comparing the calculated deflection to the measured deflection the maximum error is in the order of 8.5%. This analysis proves the direct relationship between the tyre stiffness and the lug geometry, which is independent of the tyre inflation pressure.

Table 11: Stage 1 to Stage 2 transition point, measured vs. calculated

	Cleat orientation		Tread Condition		
			100%	50%	0%
Measured Deformation[mm]	Lateral		40	55	75
	Longitudinal		30	36	55
Calculated Deformation[mm]	Lateral		40.5	52.1	78.6
	Longitudinal		30.4	39.0	59.0
	% Difference from measured	Lateral	-1.2	5.3	-4.8
		Longitudinal	-1.2	-8.5	-7.2

4.4.4. Longitudinal Static Tyre Characteristics as a Function of Tread Wear

The longitudinal static/non-rolling stiffness measurements were conducted on the STTR on P80 grit sandpaper as shown in Figure 10 a). This directional characteristic can also be referred to as the tangential stiffness. Similar longitudinal stiffness is measured in the linear section between -40mm and 40mm longitudinal displacement of 100% to 50% tread condition at an inflation pressure of 80kPa and 200kPa. The longitudinal stiffness and maximum traction force increase significantly as the tread wear condition nears 0% as shown in Figure 53.
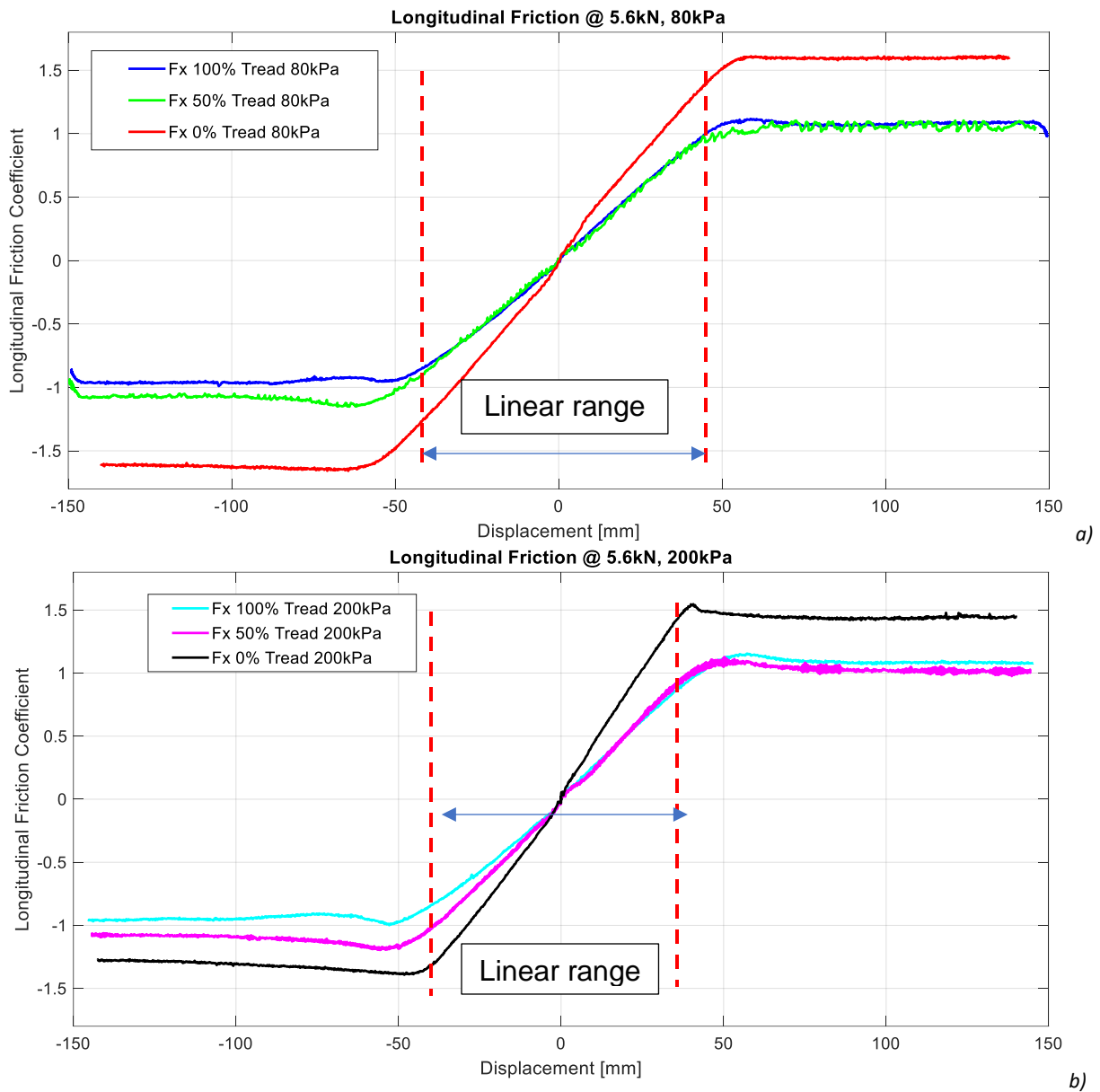
Figure 53: Longitudinal stiffness measurements for inflation pressure of a)80kPa and b)200kPa, respectively for different tread wear conditions.

The increase in maximum traction force at 0% tread condition is directly related to the

dramatic increase of rubber in contact with the surface in the contact area as shown in

Figure 22. At 0% tread the sidewall tangential stiffness is measured and is directly

proportional to the inflation pressure as shown in Figure 53. At 200kPa inflation pressure

the effect of the lugs in the tread deforming differently for positive and negative displacements are noted in Figure 53 b). This indicate that the tread stiffness varies for opposite deformation as one might expect from a directional lug pattern tread design. At 0% tread condition the tyre carcass is the only component contributing to the longitudinal stiffness of the tyre, compared to the 50% and 100% tread condition where the lugs in the tread supply reduced stiffness to the system. The tyre carcass and lugs can thus be simplified to two springs in series, where the spring with the lowest stiffness will deform/displace the most. This indicates that the tread has a lower stiffness compared to the tyre carcass. It is found that the change in longitudinal stiffness in the linear region for different tread wear conditions and inflation pressures can increase by up to 24% with a tread wear change from 100% tread to 50% tread and an increase of up to 63% between 100% tread and 0% tread condition. The change in longitudinal stiffness can be a function of the carcass construction depending on whether the tyre is used as a driven or non-driven wheel. The lateral deformation of the lugs in the contact patch can also contribute to the longitudinal stiffness, where the lugs are compressed together or pulled apart during opposite longitudinal displacement as shown in Figure 54.

Lateral deformation of lugs in contact patch
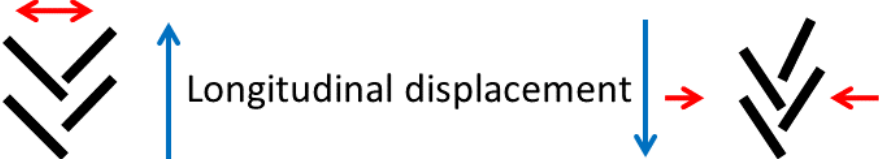
Figure 54: Lateral lug deformation in contact patch during longitudinal displacement.

A visual analysis is conducted to present and quantify the deformation of the tyre during the longitudinal displacement of a non-rolling tyre. In this analysis the deformation of a tyre before and after longitudinal displacement is compared. The bending of the lugs during the longitudinal displacement for a tyre with 50% tread depth at 200kPa is shown in Figure 55. In this figure the tyre on the right represents a tyre with only vertical deformation present. The tyre on the left is displaced by 150mm in the longitudinal direction to the left. It can be seen how the sidewall deforms in a tangential direction during the 150mm longitudinal deformation, this is shown by the red lines relative to the white markings on the tyre sidewall in Figure 55. The yellow line in Figure 55 represents the orientation of the top of the tread block before any longitudinal deformation. The green line in Figure 55 shows how much the tread block deforms due to the bending moment generated as described previously.

Figure 55: Tread deformation at 150mm and 0mm longitudinal deflection, respectively from left to right at 50% tread and 200kPa inflation pressure.

The bending of the lugs during the longitudinal displacement for a tyre with 100%, 50% and 0% tread depth, respectively, at 200kPa is shown in Figure 56. It can be seen that the sidewall tangential stiffness remains constant and is independent of the tread depth. This is shown by the red line in Figure 56 which remains in-line with the white markings on the tyre sidewall, irrespective of the amount of tread on the belt. The green line in Figure 56 shows how much the tread block deforms due to the bending moment generated as described previously. This deformation is the same for 100% tread and 50% tread. The yellow line in Figure 56 again represents the orientation at the top of the tread block before any longitudinal deformation. It can be seen that no deformation is noted at this position when the tread blocks have been removed from the tyre.
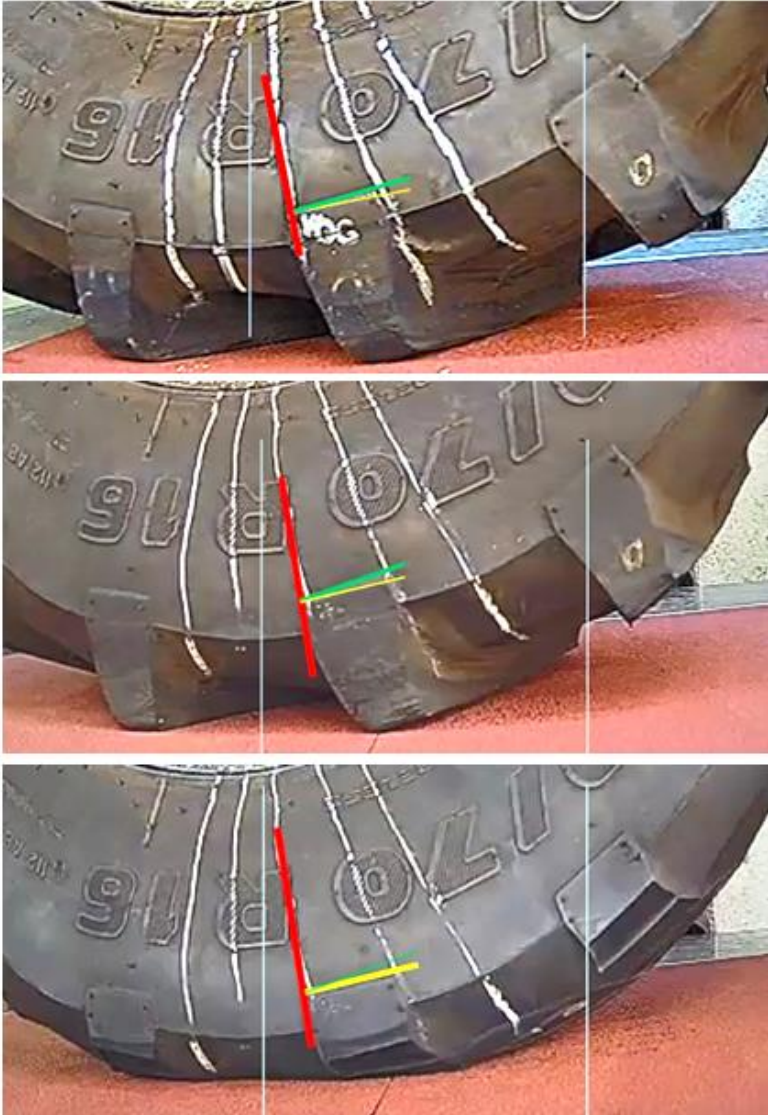
Figure 56: Longitudinal lug and carcass deformation at 200kPa inflation pressure for 100% tread, 50% tread and 0% tread, respectively from top to bottom.

The graphic representation that the sidewall tangential stiffness is directly dependent on the inflation pressure is shown in Figure 57. The red lines in Figure 57 have the same inclination as the red lines in Figure 55 and Figure 56 for the tyre at an inflation pressure of 200kPa. When comparing the red line on the left tyre in Figure 57 to the white markings in the tyre one can see the change in the sidewall tangential stiffness as the inflation

pressure is decreased to 80kPa. The belt rotation can also be seen when comparring the tyre tread block location to the yellow lines.

Figure 57: Sidewall tangential stiffness change at 150mm and 0mm longitudinal deflection, respectively from left to right at 0% tread and 80kPa inflation pressure.

4.4.5. Lateral Static Tyre Characteristics as a Function of Tread Wear

The lateral static/non-rolling stiffness measurements were conducted on the STTR on P80 grit sandpaper. Similar lateral stiffness is measured in the linear section between -50mm and 50mm lateral displacement for 100% to 50% tread condition at an inflation pressure of 80kPa. The lateral stiffness and maximum friction coefficient increase as the tread wear condition nears 0% as shown in Figure 58.
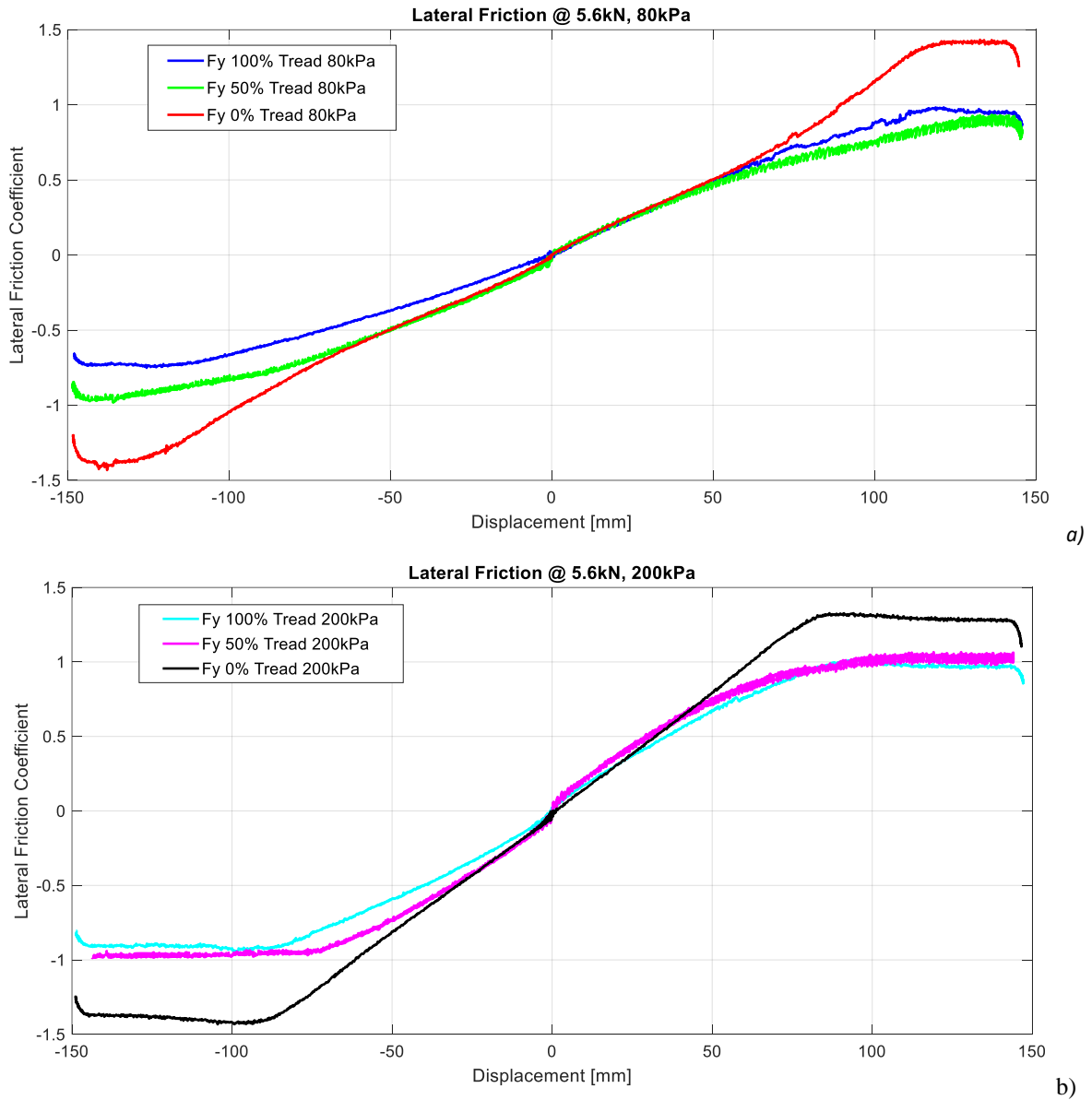
Figure 58: Lateral stiffness measurements for inflation pressure of a) 80kPa and b)200kPa, respectively for different tread wear conditions.

An increase in maximum lateral force at 0% tread condition is again directly related to the dramatic increase of rubber in contact with the surface in the contact area as shown in Figure 22. At 200kPa inflation pressure the effect of the lugs in the tread deforming differently for positive and negative displacements are noted in Figure 58b). This indicates

that the tread stiffness varies for opposite lateral displacement and is dependent on the position of the lugs in the contact patch as an un-symmetrical lug distribution is always present in the contact patch as seen in Figure 22. At 0% tread condition the tyre carcass is the only component contributing to the lateral stiffness of the tyre, thus a symmetrical characteristic is measured, compared to the 50% and 100% tread condition where the lugs in the tread supply additional stiffness to the system. This will continuously change as the lugs move through the contact patch, as a result an oscillating lateral force is always present during measurements on a rolling tyre. The most efficient way to eliminate this occurrence is to inflate the tyre at the required static load until equal amounts of lugs are in the contact patch. The tyre carcass and lugs can again be simplified to two springs in series, where the spring with the lowest stiffness will deform/displace the most and as a result lowers the lateral stiffness. It is noted that the tread's stiffness increases as the tread wear condition lowers from 100% tread to 50% tread. It is found that the change in lateral stiffness (from -50 to 50mm displacement) in the linear region for different tread wear conditions and inflation pressures can increase up to 29 % with a tread wear change from 100% tread to 50% tread and an increase of up to 51% between 100% tread and 0% tread condition at an inflation pressure of 200kPa. The same correlation is seen in the maximum sliding friction coefficient (at -120mm and 120mm displacement) as the tread wear conditions changes.

The drastic change in grip at 0% tread can change the characteristic of a vehicle which tends to slide/under steer in an emergency evasive maneuver, such as a lane change, to a vehicle that may roll-over during the same maneuver. As agricultural vehicles tend to

have high centers of gravity and are prone to roll-over, the change in lateral grip is a very important aspect to take note of during tyre wear.

Postulate conclusions:

V.   *The sliding friction coefficient value changes for different tread depths on an agricultural tyre as a result of the increase in the amount of rubber in the contact patch.*

VI.   *This section has indicated that the cleat orientation does affect the vertical characteristics of the tyre. This is noted when the vertical stiffness changes from a lower to a higher stiffness, at different vertical displacements for different cleat orientations. It is noted that the location of the cleat has a small affect.*

VII. *Asymmetric longitudinal and lateral stiffness characteristics were detected. These asymmetric characteristics were not present at 0% tread conditions, this points to the lugs as the cause of the asymmetry. It is also noted that the lateral and longitudinal stiffness increases with tread wear.*

4.5.   Rolling Tyre Characteristics

Postulate:

VIII.   *Static/non-rolling tyre characteristics can be used to predict dynamic/rolling tyre*

characteristics on an agricultural tyre

The dynamic/rolling tyre friction tests were conducted with the use of the DTTT at a

vertical load of 5.68kN in order to obtain the characteristics that describe the following:

- Longitudinal force vs. longitudinal slip under braking
- Lateral force vs. slip angle
- Friction circle (combined lateral and braking force application)

Unfiltered data for a typical rolling tyre longitudinal friction coefficient vs. longitudinal slip

under braking test is shown in Figure 59. The graph shows the longitudinal forces

normalized with the vertical force to give the friction coefficient. Instead of only testing at

80kPa and 200kPa inflation pressure as used throughout this study, tests were also

performed for inflation pressures of 120kPa and 160kPa. It can be seen that the

longitudinal stiffness is very consistent and independent of the inflation pressure at 100%

tread condition. This corresponds very well to the static/non-rolling longitudinal tests

conducted on the STTR as shown in Figure 36. Tests were conducted at a speed of

11km/h with a vertical load of 5.68kN.
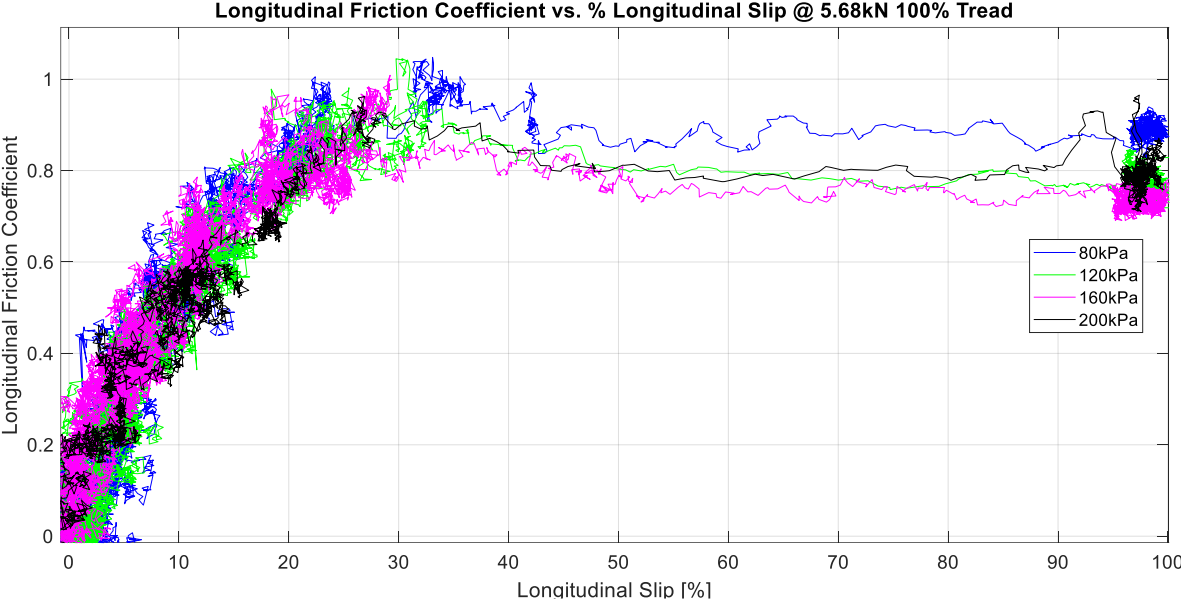
Figure 59: Longitudinal friction coefficient vs. longitudinal slip measurements under braking on Trelleborg TM700 280/70R16 at a speed of 11km/h at multiple inflation pressures.

The lateral friction coefficient vs. slip angle of a rolling tyre is as repeatable as the longitudinal test. An example of the unfiltered measured test data is shown in Figure 60, where it can be seen that the lateral stiffness of the rolling tyre is consistent and relatively independent of the inflation pressure, as the lateral stiffness only increases in the order of 10% at 200kPa inflation pressure when compared to 80kPa inflation pressure. This is the opposite of the observations (as seen in Figure 58) for a static/ non-rolling tyre where up to 50% increase is noted in lateral stiffness at 200kPa inflation pressure. This is caused by the stiffening of the carcass belt as the tyre rotates. The effect of the lugs in the tread pattern and radial runout are clearly seen in the vertical force oscillations in the data as seen in Figure 60.
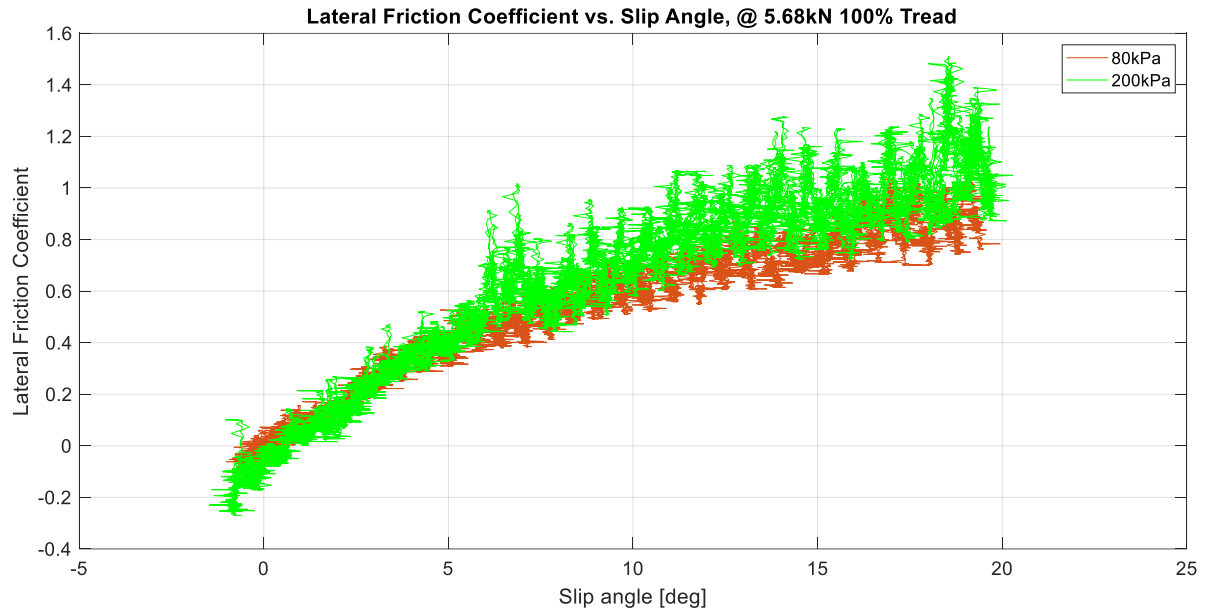
Figure 60: Lateral friction coefficient vs slip angle measurements on Trelleborg TM700 280/70R16 at 11km/h, at 80kPa and 200kPa inflation pressure.

During the friction envelope tests the tyre is rolling at a set slip angle with the brakes applied up to wheel lockup. Figure 61 shows the state of the lateral deformation of the tyre before and during lockup. This is a clear representation of why a vehicle that is operating at the limit can only generate a maximum steering force or only apply a maximum braking force. The maximum combined forces will always be lower.

Figure 61: Friction envelope tests on Trelleborg TM700 280/70R16 at 11km/h, vertical load at 5.68kN before and during lockup at a constant lateral slip angle, respectively.

The friction envelope describes the combination of the applied longitudinal and lateral forces during different slip angles and longitudinal wheel slip, as shown in Figure 62. It can be seen that at 80kPa inflation pressure a larger longitudinal friction coefficient can be generated due to a larger footprint at 80kPa, also noted in Figure 59 during pure longitudinal slip tests. The increased side wall stiffness, due to the increased inflation pressure, correlates to the increased maximum lateral friction coefficient generated at 200kPa.
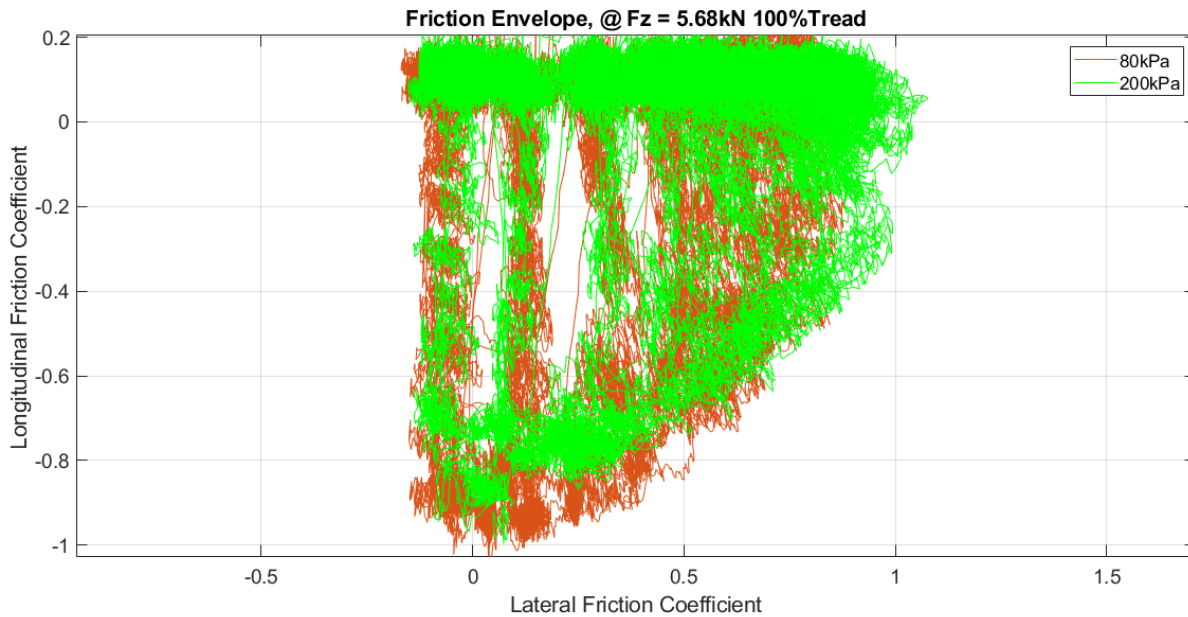
Figure 62: Friction envelop measurement on Trelleborg TM700 280/70R16 at 11km/h, at 80kPa and 200kPa inflation pressure, respectively.

4.5.1. Static/Non-rolling Tests vs. Dynamic/Rolling Tests

Outdoor dynamic tyre tests are time consuming, expensive and less repeatable than tests conducted in a laboratory. Tyre size/load limitations are a major factor when conducting dynamic/rolling tests on large tyres. If static test rig results could be used to, estimate/predict, tyre parameters that represent dynamic/rolling characteristics, it can become more affordable to obtain tyre characteristics in order to parameterize more tyre models. A method to compare the longitudinal friction coefficient as a function of % longitudinal slip of a rolling tyre to static/non-rolling longitudinal friction coefficient as a function of longitudinal displacement, is to translate longitudinal slip of the contact patch to longitudinal displacement, $D_{longStatic}$. For the dynamic longitudinal slip tests this can be

achieved by calculating the longitudinal displacement of the contact patch, D_{wheel}, relative

to the displacement of the vehicle ($D_{vehicle}$) and dividing it by the number of wheel rotations,

N_{rotate}, during the longitudinal slip period from 0% to 100% slip as shown in eq. (18):

$$D_{longStatic} = \frac{(D_{vehicle} - D_{wheel})}{N_{rotate}} \qquad \text{eq. (18)}$$

The result of this transformation of the contact patch from % longitudinal slip (% of

velocity) to relative longitudinal displacement in mm, is shown in Figure 63.
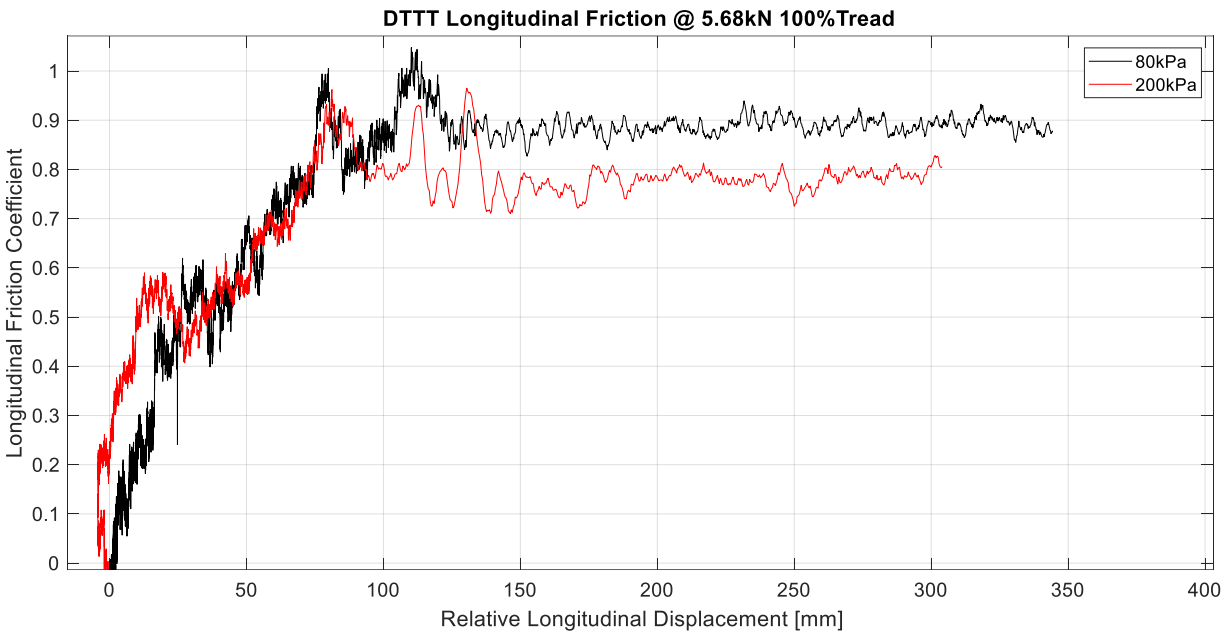
Figure 63: Translated Rolling Longitudinal Friction Coefficient vs. Relative Longitudinal Displacement at 80kPa and 200kPa inflation pressure, respectively.

Figure 64 shows the comparison between the static tests conducted on the STTR on

concrete, the DTT static tests at Gerotek and the translated DTTT tests.

Longitudinal Friction, @ 5.68kN 100%Tread
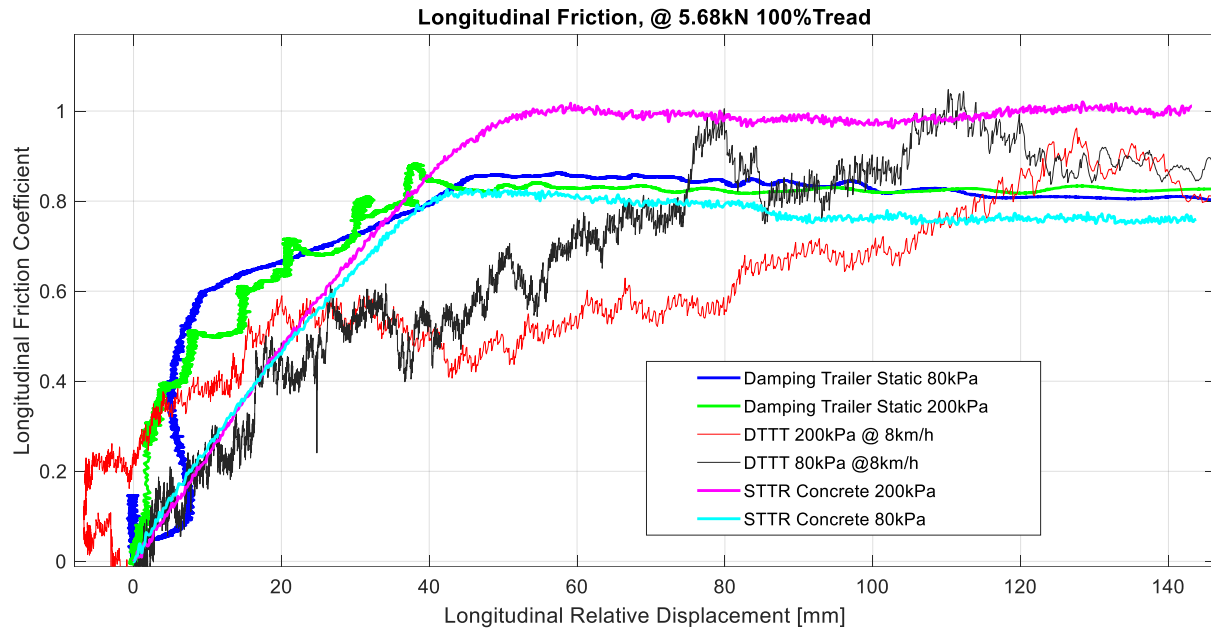
Figure 64: Longitudinal Friction Coefficient vs. Longitudinal Displacement from different test methods.

Relatively good correlation is seen between the three test methods. The initial longitudinal stiffness correlates very well (first 30mm displacement, where vehicles operate most of the time), with the maximum sliding friction coefficient within 10 to 20% for the tests conducted on the Gerotek track with the DTTT. The DTT results correlate very well with the STTR results at 80kPa, the difference at 200kPa is due to the difference in boundary conditions, which also contributes to the results from the DTTT. Digital Image Correlation techniques is a possible method to use in order to correlate the static tests to dynamic tests where the longitudinal force vs. % longitudinal slip can be compared (Botha and Els, 2015). This needs to be investigated further and is beyond the scope of the current study.

The lateral friction coefficient vs. slip angle tests can be translated to the lateral friction coefficient vs. 90-degree lateral displacement with the use of trigonometry to calculate

the lateral displacement component, $Slip_{Lat\_mm}$, at the specific lateral slip angle, β, and the

contact patch length, L, as shown in eq. (19):

$$Slip_{Lat\_mm} = Ltan\beta \qquad\qquad \text{eq. (19)}$$

As seen in Figure 65, the lower inflation pressure tests on the STTR does not correlate

very well due to the stiffening of the belt when the tyre rotates on the DTTT. The belt

stiffening has the largest effect on the lateral force generated at lower inflation pressures.

The result of the comparison between the static tests on the STTR on concrete with the

lateral translation of the friction envelope tests and lateral force vs. slip angle tests at

200kPa inflation pressure with 100% tread is shown in Figure 66. Very good correlation

is seen at the high inflation pressure tests. This shows consistency for all three tests

methods being either static or dynamic.
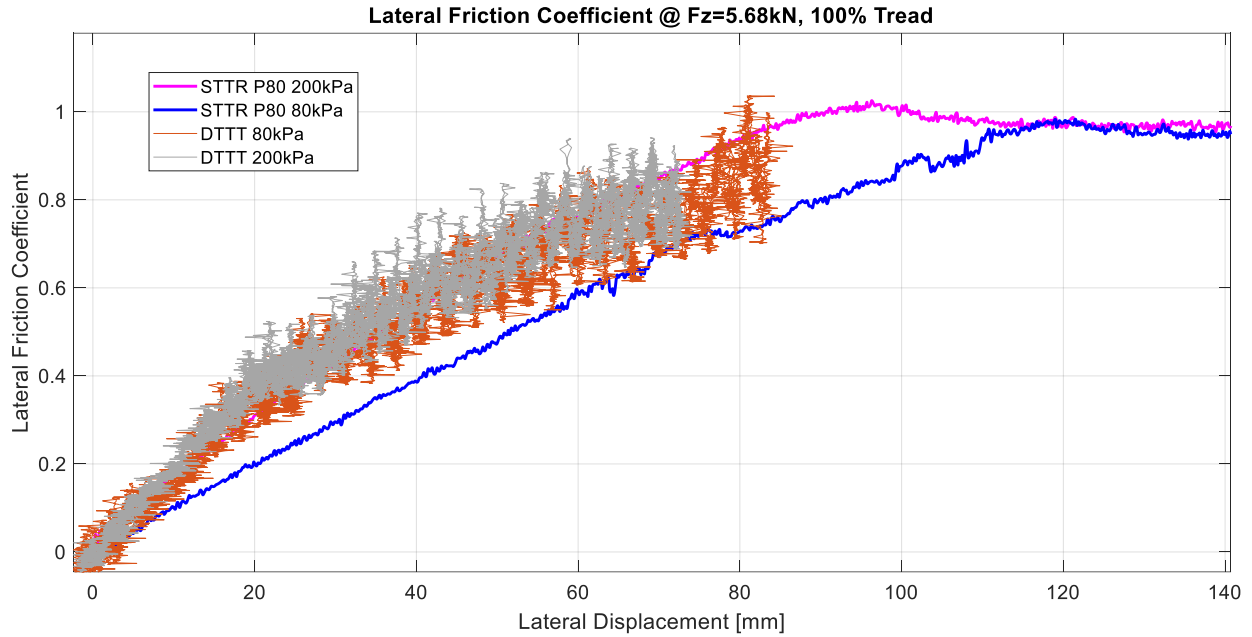
Figure 65: Dynamic lateral friction coefficient tests compared to static testes on P80 at 80kPa and 200kPa inflation pressure for 100% tread, respectively.
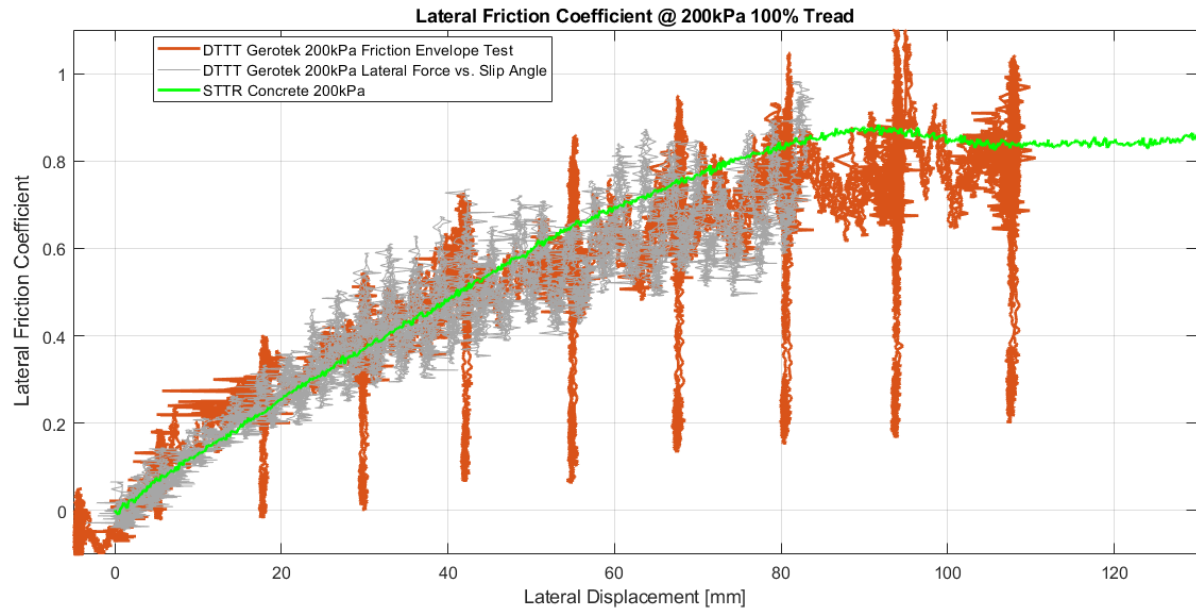
Figure 66: Dynamic lateral friction coefficient tests compared to static tests on concrete at 200kPa inflation pressure for 100% tread.

DIC techniques can possibly be used to measure the amount of lateral tyre deflection during lateral force vs. slip angle tests. This can then be used to validate the current findings. The use of DIC was beyond the scope of this study but can be investigated in future work.

Postulate conclusion:

VIII.   *Friction coefficients obtained from static/non-rolling tyre can be used to predict dynamic/rolling friction coefficients on an agricultural tyre at high inflation pressures. Construction vehicle tyres tend to have very stiff sidewalls and may be a very good application to test this theory.*

4.6.   Damping

Postulate:

IX.   Tyre damping correlates to inflation pressure and not to tread condition on an agricultural tyre

The damping coefficient is calculated with the tyre rolling over the same 28x28mm cleat as used during the static tests on the STTR. The response of the DTT is measured when driving over the cleat at 11km/h on a flat surface described in section 3.4.1. The vertical force measurement on the wheel is used during these calculations with the static load deducted to work with a mean value of zero. It can be seen in Figure 67 and Figure 68 that the measured response and calculated damping curve amplitude, as described with eq (7), correlate well for both the 80kPa and 200kPa inflation pressures, respectively. It is noted that the tyre force at 80kPa inflation pressure is in the order of 50% lower compared to 200kPa inflation pressure. The vibration seen after 5 seconds is not free vibration any longer, but rather forced vibration caused by the tread blocks, tyre imbalance, and radial runout as well as inputs from the expansion joints in the concrete road. The forced vibration is seen due to the fact that the DTT is not fitted with suspension and dampers.
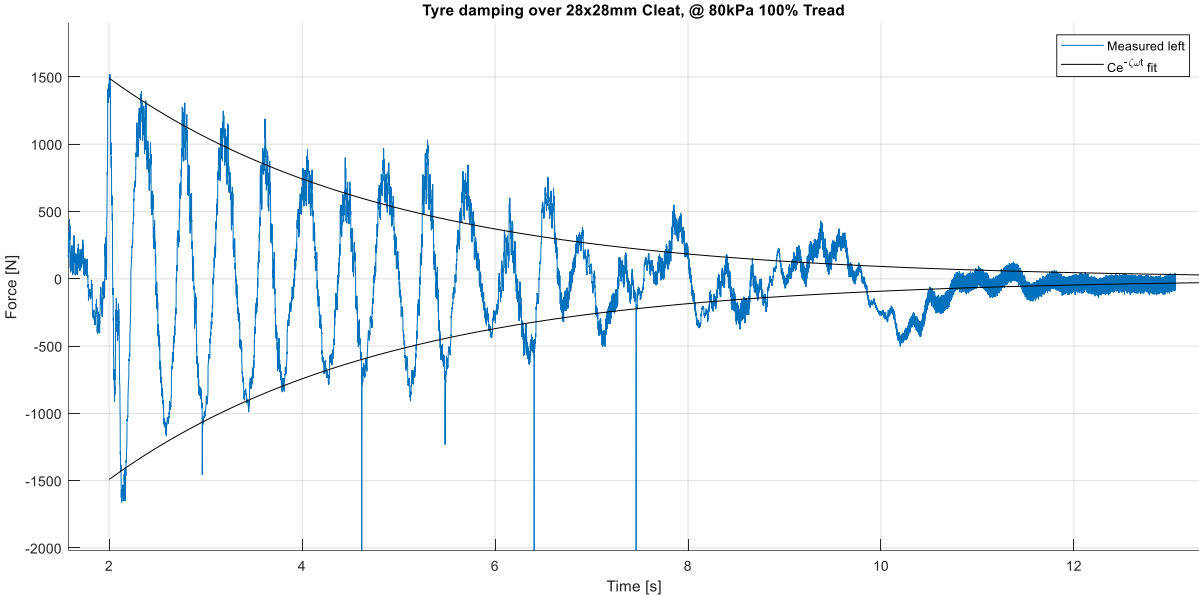
Figure 67: Measured vertical damping force and calculated damping curve amplitude on Trelleborg TM700 280/70R16 over 28x28mm cleat (11km/h) at 80kPa inflation pressure.
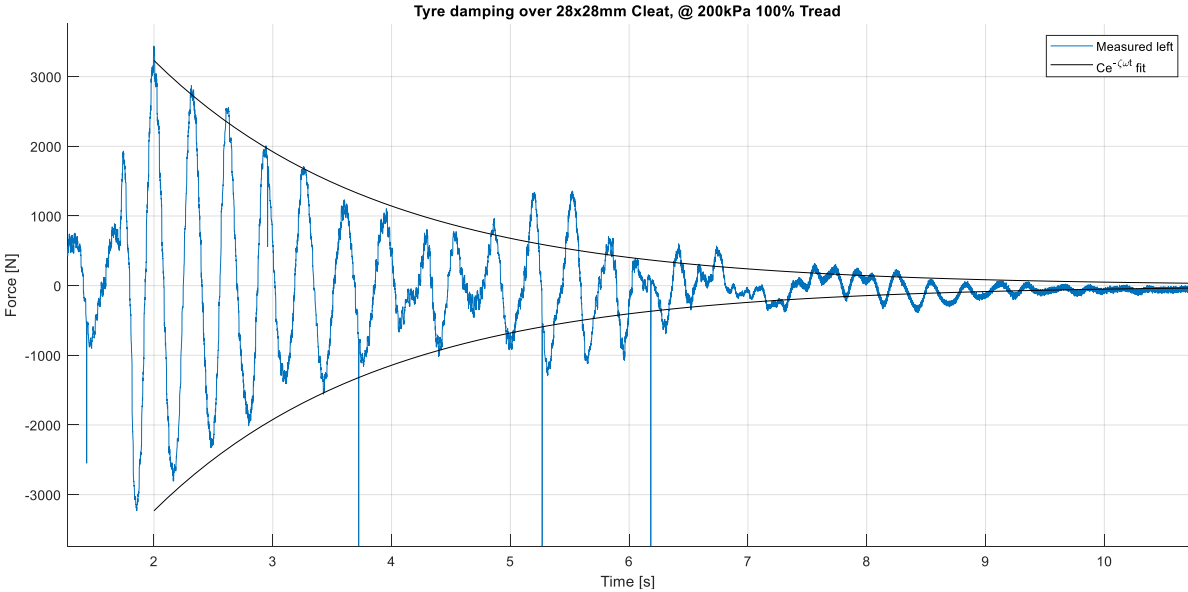
Figure 68: Measured vertical damping force and calculated damping curve amplitude on Trelleborg TM700 280/70R16 over 28x28mm cleat (11km/h) at 200kPa inflation pressure.

The linearized and averaged damping coefficient and natural frequency, as calculated using the logarithmic decrement, as described in section 3.4.1 of the DTT setup is supplied in Table 12:

Table 12: Trelleborg TM700 280/70R16 Damping results at 5.68kN wheel load @ 11km/h

Damping Results	*200kPa*	*80kPa*	*200kPa*	*80kPa*	*200kPa*	*80kPa*
Tyre Tread [%]	100		50		0	
Damping Coefficient [N s/m]	706	431	685	411	615	378
Damped natural frequency [Hz]	3.14	2.47	3.19	2.50	2.83	2.43

The results from Table 12 show that the inflation pressure has a larger impact on the damping coefficient compared to the tyre tread wear. The damping coefficient decreases on average by 39% with a decrease in inflation pressure from 200kPa to 80kPa. The effect the tyre tread wear has on the damping coefficient is only in the order of a 3% decrease from 100% tread to 50% tread, with a 12% decrease from 100% tread to 0% tread, irrespective of the inflation pressure.

Postulate conclusion:

IX.   *This section has shown that the damping coefficient increases with an increase in inflation pressure and that the tread condition has a much smaller affect.*

4.7. Motion Resistance

Postulate:

X.   *Motion resistance measurement on an agricultural tyre is dependent on the method used*

XI.   *Inflation pressure has a larger effect on motion resistance compared to tread wear condition on an agricultural tyre*

The equipment used in this study for measuring motion resistance was not aligned to a master laboratory, however the same measuring equipment was used as far as possible during all of the tests conducted during this study, with the aim of comparing measurements from different test methods on the same tyre. This means that the accuracy of the absolute values cannot be guaranteed, but the measurement methods can be compared to each other with high confidence. Testing was conducted over a period of six weeks with the tyres at 100% tread condition. The intent of this part of the study is to compare motion resistance values calculated from different test methods, namely drum, coast down, towed vehicle and trailer tests, on the same tyre. A test speed of 11 to 18km/h was selected as this is the normal operating speed range of the vehicle that these tyres would be used on. The speed rating of the tyre is 40km/h. The same non-deformable, concrete test section was used for the coast down, towed vehicle and motion resistance trailer measurements, thus eliminating the effect of the terrain from these measurements. All tests were conducted at unregulated tyre pressures, which allowed

the tyre pressure to increase and stabilize during the tests. The tyre pressures were verified at cold/start conditions and not adjusted during tests, only monitored with the use of a pressure transducer mounted in the rim during some of the tests.

4.7.1. Drum Tests

The drum tests were conducted with the tyre mounted on a steel rim and running on a smooth aluminium surface drum with a radius, R_{drum}, of 0.8m. the surface roughness of the drum was measured to be in the order of R_a = 0.896µm. The ambient temperature, t_{amb}, during the tests were kept at 25 °C in an air-conditioned laboratory. The applied vertical load, L_m, was measured with the use of a load cell with a maximum rating of 10kN. The input torque on the drum, T_t, was also measured. The drum test setup is shown in Figure 69. Tests were conducted at a vertical load, L_m, of 2452N at multiple velocities, v, including 18km/h and cold inflation pressures of 80 and 200kPa respectively. A lower vertical load, compared to the vehicle and trailer tests were used due to the width limitation of the drum, as the tyre should not deform around the drum surface during the test. Tyre carcass temperature and pressure were monitored with the use of a FLIR thermal imaging camera and pressure transducer mounted in the rim. All coordinate systems are defined as per ISO 8855:2013.

The torque method described in ISO 28580:2009 was used to measure the motion resistance coefficient, C_r, of the tyre on the drum test rig. During these tests the input

torque, T_t, on the drum was measured, with L_m at 2452N. The parasitic losses, F_{pl}, are

calculated using eq. (20)

$$F_{pl} = \frac{T_{no\_load}}{r} \qquad \text{eq. (20)}$$

The measured torque, T_{no_load}, is the torque required to keep the drum rotating with no

applied load on the drum from the tyre, with r, the radius of the test drum. The motion

resistance force, F_r, expressed in Newton is calculated using eq. (21)

$$F_r = \frac{T_t}{r} - F_{pl} \qquad \text{eq. (21)}$$

The C_r is then calculated using eq. (22)

$$C_r = \frac{F_r}{L_m} \qquad \text{eq. (22)}$$
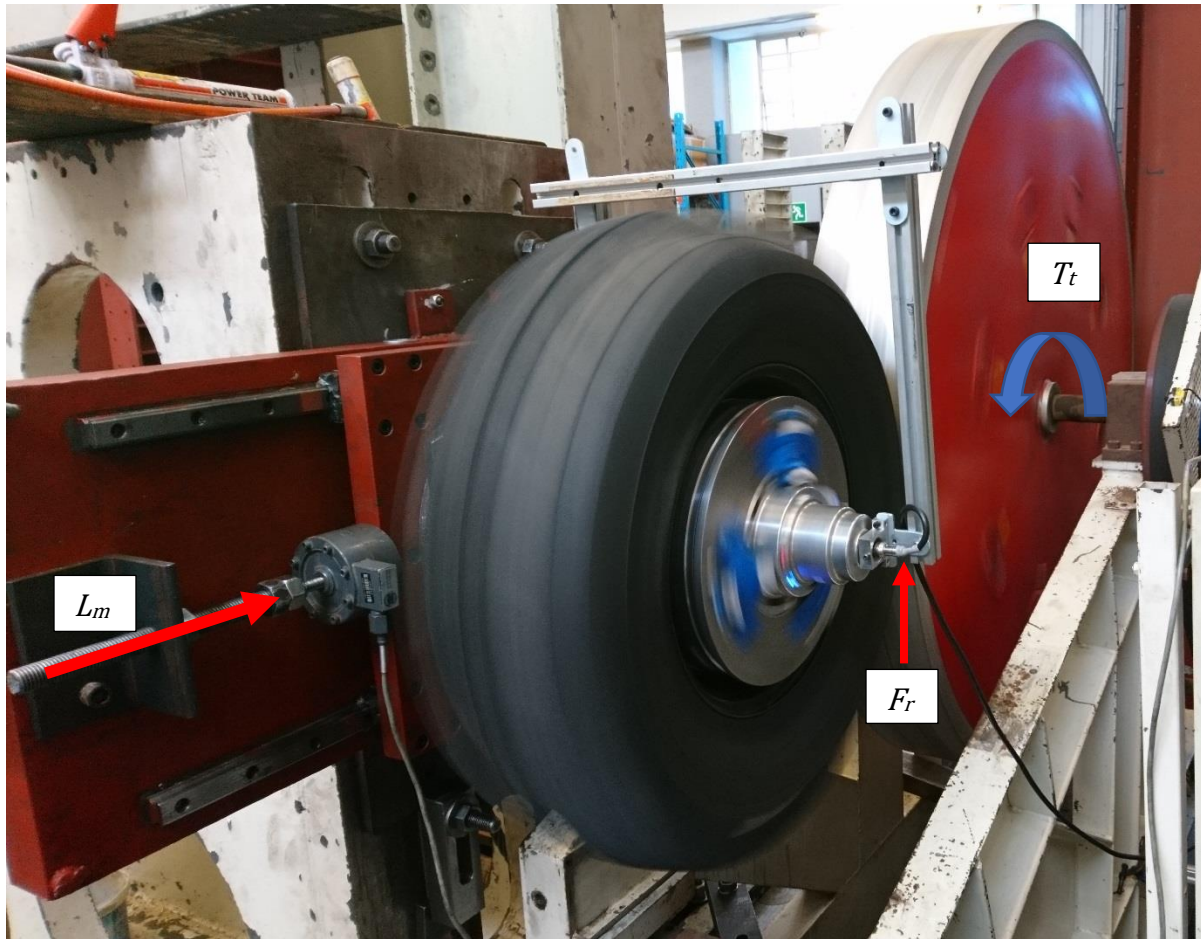
Figure 69: Drum test rig.

Temperature correction for tests conducted at different ambient temperatures, are applied using eq. (23).

$$F_{r25} = F_r[1 + K_t(t_{amb} - 25)] \qquad \text{eq. (23)}$$

where the temperature constant, K_t, is a constant value of 0.010, as described in ISO 28580:2009.

Drum diameter correction is performed using eq. (24).

$$F_{r02} \cong K_r F_{r01} \qquad\qquad \text{eq. (24)}$$

Where eq. (25) describes K_r:

$$K_r = \sqrt{\frac{(r_1/r_2)(r_2+r_T)}{r+r_T}} \qquad\qquad \text{eq. (25)}$$

With

$r_1 =$ 0.8m (for the 1.6m diameter drum used in the current study)

$r_2 =$ 1m (for the standard drum as described in ISO 28580:2009)

r_T is one half of the nominal tyre diameter, 0.4m (for the test tyre used in current study)

$F_{01} = F_{r25}$

It should be noted that the radial run out of these agricultural tyres with large lugs are more than the allowed 0.5mm, as specified in ISO 28580:2009, however the ISO specification was used as a baseline/reference for the tests conducted.

The results for the tests conducted on the drum test rig, revealed the relationship between motion resistance coefficient, inflation temperature and tyre carcass temperature as they are all directly related. Tests were conducted at a constant speed of 18km/h, from an ambient temperature of 25 °C and initial inflation pressure of 200kPa, for 10 hours on day 1 and for 5 hours on day 2. Data sets were recorded at 1kHz, on a 16-bit resolution data acquisition system, for one minute out of every 10 minutes rolling. Figure 70 shows how the pressure and temperature are directly proportional to each other, compared to the C_r

which decreases as the pressure inside the tyre and tyre carcass temperature increase and stabilize as seen in Figure 71 and Figure 72.
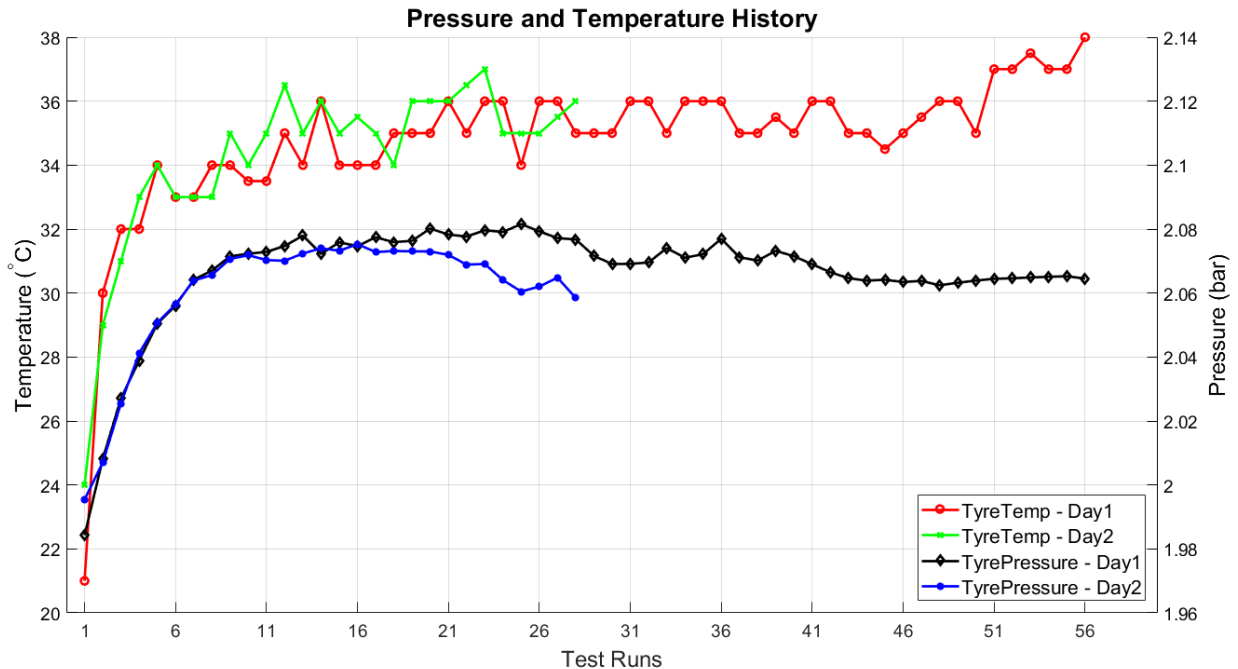
Figure 70: Pressure and temperature during drum test with a test run every 10 minutes.

The boxplots in Figure 71 and Figure 72 show the mean (in red) and variance in the measured data on this tyre with large lugs. The variance is due to a combination of factors in the form of the imbalance, radial run out of tyres with large lug and rolled steel rims being not concentric when compared to a machined Aluminium rim. The natural frequencies and mode shapes of the tyre can also contribute as they occur at very low frequencies and sometimes fall within the operating frequencies of tyres with large lugs (Becker and Els, 2011). Investigating all these geometry effects was outside the scope of this study.
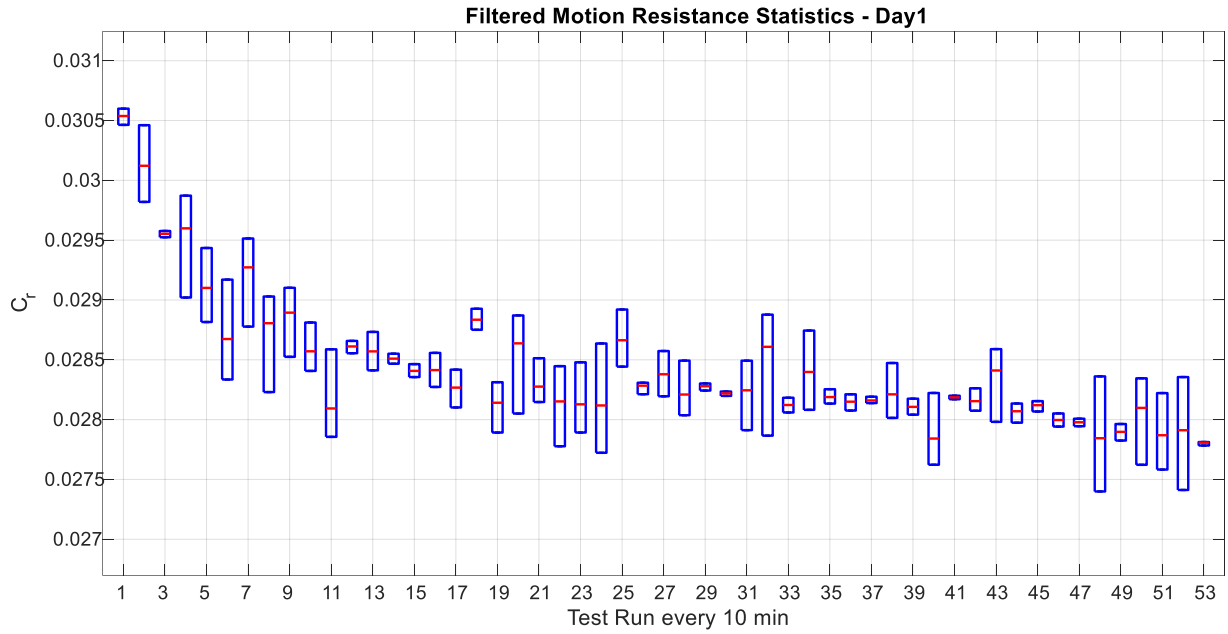
Figure 71: Drum Test results day 1, with a test run every 10 minutes.
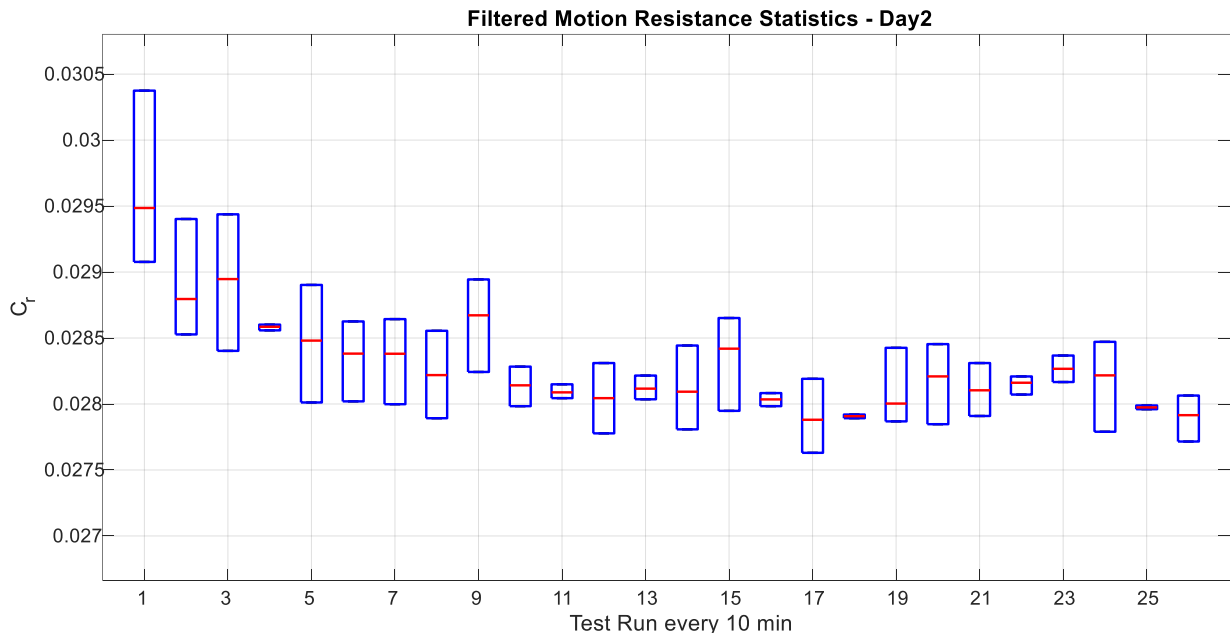
Figure 72: Drum test results day 2, with a test run every 10 minutes.

It is known that the C_r decreases as the tyre pressure is increased. The same trends are seen for both test days as the tyre pressure increases and temperature stabilizes when it

reaches operating conditions. The mean C_r from the drum test results are shown in Figure 73. The C_r stabilizes during both test days at around 0.028, which indicates a stable and repeatable test setup.
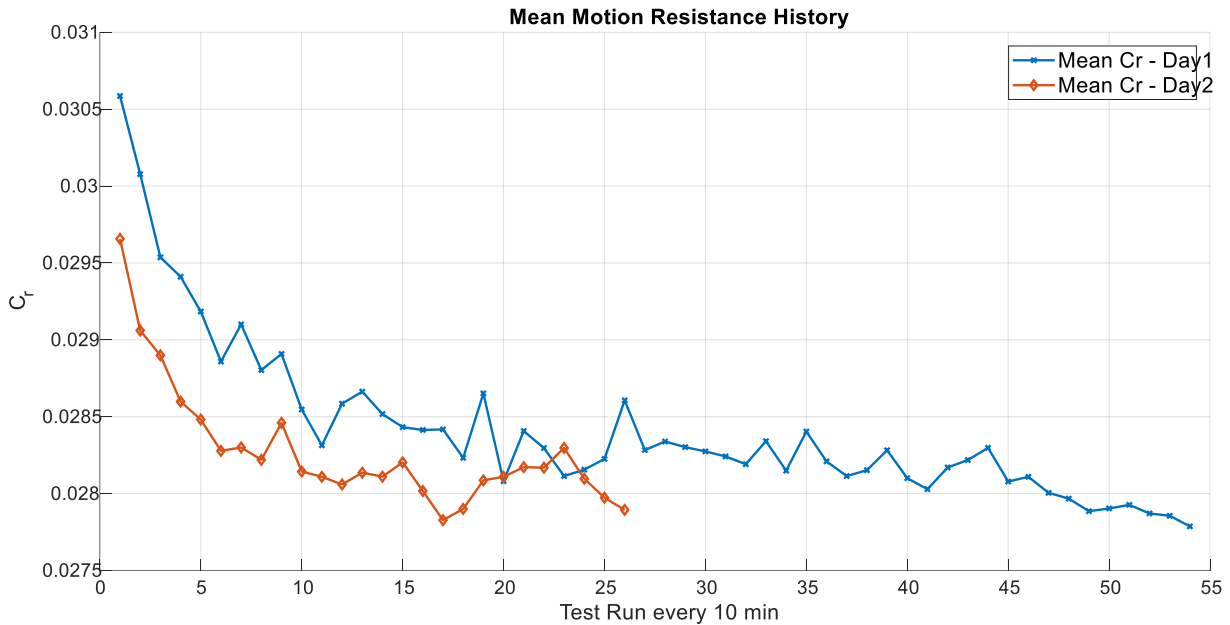
Figure 73: Mean motion resistance drum test.

4.7.2. Coast Down

The coast down tests were conducted on the K-L section of the suspension tracks at Gerotek, as described in section 3.7.1. The test vehicle fitted with the Trelleborg TM700 280/70R16 tyres was the test vehicle used, as shown in Figure 16.

Tests were conducted at tyre inflation pressures of 80 and 200kPa respectively. Test runs were done in both Easterly and Westerly directions over the same test section. The

ambient test conditions ranged from 25 to 30 °C with wind still conditions. Two drivetrain configurations were used during the tests. The first setup was a standard drive train setup where the test vehicle was driven up to a speed of just above 40km/h after which the transmission was placed in Neutral and the vehicle was allowed to coast to a standstill. SAE J2263-1996 specifies in section 12.6 that data analysis on coast down test should be restricted to velocities from 115 to 15km/h, however the maximum speed of 40km/h was a restriction set by the tyre speed rating (as is often the case with agricultural/off-road tyres). In the second drivetrain configuration, the drive shafts of the vehicle were disconnected from the hubs. This was done by replacing the splined spiders that connect the drive shafts to the hubs, with spline less spiders as shown in Figure 74.

Figure 74: Standard splined spiders (left) and custom spineless spiders (right) on wheel hubs.

For the second drivetrain configuration, the test vehicle was pushed with another vehicle up to a speed above 40km/h and allowed to coast down to a standstill. These two configurations were used to investigate the inertial and energy loss effects of the

connected and disconnected drivetrain on the measured motion resistance during coast down tests.

The inertial effects from the wheels were taken into consideration when calculating the road load from the coast down, R_{RL_cd}, with the use of the measured acceleration, a, as described in SAE J2263, 1996 as shown in eq. (26):

$$R_{RL\_cd} = Ma$$
<div align="right">eq. (26)</div>

With the acceleration, a, calculated from the speed vs. time measurements as recorded from the GPS during the coast down.

The inertia of the front and rear wheels was measured and calculated with the use of the Bifilar pendulum method as described in section B.3.2 of ISO 28580:2009. Compensated road load, R_{RL_Comp} is described in eq. (27):

$$R_{RL\_comp} = \left(M + 2 \left(\frac{I_{rw}}{(r_{rr})^2} \right) + 2 \left(\frac{I_{fw}}{(r_{rr})^2} \right) \right) * a$$
<div align="right">eq. (27)</div>

The wheel inertias effectively increase the apparent mass of the vehicle which increases the R_{RL}. The higher road load will result in a higher C_r because the equation to calculate C_r remains the same by using eq. (28):

$$C_r = \frac{R_{RL\_comp}}{M*g}$$
<div align="right">eq. (28)</div>

Figure 75 shows the coast down measured speed vs. time results. The cost down tests were very repeatable in both the Easterly and Westerly directions.
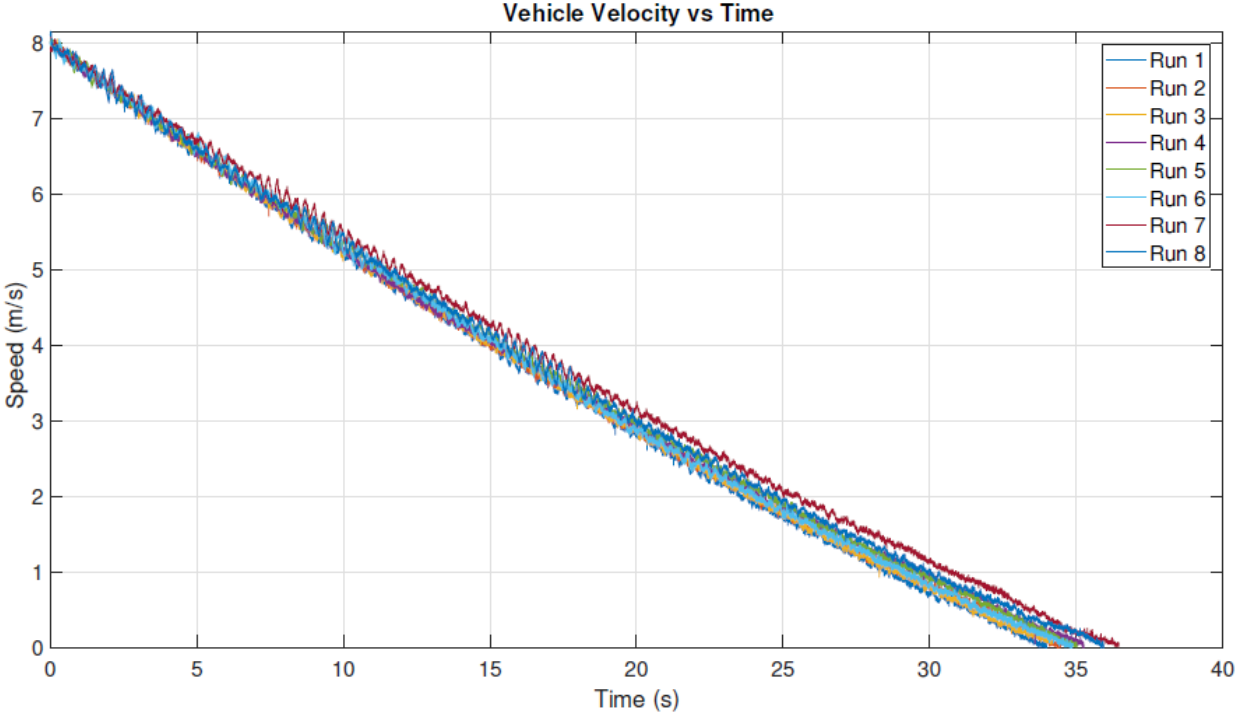
Figure 75: Coast down tests Easterly and Westerly speed vs. time results.

The calculated C_r results for the coast down tests are shown in Figure 76 and Figure 77 for inflation pressures of 200kPa and 80kPa respectively. In these graphs the inertial effects as well as the disconnected drivetrain (DT) effects are shown. The aerodynamic drag contribution to the motion resistance or road load varies from a calculated 146N down to zero during the coast down from 40-0km/h. All of the different combinations of inertial effects and drivetrain disconnected can result in a 16% difference in C_r measurements.

Additional tests were conducted on the drum test rig at velocities from 3 to 24km/h in 3km/h increments at inflation pressures of 200kPa and 80kPa respectively. This was done to facilitate the comparison of the drum tests at different velocities to the coast down tests. These results are also shown in Figure 76 and Figure 77 respectively together with the

coast down methods. From these results it is clear that the C_r is directly proportional to the velocity and inflation pressure. It is noted that the C_r as calculated with the use of the coast down methods diverge considerably when compared to the drum tests at different velocities.

An interesting phenomenon noted in Figure 76 and Figure 77 is that the C_r as measured with the drum test and motion resistance test trailer resulted in a higher value compared to the coast down test at very low velocities. It is expected that the C_r values calculated from the coast down test would result in a higher C_r due to the aerodynamic drag, inertia of the wheels and drive train of the vehicle, which appears not to be the case. Due to the low testing speed of the coast down test, it is difficult to state an accurate value for the aerodynamic drag force. On the specific tyre used in this paper an increase of 26-30% in C_r was measured with the decrease of inflation pressure from 200kPa to 80kPa, as shown in Figure 77. This highlights the importance of running tyres at the correct inflation pressure for the specific vertical load that the tyre is operating at, as this has a direct impact on fuel efficiency. This effect is especially applicable when driving on non-deformable terrain.
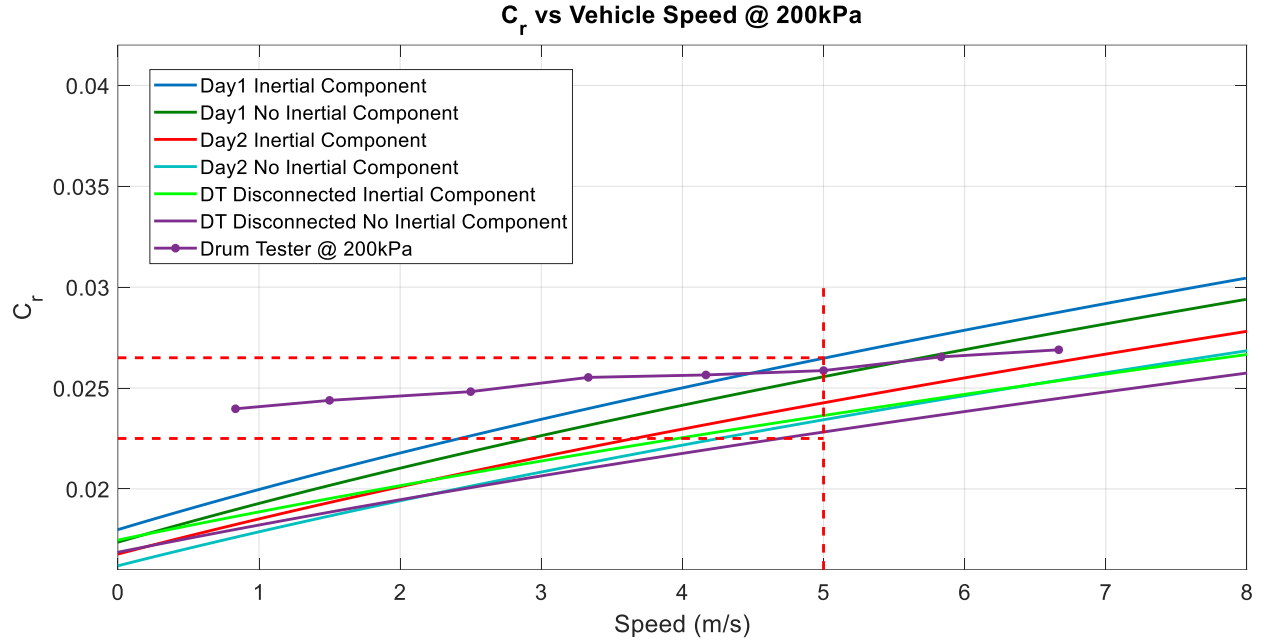
Figure 76: Coast down with and without inertial effects and drivetrain disconnected at 200kPa.
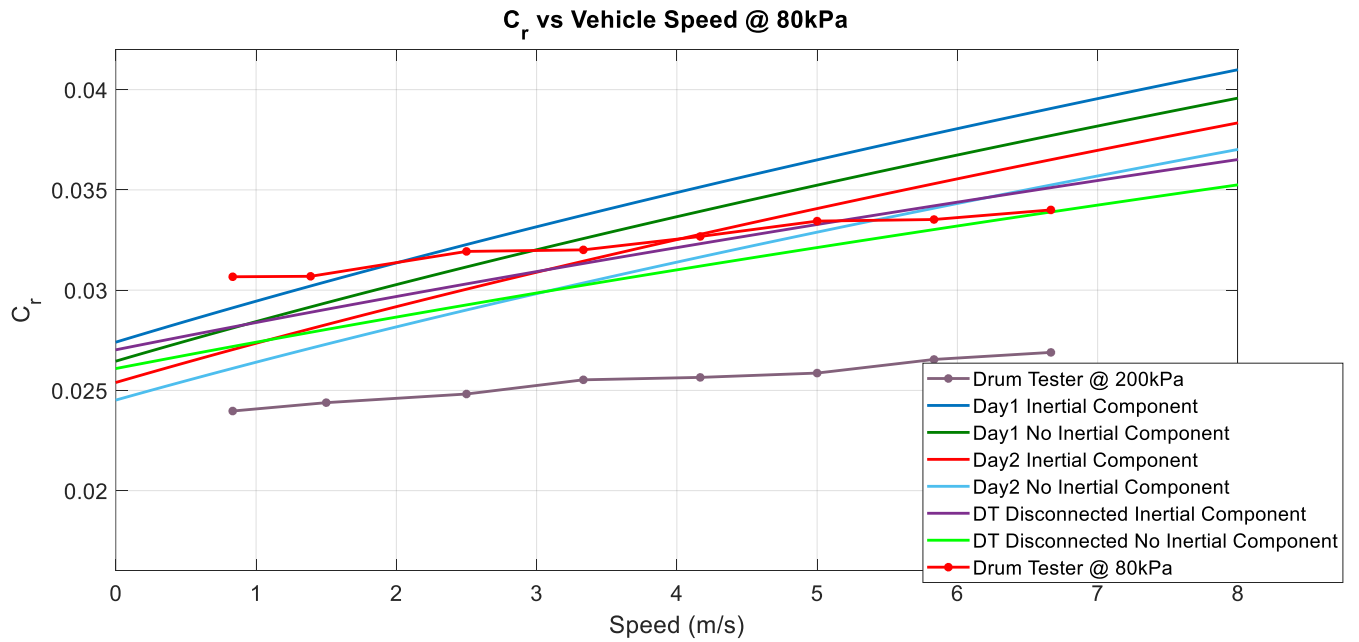
Figure 77: Coast down with and without inertial effects and drivetrain disconnected at 80kPa.

4.7.3. Towed Vehicle

The towed vehicle tests were conducted on the K-L section of the suspension tracks at Gerotek, as described in section 3.7.1. Test runs were performed in both Easterly and Westerly directions over the same test section, with the test vehicle, as shown in Figure 78. The test vehicle was towed by another vehicle at a constant speed of 18km/h. The vertical load on the tyres due to the weight of the vehicle, W_w, on each tyre was on average 5.78kN due to the 50:50 weight distribution of the vehicle. Tests were conducted in both directions on the same test section with tyre inflation pressures of 80 and 200kPa respectively. Ambient test conditions were 25 to 30 °C with an 11km/h easterly wind. The effect of the wind speed is noticed during the analysis of the results. The towed vehicle tests were conducted from ambient conditions to see the effect that the tyres and drivetrain warming up to operating conditions have on the C_r. The test vehicle's speed was measured with the use of a VBOX III differential GPS. The longitudinal towing force, F_{xDB}, was measured with the use of a S-Type load cell with a maximum rating of 5kN. The tow rope was in-line with both vehicles in a horizontal position to ensure that a pure longitudinal force was measured.
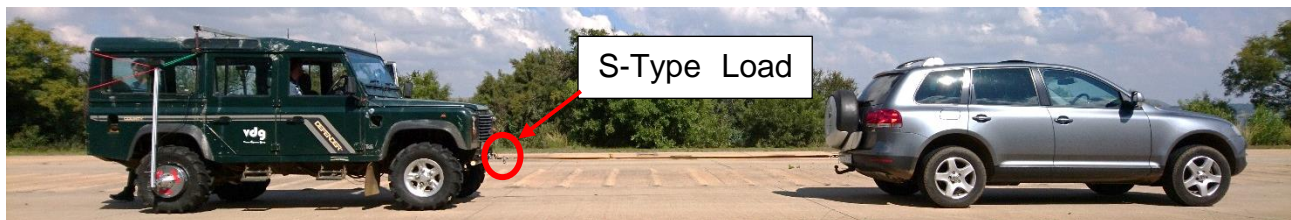
Figure 78: Towed vehicle test setup.

F_{xDB} measures the total road load, R_{RL}, as described by Gillespie, (1992). The total road load is given in eq. (29) as:

$$R_{RL} = C_{vr}W_N + {}^1/_2\,\rho V^2 C_d A + W_N sin\theta \qquad \text{eq. (29)}$$

Tests were conducted at a constant speed of 18km/h; thus, the aerodynamic drag of the vehicle was low and in the order of 30N. The tow vehicle also reduced the aerodynamic drag even further as it caused the air to flow around the trailer.

The C_{rDB} was thus calculated using eq. (30)

$$C_{rDB=}\frac{F_{xDB}}{W_N} \qquad \text{eq. (30)}$$

The C_r calculated from the towed vehicle tests are shown in Figure 79. Data sets were recorded over the same 400m section as per the motion resistance trailer tests and in both directions. Tests were conducted at an ambient temperature of 28°C. The same trends are noted as in the previous tests except that measurements stabilized faster due to a higher ambient temperature on the day of testing. The box plot again shows the variation in the measurement values and it is concluded that the stretch in the tow rope may also have been a contributing factor to the larger variations.
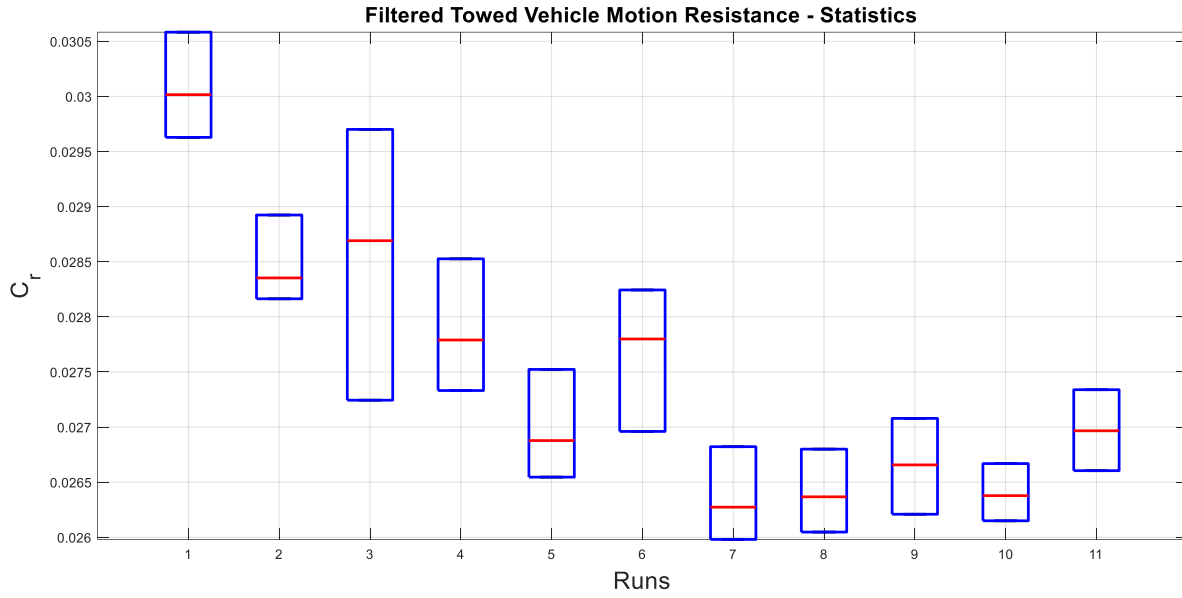
Figure 79: Towed vehicle motion resistance test results at 200kPa.

The mean Cr for both directions during the towed vehicle tests at 200kPa is shown in

Figure 80.
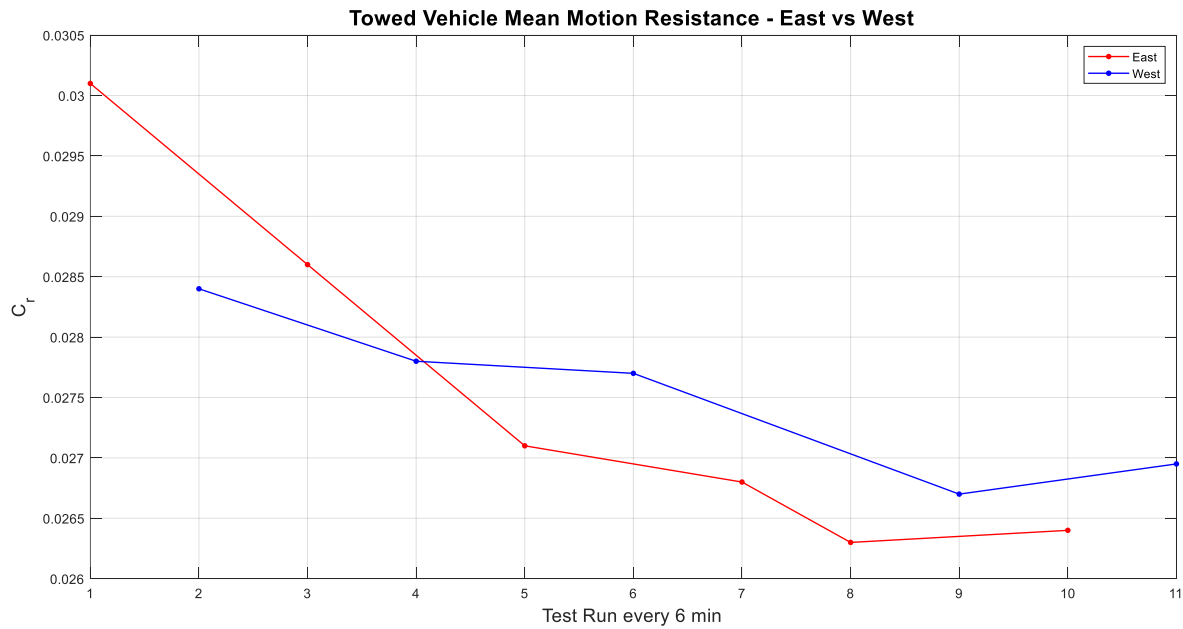
Figure 80: Towed vehicle motion resistance tests Easterly and Westerly results at 200kPa.

4.7.4. Motion Resistance Trailer

The Motion Resistance Trailer tests were conducted with the use of the DTT on the K-L section of the suspension tracks at Gerotek, as described in section 3.7.1. Test runs were performed in both Easterly and Westerly directions over the same test section. The ambient test conditions ranged from 25 to 30 °C with wind still conditions. The DTT was used to measure the motion resistance as shown in Figure 12. Tests were conducted at a constant speed of 18km/h with a vertical load, F_z, of 5.68kN on each of the tyres at inflation pressures of 80 and 200kPa respectively. This vertical load was selected to facilitate a direct comparison of motion resistance measurements, from the trailer measurements, to the motion resistance measurements from the towed vehicle and coast down tests conducted on a test vehicle. The inflation pressures were set at the beginning of the test and not adjusted during the tests. A six-component load cell was used to measure the longitudinal force, F_x, at the tow hitch. The orientation of the six-component load cell had one S-Type in the longitudinal direction, two S-Types in the lateral direction and three S-Types in the vertical direction. The S-Type load cells used in the six-component load cell each has a 1kN rating. Data was sampled at 1 kHz with 16-bit resolution. A VBOX 3I differential GPS was used to measure the tow vehicle's speed and ensure that the test was conducted at a speed as constant as possible. The motion resistance was calculated using eq. (31) and eq. (32)

$$F_r = \frac{mean(F_x)}{2} \qquad\qquad \text{eq. (31)}$$

with

$$C_{r=}\frac{F_r}{F_z}$$ eq. (32)

The drum tests indicated that the measured motion resistance is inversely proportional to the tyre inflation pressure which is directly proportional to the tyre carcass temperature. As the tyre pressure and operating temperature increase and stabilize, the motion resistance also decreases and stabilize when the tyre reaches operating temperature. The typical stabilization time for the tyres used during these field tests were in the order of 90 minutes of running at a constant speed of 18km/h. This is due to the tyre being an undriven tyre with no braking torque applied during the tests.

The results for the motion resistance trailer, DTT tests are shown in Figure 81. Tests were conducted from an ambient temperature of 25°C on the concrete sections between the suspension tracks at Gerotek with no wind. The C_r decreases as the tyre reaches operating temperature and pressure. From this graph one can note the effect the 0.03° gradient of the test track has on the results. The difference is apparent between the measurements taken in the Easterly vs. Westerly directions, however the mean C_r value of these tests correspond to the drum test rig measurements of 0.028.
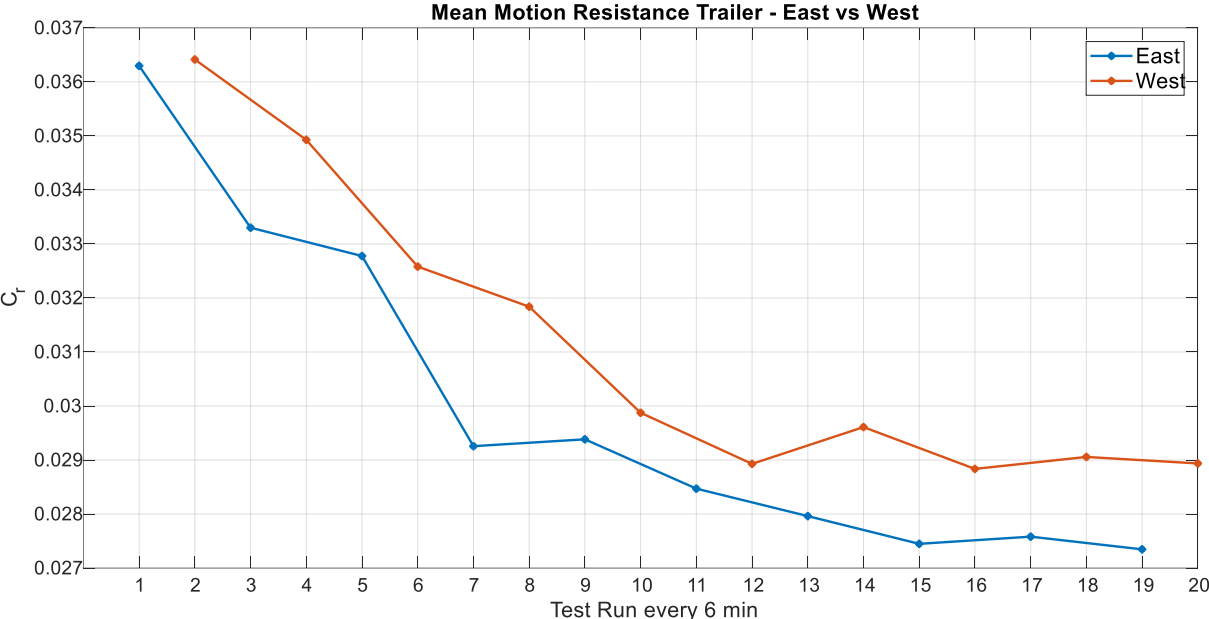
Figure 81: Motion resistance trailer, DTT test results at 200kPa.

A summary of the different motion resistance test methods is tabulated in Table 13. It can

be seen that the results from the different measurements methods can differ by 12 to 18%

depending on the inflation pressure.

Table 13: Motion resistance values at 18km/h form different test methods.

Inflation Pressure [kPa]	Drum	Coast Down	Coast Down, No Drivetrain	Towed vehicle	Motion resistance trailer
80	0.033	0.036	0.032	0.034	0.035
200	0.026	0.025	0.023	0.0265	0.028

4.7.5. The Effect of Wear on Motion Resistance

The results from the different C_r measurements methods indicated that the results from the DTT is very representative, therefore this method was chosen to compare the effect that tread depth has on motion resistance. Results are shown in Figure 82. At the higher inflation pressure (200kPa) a 25% decrease in C_r is noted as the tread wears down to 0%, compared to 80kPa inflation pressure where the C_r first increases by 8% and then decreases as the tread wears down to 0%. The change in C_r is due to the large tyre deformation at the lower inflation pressure.
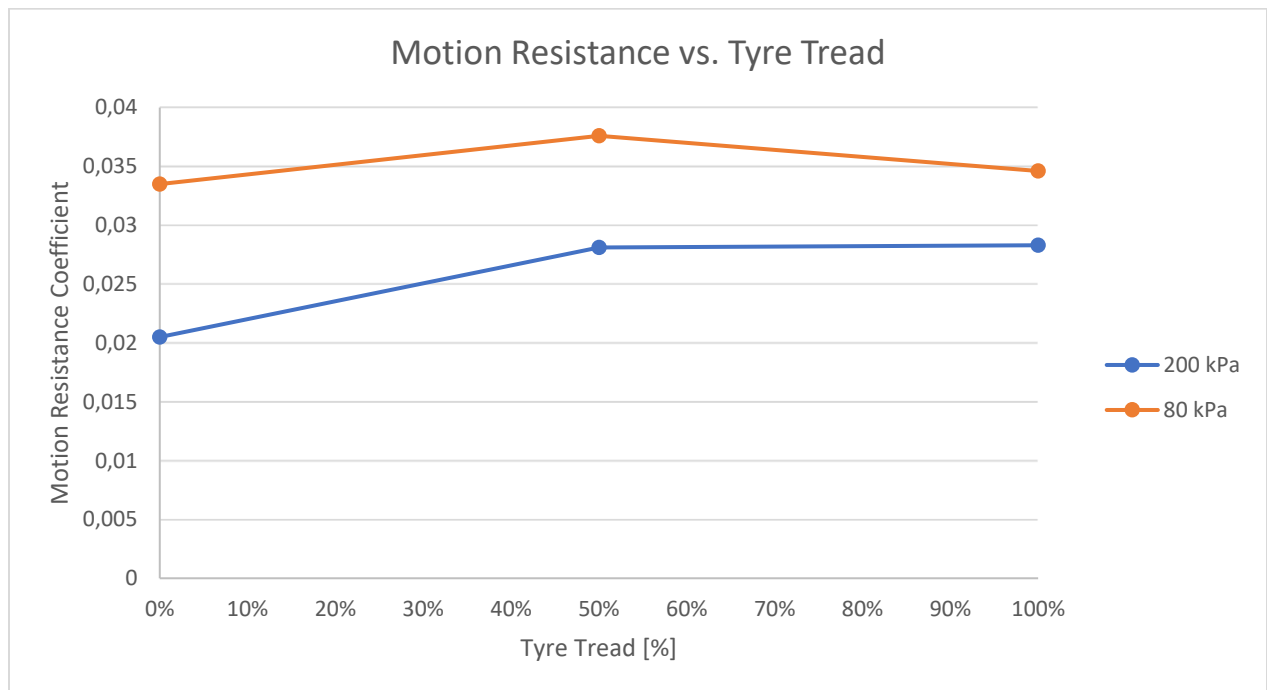
Figure 82: Motion Resistance vs. % Tyre Tread.

From these results it can be concluded that the inflation pressure has a larger influence on the motion resistance compared to the tread depth when a tyre operates at multiple inflation pressures.

Postulate conclusion:

XI.   *The motion resistance study concluded that in general, the inflation pressure is the dominant factor in motion resistance on the tyre in question. Other possible factors can include the tread pattern, which did not form part of the current study.*

4.8.   Results Summary

As tyre models are application dependent, tests conducted in this study have indicated the importance of using actual test data to parameterise tyre models due to the non-linearities in the tyre characteristics. Linearization of tyre stiffness should be done with extreme caution as it will have a direct effect in the simulation results and is suggested to be avoided if possible. In order to parameterise a tyre model that will represent the actual expected tyre characteristics in field tests it is important to use a representative surface during laboratory tests as seen in this study. The change in tyre characteristics as the tyre deforms over a cleat has been investigated. Different characterisation methods (Static/Non-rolling vs. Dynamic/Rolling) have been compared with good correlation between the different methods. The study has indicated that the carcass stiffness is the dominating factor in both the damping and motion resistance values in the current study, the tread pattern is an additional factor that may contribute and should be investigated in future studies. Both damping and motion resistance relate to rubber hysteresis as parts of the tyre deform in the contact patch. The influence the amount of tread has on the tyre characteristics of an agricultural tyre has also been investigated during all of the tests in this study. The results indicate that the amount of tread on a tyre is a parameter that needs to be considered by the designers and end users of a vehicle, as this contributes to the tyre's stiffness and sliding friction characteristics which will affect the handling of the vehicle.

5. Conclusions and Recommendations

This study has shown the importance of knowing how the tyre characteristics change due to tyre wear and why actual tyre data may assist vehicle designers with improved simulation results for ride and handling simulations. Although it is the responsibility of the end user to maintain the tyres on the vehicle, it remains the OEM's responsibility to design a vehicle that can function reliably for different tyre wear conditions. It is also shown that running tyres at the correct inflation pressure, for the specific vertical load that the tyre is operating at, has a direct impact on the tyre's response. The standard procedure of testing a tyre only in the "new" condition and using only this data to parameterize the tyre model can lead to substantial errors in the design process of a vehicle. Test methods applied to passenger car or commercial vehicle tyres have to be modified, or at least thought about carefully when applied to tyres with large lugs such as agricultural tyres.

5.1. Contact Area

The contact area of the tyre in question increases dramatically at the 0% tread condition. The 0% tread condition has the smallest perimeter measurements; however, this condition has the highest rubber contact areas of the three conditions, thus it has the lowest contact pressure. At the same time the mass of the tyre is reduced by 31%. The

contact area, for 0% tread condition and an inflation pressure of 80kPa, increases by 202% compared to the 100% tread condition at 80kPa. The contact area for 0% tread condition for an inflation pressure of 200kPa increase by 147% compared to the 100% tread condition at 200kPa. A 60 to 66% contact pressure drop is noted at 0% tread condition due the increase in actual rubber in contact with the test surface. This indicates that running an agricultural tyre close the 0% tread will have a very large effect on the handling characteristics of the vehicle.

5.2.   Surface Roughness and Friction

This study presented friction coefficient measurements on different dry non-deformable surfaces in a laboratory and field test tracks. Different friction coefficient measurements are presented for the same tyre at three tread wear conditions over nine different terrains. This study has shown the effect a test surface with a low surface roughness and a high surface roughness will have on the measured tyre characteristics. In general, the test results on concrete surfaces on the static tyre test rig and static trailer tests at Gerotek Test Facilities correlate well when considering the different boundary conditions. It is known that the friction coefficient on all test surfaces differ in every environment/ different test facility, thus it is suggested that the surface roughness of the test surface on which the tyre will be used the most, is measured before tyre characterisation tests are conducted in a laboratory. This surface roughness can then be used to determine which grit sandpaper or corundum tracks will be best suited to represent the outdoor environment during laboratory tests. It was found that, for the concrete field test surfaces

in question, the recommended laboratory test surface needs to have a surface roughness value of between 10<R_a<15µm. This roughness is equivalent to a P220 to P180 grit sandpaper, however, using only the sandpaper grade is not a good measure to use. The grading system of sandpaper is based on the number of abrasive particles per square inch on the sandpaper. A more accurate method is to compare the Displacement Spectral Densities of the field test surface with that of the sandpaper. The spatial frequency of interest that needs to be compared is between 10^4 and 10^6 cycles/m, with corresponding surface index, *H2*, and roughness coefficient at a spatial frequency of 75000 cycles/m.

The majority of the road surface contains exposed aggregate, which is in direct contact with the rubber in the contact patch, thus the dominating factor in friction generation. This study has also indicated that stick-slip phenomena are not just possible on smooth surfaces where R_a<1µm (as suggested in literature), as stick-slip was measured on surfaces with R_a as high as 3µm. The stick-slip was independent of the size of the contact area and contact pressure in the contact patch. It is concluded that the stick-slip measured on the agricultural tyre of interest was caused by the lower stiffness of the lugs in the tread at 100% tread condition.

It is recommended that an artificial surface is used in laboratory tests during tyre characterisation. This surface must represent the actual field test surface on which validation tests, or any other tests, are to be conducted.

5.3.   Quasi-Static Tyre Characteristics

The importance of understanding the effect the condition of tyres will have on the response from a vehicle is shown. This is especially the case on agricultural vehicles where the tyre is the primary suspension of the vehicle. The vertical stiffness measurements have shown that the change in tread condition does not have a drastic change in gradient of the vertical stiffness between 100% and 50% tread around the static load condition. However, as the tread nears 0% tread condition the gradient of the vertical force vs. displacement curve is increased. When extrapolating the linear stiffness around the static vertical load, a 16% to 21% error can be made in the estimated tyre deformation. As a tyre travels over a cleat one can expect a 46% decrease in vertical stiffness, which leads to a multistage stiffness graph where the vertical stiffness increases again to the stiffness of a tyre on a flat surface as the tyre deforms around the cleat. At 100% tread condition the tyre vertical stiffness is relatively similar over lateral and longitudinal orientated cleats, however this change as the tread wear condition changes. It is noted that the transition point, from a lower to a higher stiffness on the vertical force vs. displacement graph, is dependent on the tread wear condition and independent of the inflation pressure. It is found that the transition point can be calculated within 8.5% with the use of simply supported beam deflection theory and the cross-section geometry of the lug at different tread wear conditions.

It is found that the change in longitudinal stiffness in the linear region for different tread wear conditions and inflation pressures can increase up to 24% with a tread wear change from 100% tread to 50% tread. Longitudinal stiffness increases of up to 63% between

100% tread and 0% tread condition at an inflation pressure of 80kPa is measured. The dramatic increase in friction coefficient in the longitudinal direction, at 0% tread, can place high levels of unintended strain on the driveline of the vehicle which may lead to driveline failures.

The change in lateral stiffness in the linear region for different tread wear conditions and inflation pressures can increase by up to 29% with a tread wear change from 100% tread to 50% tread. Lateral stiffness increases of up to 51% between 100% tread and 0% tread condition at an inflation pressure of 200kPa is measured. This drastic change in grip at 0% tread can change the characteristic of a vehicle which tends to slide/under steer in an emergency evasive maneuver, such as a lane change, to a vehicle that may roll over during the same maneuver. It is recommended that each tyre model, used in a simulation environment, is parameterized with representative tyre data so that the non-linearities are captured in the tyre model.

In general, new tyres are always used to measure tyre characteristics for parameterisation purposes, no matter which tyre model is used. From the results in section 4.4, it is highly recommended, especially when a physics based tyre model (as FTire, for example) is used, to characterize the tyre stiffness on a new tyre with 100% tread as well as the same tyre with 0% tread. It is then further recommended that the 0% tread data is used to parameterize only the carcass stiffnesses, followed by the 100% tread data to adjust the parameters related to the tread/lug stiffness (brush model). This is highly recommended for agricultural tyres or any other tyre with large lugs.

5.4.   Dynamic/Rolling Tyre Characteristics

The results from the dynamic/rolling tyre field tests at a 100% tread condition is successfully compared to the static characterisation tests, with limited success at low inflation pressures due to the tyre belt stiffening for a rolling tyre. This indicates that it is possible to obtain accurate tyre characteristics from static tests which are representative of a rolling tyre at lower velocities and high inflation pressures. This is an important observation as most agricultural vehicles operate at low speeds. This will allow designers to obtain valuable tyre parameterisation data at a lower cost with the use of static tyre testing. This data can also be used to parameterise physics-based tyre models for rolling tyre simulations.

5.5.   Damping

It was found that the damping coefficient decrease with the inflation pressure as the damping coefficient decreases on average by 39% with a decrease in inflation pressure from 200kPa to 80kPa at 0% tread. The effect the tyre tread wear has on the damping coefficient is only in the order of a 3% decrease from 100% tread to 50% tread, with a 12% decrease from 100% tread to 0% tread. The tread pattern may be an additional factor that may contribute to the damping coefficient, this was outside the scope of this study, however it may be investigated in future projects.

5.6.   Motion Resistance

The four methods used to measure the Motion resistance (C_r) in this study have produced very interesting results. Very consistent C_r values were obtained with the use of the drum test rig, motion resistance test trailer (DTT) method, as well as with the towed vehicle test method. The coast down C_r measurement illustrates the inertial effect, drive train inertia and aerodynamic drag have on the measurements. The fact that a lower C_r is calculated below 5m/s with the coast down method compared to the other three methods, does raise concerns with regards to the accuracy of the coast down method at velocities lower than 5m/s. It is expected that the coast down method will always produce a higher C_r compared to the other three test methods due to the inclusion of the complete vehicle and all of the losses. The drum, towed vehicle and trailer tests result in very similar results. The trailer test is found to be the preferred test method as it is independent of the inertial effects of the vehicle's drivetrain. Various tyre sizes, inflation pressures and vertical loads can be tested with the use of a single tow-vehicle-trailer combination. At 200kPa inflation pressure a 23% decrease in C_r is noted as the tread wears down to 0%, compared to the 80kPa inflation pressure where the C_r first increase by 8% and then decrease as the tread wears down to 0%. This is due to the large tyre deformation at the lower inflation pressure, which indicated that the inflation pressure has a larger effect on the motion resistance compared to the tread depth.

It is thus noted that the coast down test method should be used with caution. Especially when determining the C_r on agricultural or construction vehicles which operates most of the time below 5m/s. SAE J2263-1996 specifies in section 12.6 that data analysis on coast down test should be restricted to velocities from 115 to 15km/h. The 15km/h or 4.1m/s lower limit correlates to the data shown in Figure 76 and Figure 77. With this in mind it is recommended that coast down tests conducted on agricultural or construction vehicles are conducted from the maximum self-propelled speed that the vehicle can run at, as it may even be lower than 15km/h. It is suspected that for these slow-moving vehicles a more linear speed vs time graph will be measured during the coast down tests. This was also seen for the tests conducted in this study as the initial vehicle speed was only at 40km/h (speed rating of tyre), when compared to standardised tests conducted from 115km/h.

The importance of running tyres at the correct inflation pressure for the specific vertical load that the tyre is operating at is shown, as this has a direct impact on fuel efficiency and traction. This can be used to justify the additional capital cost of running a vehicle with a Central Tyre Inflation system, especially if the vehicle is operated on deformable terrain at low inflation pressures and non-deformable terrain at high inflation pressures.

Test results for the motion resistance trailer tests indicate that at a higher inflation pressure (200kPa) a 25% decrease in C_r is noted as the tread wears from 100% tread down to 0%, compared to 80kPa inflation pressure where the C_r first increase by 8% and then decrease as the tread wears down to 0%. From these results it can be concluded that the inflation pressure has a larger impact on the motion resistance compared to the tread depth.

6. Future Work

The results for the current study have inspired some possible future investigations. The following aspects needs to be investigated further:

- The results from the current study need to be investigated on larger diameter tyres as some dynamic effects are expected on a rotating tyre due to increased inertia effects on large tyres.

- Use Digital Image Correlation techniques to comparing the % longitudinal slip obtained during static tests on the STTR from a video clip with the % longitudinal slip measured on the DTTT.

- Investigate the longitudinal lug deformation with the cantilever beam approximation, as described in section 4.3, where the belt stiffness needs to counter the moment generated by the deformation of the lug and stick-slip phenomena at 100% tread condition with the use of the T2CAM system as described in section 2.2, Guthrie et al., (2017) and Pegram et al., (2020).

- The surface roughness value of $10 < R_a < 15 \mu m$ correlates directly to the surface texture of the aggregate used in the construction of road surfaces. An investigation into the roughness of the aggregate used in multiple road surfaces relative to the friction coefficient of these roads needs to be compared and related to representative laboratory test surfaces.

- Use the data captured in this study to parameterise tyre models.

- Conduct simulation analysis with the use of the newly parameterised tyre models together with the VDG's Land Rover Defender model and compare the simulation results with actual test data.

References

Acuity, 2015, AR700 laser displacement sensor, Oregon: Schmitt Industries.

Ambruster, K, Kutzbach, H.D., 1989, Development of a single wheel tester for measurement on driven angled wheel. In: Proceedings of 5th European conference of the ISTVS, Wageningen, The Netherlands; p. 8–14.

American Institute of Physics, 2015. Phys org. [Online] Available at: https://phys.org/news/2015-05-simple-leonardo-da-vinci-combined.html (accessed 14 May 2018).

Bakker, E, Nyborg, L and Pacejka, H.B., 1987, Tyre modelling for use in vehicle dynamics studies, Society of Automotive Engineers, Warrendale, PA.

Becker, C.M, 2009, Profiling of rough terrain, Master of Engineering Thesis, University of Pretoria, South Africa, http://hdl.handle.net/2263/29833.

Becker, C.M. and Els, P.S., 2011, Modal analysis on a large off-road tyre using Scanning Laser Vibrometry, Proceedings of the 17th International Conference of the ISTVS, Blacksburg, USA, 18 to 22 September 2011.

Becker, C.M. and Els, P.S., 2014, Profiling of rough terrain. International Journal of Vehicle Design, Vol. 64, pp240-261.

Becker, C.M. and Els, P.S., The applicability of the friction circle concept to off-road tyres, Proceedings of the 13th European Conference of the ISTVS, Rome, Italy, 2015.

Becker, C.M. and Els, P.S., 2018, Static and Dynamic Parameterization Test Rigs for Large Tyres, Proceedings of the 10th Asia-Pacific Conference of the ISTVS, Kyoto, Japan, July 11-13.

Becker, C.M. and Els, P.S., 2020, Motion Resistance Measurements on Large Lug Tyres, Journal of Terramechanics, Vol.88(1), p.17-27.

Bekker, M.G., 1956, Theory of Land Locomotion the Mechanics of Vehicle Mobility, University of Michigan Press.

Billington, P.W., 1973 The NIAE Mk II single wheel tester. J Agric Eng Res; 18:67–70.

Bondetec, 2021, website: https://bondetec.en.ecplaza.net/products/bondetec-portable-shore-a-hardness-tester_2398779 accessed on 28 July 2021.

Botha, T.R. and Els, P.S., 2015, Digital image correlation techniques for measuring tyre-road interface parameters: Part 2 - Longitudinal tyre slip ratio measurement, Journal of Terramechanics, Vol 61, pp.101-112.

Cosin scientific software, 2017, FTire, Modelization and Parameter Specification. 2017-1-r14630. [pdf]. Software documentation and user guide.

Crolla, D.A. and El-Razaz, A.S.A., 1987, A Review of The Combined Lateral and Longitudinal Force Generation of Tyre on Deformable Surfaces. Journal of Terramechanics, Vol. 24(3), p199-225.

Crolla, D.A., and Maclaurin, E.B., 1985, Theoretical and Practical Aspects of The Ride Vibration Dynamics of Off-road Vehicles., Journal of Terramechanics, Vol 22(1), p17-25.

Du Cross, Sir Arthur, 1938, Wheels of Fortune, a salute to pioneers, Chapman and Hall, London.

Els, P.S., 2012, Wheel Force Transducer Research and Development, W911NF-10-1-0463, Final report, August 2011 – February 2012, https://apps.dtic.mil/sti/pdfs/ADA557517.pdf

Ergun, M., Iyinam, S., and Iyinam A.F., 2005, Prediction of Road Surface Friction Coefficient Using Only Macro- and Microtexture Measurements. Journal of Transport Engineering, 131(4), p 311-319.

fka, 2021. Chassis Truck Tyre Test Rig, Aachen, Germany, https://www.fka.de/en/testing/chassis/114-truck-tyre-test-rig.html, assessed on 26 March 2021.

Gerotek Test Facilities, 2021, https://www.armscor.co.za/?page_id=3967 , accessed on 16 April 2021.

Gillespie T.D., 1992, Fundamentals of Vehicle Dynamics, p79-120.

Google earth, 2018, Gerotek Test Facility, Pretoria, South Africa, 25° 45' 30.19" S 28° 00' 27.82" E, Accessed 2018/05/13.

Gorsich, D.J., Chaika, M., Gunter, D., Karlsen, R., Haueisen, B., Sun, T. and Ferris, J., 2003, Terrain Roughness Standards for Mobility and Ultra-Reliability Prediction, SAE 2003-01-0218.

Guthrie, A.G., Botha, T.R., Jimenez, E., Els, P.S. and Sandu, C., 2017. Dynamic 3D Measurement of Tyre-Terrain Interaction. Proceedings of the 19th International & 14th European-African Reginal Conference of the ISTVS, Budapest, September 25-27.

Heinrich G. and Klüppel M., 2008, Rubber Friction, Tread Deformation and Tire Traction, Wear, 265:1052-1060.

ISO 28580: 2009. International Organization for Standardization 28580: Passenger car, truck and bus tyres – Methods of measuring rolling resistance – Single point test and correlation of measurements results. Switzerland.

ISO 4287: 1997, International Organization for Standardization 4287: Geometrical Product Specifications (GPS), Surface texture: Profiling method – Terms, definitions and surface texture parameters.

ISO 8608: 1995, International Organization for Standardization 8608: Mechanical vibration - Road surface profiles - Reporting of measured data, ISO 8608:1995(E).

ISO 8855: 2013. International Organization for Standardization 8855: Road vehicles – Vehicle Dynamics and Road-holding Ability – Vocabulary. Beuth, Berlin.

ISO 13473: 1997. International Organization for Standardization 13473: Characterization of Pavement Texture by Use of Surface Profiles.

Karafiath, L.L. and Nowatzki, E.A., (1978). Soil Mechanics for Off-Road Vehicle Engineering (1st ed.). Germany: Trans Tech Publications.

Klingspor, 2021a), Abrasive belt CS 308 Y premium with extra tear-resistant backing, website: https://www.klingspor.co.za/products/belts/cs-308-y, accessed on 29 May 2021.

Klingspor, 2021b), Abrasive belt CS 311 Y ACT with cloth backing, website: https://www.klingspor.co.za/products/belts/cs-311-y-act-1, accessed on 29 May 2021.

Lines, J.A., 1991, The Suspension Characteristics of Agricultural Tractor Tyres. PhD Thesis, Cranfield Institute of Technology Silsoe College.

Le Gal, A., Guy, L., Orange, G., Bomal, Y., Klüppel M., 2008. Modelling of Sliding Friction of Carbon Black and Silica Filled Elastomers on Road Tracks. Wear, Volume 264, Issue 7-8, pp 606-615.

Loadcell Services, 2021, ULP loadcell Specifications, data sheet on website: https://loadcell.co.za/wp-content/uploads/downloads/productsLoadcells/ulpSpecifications.pdf accessed on 26 July 2021.

Mardani, A., Shahidi, K. and Maslak H. K., 2010, An Indoor Traction Measurement System to Facilitate Research on Agricultural Tires. Journal of Food, Agriculture and Environment, Vol. 8(1), p.642-646.

Macmillan, R.H., 2002, The Mechanics of Tractor-Implement Performance, University of Melbourne.

McKibben, E.G., and Davidson, J.B., 1940, Effect of outside and cross-sectional diameters on the rolling resistance of pneumatic implement tyres, Agricultural Engineering, 21(2) 57-58.

Meriam, J.L. & Kraige, L.G., 1998, Engineering Mechanics Volume 2 Dynamics, 4th edition, Chapter 8 Vibration and time response.

Misiewicz, P.A., 2010. The Evaluation of the Soil Pressure Distribution and Carcass Stiffness Resulting from Pneumatic Agricultural Tyres. (PhD. Thesis) Cranfield, UK: Cranfield University.

Misiewicz, P.A., Terence, E.R., Blackburn, K., Godwin, R., 2016, Comparison of Methods for Estimating the Carcass Stiffness of Agricultural Tyre on Hard Surfaces, Biosystems Engineering, Vol 147, pp 183-192.

Mitutoyo, 2021, SJ210 Portable Surface Roughness Tester, https://www.mitutoyo.com/wp-content/uploads/2015/08/Surftest_SJ210.pdf, Assessed 23 July 2021.

MSC Software, 2014, ADAMS/Tire help file.

MTS, 2021. Flat-Trac Tire Force & Moment Measurement Systems, MN USA https://test.mts.com/en/products/automotive/tire-test-systems/flat-trac-tire-system#technical, accessed on 26 March 2021.

Murphy, K. and Lines, J.A., 1991.The Stiffness of Agricultural Tractor Tyres. Journal of Terramechanics, Vol. 28(1), pp49-64.

Pegram M.S., Botha T.R., Els P.S., 2020, Full-Field Strain Measurement of the Contact Patch via the Inside Tyre Surface. In: Klomp M., Bruzelius F., Nielsen J., Hillemyr A. (eds) Advances in Dynamics of Vehicles on Roads and Tracks. IAVSD 2019. Lecture Notes in Mechanical Engineering. Springer, Cham. https://doi.org/10.1007/978-3-030-38077-9_212.

Persson, B.N.J., 2001, Theory of rubber friction and contact mechanics. Journal of Chemical Physics, vol.115:3840-3860.

PIARC, 1995, Technical Committee on Surface Characteristics, "International PIARC Experiment to Compare and Harmonize Texture and Skid Resistance Measurements", Paris.

Racelogic, 2018a, RLVB3I-V5_Data.pdf document, downloaded from website: https://www.racelogic.co.uk/_downloads/vbox/Datasheets/Data_Loggers/RLVB3i-V5_Data.pdf, accessed on 6 August 2018.

Racelogic, 2018b, RLVB3I-iSLR_Data.pdf document, downloaded from website: https://www.racelogic.co.uk/_downloads/vbox/Datasheets/Data_Loggers/RLVB3iSLR_Data.pdf, accessed on 6 August 2018.

Rao, S.S. Mechanical Vibrations, 4th edition, 2004, Chapter 2 Free vibration of single degree of freedom systems.

Reece, A.R. 1965 Principles of soil - vehicle mechanics, Proceedings Institution of Mechanical Engineers, 180 Part 2A ,125-31.

Rukes, B.,2002, John Deere Industrials. ISBN 0-7603-1023-8.

SAE J2263, 1996. Road Load Measurement Using Onboard Anemometry and Coast down Techniques.

Sandberg, Ulf., 2011, Rolling Resistance – Basic Information and State-of-the-Art on Measurement methods, Report MIRIAM_SP1_01, project MIRIAM SP 1, final version, updated 2011-06-01.

Sandu, C., Taheri, Sh., Taheri, S., Els, S., Jimenez, E., 2020, Hybrid soft soil tire model (HSSTM). Part III: Model parameterization and validation. Journal of Terramechanics, 88:1-5.

Salehi M., Noordermeer J.W.M., Reuvekamp L.A.E.M., Dierkes W.K., Blume A., 2019, Measuring Rubber Friction Using a Laboratory Abrasion Tester (LAT100) to Predict Car Tire Dry ABS Braking. Tribology International, 131, p 191-199.

Scholtz, O. and Els, P.S., 2020, Tyre Rubber Friction on a Rough Road, Journal of Terramechanics, 93:41-50.

Shigley, J.E., 1986, Mechanical Engineering Design, First Metric Edition, Appendix Tables A-9, #5 Simple supports-center load.

Shmuleviuch, I., Ronai, D., Wolf, D., 1996. A new field single wheel tester. Journal of Terramechanics, Vol. 33(3), p133–41.

Stallmann, M.J., 2013, Tyre model verification over off-road terrain. Master's Thesis, University of Pretoria, South Africa, https://repository.up.ac.za/handle/2263/41012

Stallmann, M.J., 2018, Cost effective FTire parameterisation methods for ride simulations with large off-the-road tyres. PhD Thesis, University of Pretoria, South Africa, https://repository.up.ac.za/handle/2263/70496

Stayner, R.M., Collins, J.A. and Lines, J.A., 1984, Tractor Ride Vibration Simulation as an Aid to Design. Journal of Agriculture Engineering Res. 29.345-355.

Tekscan Pressure Mapping, Force Measurement and Tactile Sensors, 2021, South Boston, MA, USA: https://www.tekscan.com/products-solutions/systems/tirescan-versatek-system, accessed on 9 April 2021.

The Transtec Group, 2021, What is Pavement Texture?, https://www.thetranstecgroup.com/pavement-surface-characteristics/basics/texture/ accessed 23 July 2021.

Trelleborg TM700 Brochure, 2018, downloaded from website: https://www.trelleborg.com/en-za/wheels/products--and--solutions/tractor--tyres/utility--and--specialty--tractors/tm700, accessed on 6 August 2018.

TüV SüD, 2021, Virtual Simulation to Ensure the Safety of Vehicles, website: https://www.tuvsud.com/en/e-ssentials-newsletter/automotive-essentials/e-ssentials-3-2017/virtual-simulation-to-ensure-the-safety-of-vehicles, accessed 5 October 2021.

VSM, 2021, RK700X Ilumeron long-term abrasive spec sheet, website: https://uk.vsmabrasives.com/rk700x/, accessed on 29 May 2021.

Wismer, R.D., and Luth H.J., 1974, Off-road traction prediction for wheeled vehicles Transactions of American Society of Agricultural Engineers, 17(1) 8-10,14.

Witzel, P., 2018. The Hohenheim tyre model: a validated approach for the simulation of high-volume tyres – Part I: Model structure and parameterisation. Journal of Terramechanics. 75, 3–14.

Wright, K.R.S., Botha, T.R. & Els, P.S., 2019, Effects of age and wear on the stiffness and friction properties of an SUV tyre, Journal of Terramechanics, vol. 84, pp. 21-30.

Wong, J.Y., 1993, Theory of Ground Vehicles, 2nd edition, ISBN 0-471-52496-4.

Zaayman, O.C.D., 1988, Terrain profile roughness measurement and characterization, Unpublished M.Eng Thesis, University of Pretoria, Pretoria, South Africa.

Zuleeg, J., 2015, How to Measure, Prevent, and Eliminate Stick-Slip and Noise Generation with Lubricants, SAE Technical Paper 2015-01-2259, doi:10.4271/2015-01-2259.